SINGLE-MOLECULE STUDY OF β-CATENIN TRANSLOCATION AND THE ROLE OF CUSTOS IN ITS REGULATION

A Dissertation

Submitted to

the Temple University Graduate Board

In Partial Fulfilment

of the Requirements for the Degree

DOCTOR OF PHILOSOPHY

by

Steven John Schnell

August 2020

Examining Committee Members:

Dr. Raymond Habas, Advisory Committee Chair, Department of Biology, Temple University

Dr. Richard Waring, Examining Committee Chair, Department of Biology, Temple University

Dr. Weidong Yang, Department of Biology, Temple University

Dr. Peter S. Klein, External Examiner, Department of Medicine, Perelman School of Medicine, University of Pennsylvania

ABSTRACT

The nuclear pore complex is closely involved in the regulation and control of many cellular processes, including the movement of molecules into and out of the nucleus along with the regulation of gene transcription. It is therefore a major barrier for controlling the passage of signaling molecules into and out of the nucleus. β-catenin is one such signaling molecule, and a primary signaling molecule of the Wnt signaling pathway. How the passage of β-catenin into and out of the nucleus is controlled remains poorly defined. This signaling pathway governs major developmental processes, including cell fate determination, proliferation, motility and primary axis and head formation during development. In this study, we use super-resolution microscopy to show that β-catenin import requires Custos as a docking protein. Custos and β-catenin form a complex in the cytoplasm and move together through the NPC into the nucleus, where they dissociate in the nucleus. Further, we provide evidence that import of β-catenin into the nucleus is a regulatory event at the NPC and define regions within the β-catenin protein required for this regulation.

TABLE OF CONTENTS

LIST OF TABLES

LIST OF FIGURES

LIST OF ACRONYMS

2D	Two dimensional
3D	Three dimensional
AA	Amino acid
APC	Adenomatous polyposis coli
ARM	Armadillo
β-TRCP	β-transducin repeats–containing protein
BCL9	B-cell CLL/lymphoma 9 protein
CK1	Casein kinase 1
CCD	charge-coupled device
CBP/p300	CREB-binding protein/E1A binding protein p300
cDNA	complementary DNA
C/H	Charged/hydrophobic (ratio)
CRM1	Chromosomal maintenance 1
CTF	C-Terminal fragment
DAPI	4′,6-diamidino-2-phenylindole
DEP	Dishevelled, EGL-10 Pleckstrin (domain)
DIX	Dishevelled/Axin (domain)
DMEM	Dulbecco's modified eagle's medium
EGTA	(ethylene glycol-bis(β-aminoethyl ether)-N,N,N′,N′-tetraacetic acid)
FBS	Fetal bovine serum
FRET	Förster resonance energy transfer

FG	phenylalanine-glycine
GEF	Guanine nucleotide exchange factor
GFP	Green fluorescent protein
GSK3	Glycogen synthase kinase 3
HEAT	Huntingtin, elongation factor 3, protein phosphatase 2A, yeast kinase TOR1
HEPES	(4-(2-hydroxyethyl)-1-piperazineethanesulfonic acid)
ICAT	Inhibitor of β-catenin and TCF4
IDP	Intrinsically disordered protein
LEF	lymphoid enhancer-binding factor
LRP5/6	low-density-lipoprotein-related protein 5/6
MSD	Mean square displacement
mRNP	Messenger ribonucleoprotein
NES	Nuclear export sequence
N/C	Nucleus-to-cytoplasm (ratio)
NLS	Nuclear localization sequence
NPC	Nuclear pore complex
NTR	Net transport rate
Nup	Nucleoporin
ONM	Outer nuclear envelope
PALM	Photoactivated light microscopy
PDZ	Post-synaptic density protein, *Drosophila* disc large tumor suppressor and zonula occludens (domain)

PP2A	Protein phosphatase 2A
PSF	Point-spread function
Ror2	Tyrosine kinase-like orphan receptor 2
SFRP	Secreted frizzled-related protein
siRNA	small interfering ribonucleic acid
SPEED	Single-point edge-excitation subdiffraction
spFRET	single-particle FRET
SPT	single-particle tracking
STED	stimulated emission depletion
STORM	stochastic optical reconstruction microscopy
TCF	T-cell factor
Vangl2	VANGL planar cell polarity protein 2
WIF	Wnt inhibiting factor protein

CHAPTER 1: INTRODUCTION

1.1 Wnt Signaling and Embryonic Development

Embryonic development, the formation of a complex multicellular organism, consists of proliferation, cell fate decisions to produce distinct cell types, and movement of cells to form tissues. These processes are tightly regulated by a number of signaling pathways, among which the Wnt signaling pathway is one of the most important [1-5]. The first Wnt gene, termed Int-1, was discovered and cloned from mouse mammary tumors in 1982 and with the identification of its homologue termed Wingless in Drosophila, the two names were fused to form Wnt [6,7]. The highly conserved Wnt proteins are secreted glycoproteins that govern major developmental processes, such as cell fate determination, cell proliferation, cell motility and establishment of the primary axis and head formation during vertebrate development [8-14]. In addition to regulating embryonic development and pattern formation, defects in Wnt signaling have been implicated in tumorigenesis [9,15-17], leading to an understanding of cancer as a form of aberrant development [3].

Wnt proteins are typically between 350 and 400 amino acids long and subject to posttranslational modification, such as including glycosylation and palmitoylation. They also contain a secretion signals on their N-termini [18,19]. They are secreted and diffuse extracellularly [46]. Wnt proteins are developmental morphogens that regulate cell fate via their position along the Wnt concentration gradient [18]. Wnt proteins were originally shown to act as long-range morphogens in *Drosophila* [3,20-22]. However, it is not clear how the Wnt protein travels in the extracellular matrix. Several Wnt transport

mechanisms have been proposed, such as vesicles, specialized signaling filopodia (cytonemes), and exosomes [3,23-25]. Mouse Wnt3a, the Wnt used in this study, was the first purified and characterized Wnt protein [19,26].

On their intercellular journey, Wnt ligands are known to interact with several classes of proteins, such as secreted frizzled-related proteins (SFRPs), themselves secreted signaling molecules, and Wnt inhibiting factor proteins (WIFs). It is not known for certain that these Wnt-interacting protein families serve to inhibit or promote movement of Wnt through the extracellular matrix [3,27-30]. At the plasma membrane, Wnt proteins are known to interact with the seven-pass transmembrane protein Frizzled as the primary receptor and low-density-lipoprotein-related protein 5/6 (LRP5/6) as a co-receptor [1]. Some extracellular inhibitors of Wnt are known to operate at the level of the cell surface receptor; for instance, Wise and Dickkopf bind to LRP5/6, interfering with binding of Wnt [3,31,32].

The destruction complex of the canonical Wnt signaling pathway is a major regulatory checkpoint of β-catenin–dependent Wnt signaling. β-catenin is a transcriptional co-activator of Wnt target genes, which are necessary for stem cell renewal as well as formation of various organ systems including the heart, lungs, kidney, skin and bone. The destruction complex keeps cytosolic levels of β-catenin low in the absence of Wnt stimulation to prevent Wnt-mediated gene transcriptional regulation [2,3,33]. This complex is comprised of the scaffold protein Axin, the tumor suppressor Adenomatous Polyposis Coli (APC), Casein Kinase 1 (CK1) and Glycogen Synthase Kinase 3 (GSK3)

[1,34]. The role and necessity of another possible player in this group, protein phosphatase 2A (PP2A), are unclear [33]. In the absence of Wnt ligand, the destruction complexes, localized around the nucleus [34], serve to target and shuttle β-catenin for degradation. Members GSK3 and CK1 of the destruction complex phosphorylate β-catenin, which targets the latter for ubiquitination by β-transducin repeats–containing protein (β-TRCP), resulting in its degradation in the proteasome [1]. A simplified diagram of the Wnt signaling pathway within the cell is shown in Figure 1.

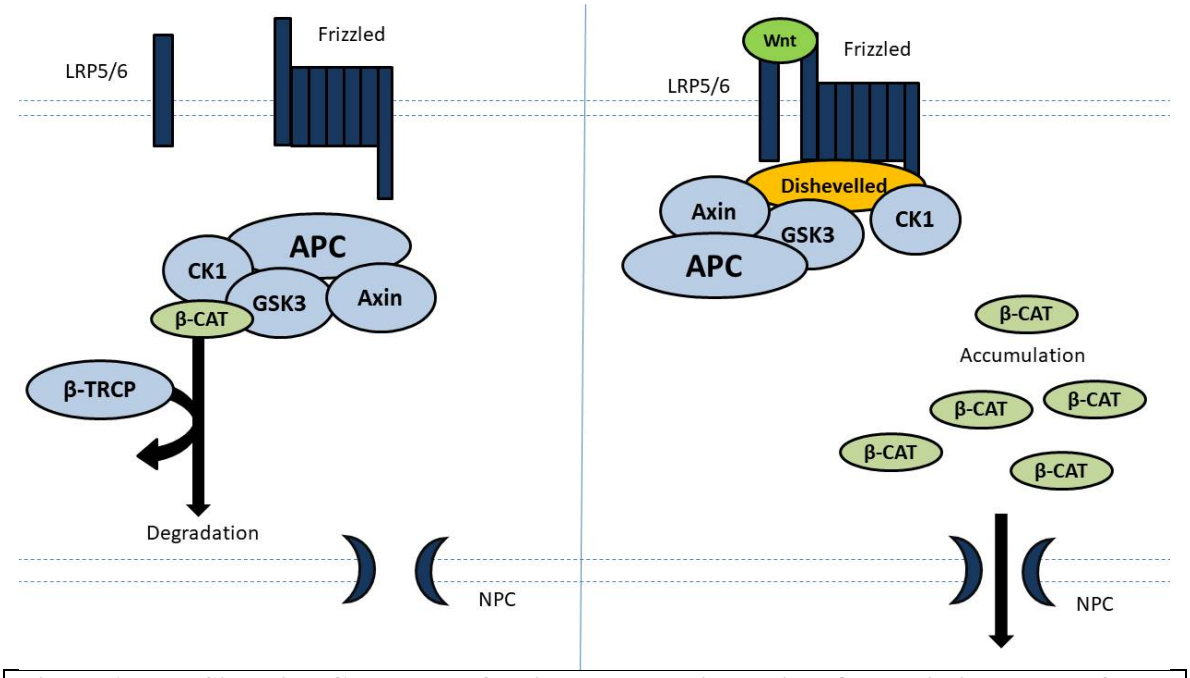

Figure 1. Wnt Signaling Cascade. Left, without Wnt stimulation, β-catenin is targeted for degradation in the cytoplasm by interaction with the destruction complex. Right, when Wnt binds the receptor complex, the destruction complex and Dishevelled are recruited to the receptor complex, resulting in accumulation of β-catenin and import to the nucleus. After [1] and [35].

Dishevelled, a central actor in all Wnt signaling cascades, was first discovered in *Drosophila* and is highly conserved [36,37]. It has many known binding partners that act as positive or negative regulators [36]. Dishevelled proteins are between 500-750 amino

acids in length and are comprised of several conserved domains, including the Dishevelled/Axin (DIX) domain; the post-synaptic density protein, *Drosophila* disc large tumor suppressor and zonula occludens (PDZ) domain; and the Dishevelled, EGL-10 Pleckstrin (DEP) domain (Figure 2) [36,38-40].

Wnt mediates the activation of two major signaling pathways; a canonical and a non-canonical pathway [9]. When Wnt binds to Frizzled and LRP5/6, the destruction complex and Dishevelled are recruited to the plasma membrane, activating the canonical wnt signaling pathway. This recruitment may be in response to an as-yet unknown signal [34], triggered by conformational change of Frizzled [3], or both. The α and β subunits detach from the γ subunit and activate Dishevelled through guanine nucleotide exchange factor (GEF) Ric8a, which leads to canonical signaling if the DIX (and PDZ) domain is activated and non-canonical signaling if the DEP (and PDZ) domain is activated [41]. Once the destruction complex is recruited to the plasma membrane, changes in the interactions between its members cause it to be inactive in regard to phosphorylation of β-catenin [1,3,22,34]. Wnt signaling via the protein Dishevelled induces the stabilization and the nuclear import of β-catenin, which controls the transcriptional regulation of Wnt target genes [1,8-12,38,42,43]. However, the mechanism of the nuclear translocation of β-catenin remains poorly defined to date.

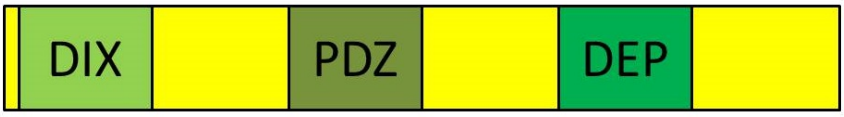

Figure 2. Dishevelled Domains. Length between 500 and 700 amino acids, with DIX, PDZ, and DEP domains. Modified from [36].

Exactly how the signal is transduced from the receptor to the destruction complex is not known for certain. However, it has been shown that the cytoplasmic-facing C-terminus of Frizzled interacts with the PDZ domain of Dishevelled [36,44]. Axin docks with LRP5/6 in response to ligand binding, causing relocation of the members of the destruction complex [3,45]. Once Dishevelled and the destruction complex are recruited to the plasma membrane, β-catenin is no longer degraded and accumulates in the cytoplasm.

Alternatively, when Wnt binds with Frizzled and co-receptors tyrosine kinase-like orphan receptor 2 (Ror2) and VANGL planar cell polarity protein 2 (Vangl2), Dishevelled is recruited and the noncanonical pathway is activated. Because the signal in both of these pathways is transduced through recruitment of Dishevelled, they are thought to be mutually antagonistic [23].

1.2 β-Catenin

β-catenin is a dual-function protein that serves as a transcriptional co-activator of Wnt target genes and as part of the protein complex that forms adherens junctions. They are vital for cell growth and adhesion between cells. As part of the adherens junction complex, β-catenin is a link between cadherin and actin cytoskeleton [46]. The majority of β-catenin in the cell is engaged in this function at the plasma membrane. More important for this study, a smaller pool of β-catenin serves to carry the Wnt signal from the cytoplasm into the nucleus, where it functions as a transcriptional coactivator with T-cell factor (TCF) and lymphoid enhancer-binding factor (LEF). β-catenin is involved in the transcription of a large cohort of genes over the course of embryonic development

[1,19,46]. The role of Custos, detailed below, in the nuclear import of β-catenin is the focus of this study. It is possible that the cell adhesion and signal transduction roles of β-catenin are unrelated; in *Caenorhabditis elegans*, β catenin is not dual-function: the two roles are carried out by two different proteins [46-48].

Human β-catenin is encoded by the *CTNNB1* gene [19,49], and in Drosophila its homolog is *Armadillo*. The β-catenin molecule consists of a central Armadillo (ARM) repeat region flanked by intrinsically disordered termini. The ARM repeat region is a superhelix of 12 helices (see Table 1) and contains the binding sites for most known binding partners. E-cadherin and TCF, in particular, have their binding sites in the ARM repeat groove [46], although there is not full agreement on the portion of the ARM repeat region is required for that binding. For example, TCF binding requires ARM repeats 5-9 according to one study [46] and ARM repeats 3-10 according to another [50]. The ARM repeats, although similar, are not identical in sequence or in structure. Each repeat consists of three consecutive β-helices that form a curl or a triangle (see Figure 3), except ARM 7, which has only two. Also, ARM 10 is longer than the other repeats, with a non-helical insertion between its second and third helices [46,51]. Whether these differences in the individual ARM repeats are the cause of functional differences is not known for certain.

The N-terminus of β-catenin contains the binding site for α-catenin as well as the GSK3 and CK1 phosphorylation sites [46], and has been shown to be necessary for transcriptional activity [52]. Dar and colleagues have shown that deletion of a portion of

the N-terminus results in human liver cancer; this region of the N-terminus (bp 286-635) has been shown to be unnecessary for import, but is required for cadherin binding. The result is a misdirection of β-catenin from the plasma membrane and increased nuclear import [53]. The full scope of the function of the C-terminus is not well understood, and the literature is contradictory. It has been asserted that C-terminus deletions increase nuclear localization [53] and transcriptional activity [54]. Others have proposed that the C-terminus may also serve to inhibit translocation [55]. Indeed, in the present study, truncation of the C-terminus causes increased nuclear localization of β-catenin and increased transcription activity. Further, it has been shown that the C-terminus is essential for transcriptional activity [52], whereas another study has asserted that the C-terminus not required for binding to the nuclear pore complex (NPC) [56].

Increasing this complexity and uncertainty, the C-terminus has been shown in several studies to interact with the ARM repeats, possibly folding back over them to inhibit interaction with cadherin or the NPC [55,57,58]. The C-terminus alone may be inhibitory or competitive of full-length β-catenin. It may be that the C-terminus' primary function at the NPC is to facilitate export, as Importin-β has been shown to inhibit β-catenin export but not import [55]. Also, it has been shown that the import and export mechanisms are not the same. Further, it may be that the C-terminus of β-catenin may change conformation in response to Wnt stimulation, which may expose ARM repeats to interact with the NPC [55,57].

Several previous studies have shown that the ARM repeat region, or portions thereof, of β-catenin are required for import to the nucleus. However, there is not universal agreement on which portions are necessary. In a developmental study, Yang and colleagues showed that ARM repeats 3-8 and 10-12 are required for translocation [56]. In another study, only ARM repeats 10-12 were shown to be necessary for import [55]. It has been shown as well that mutations in ARM 9 and in ARM 12 cause loss of signaling function [52], although this loss may be due to lack of binding with TCF or Groucho in the nucleus rather than failure to translocate [50].

Table 1. ARM Repeats of *X. laevis* β-Catenin

ARM	Starting AA Number	AA Sequence
1	146	IPELTKLLNDEDQVVVNKAAVMVHQL
2	188	IMRSPQMVSAIVRTMQNTNDVETARCTAGTLHNL
3	230	AIFKSGGIPALVKMLGSPVDSVLFYAITTLHNL
4	255	KMAVRLAGGLQKMVALLNKTNVKFLAITTDCLQILAY
5	307	KLIILASGGPQALVNIMRTYSYEKLLWTTSRVLKVL
6	339	KPAIVEAGGMQALGLHLTDSSQRLVQNCLWTL
7	395	LGTLVQLLGSDDINVVTCAAGILSNL
8	416	KMMVCQVGGIEALVRTVLRAGDREDITEPAICALRHLTS
9	472	QNAVRLHYGLPVVVKLLHPPSHWPLIKATVGLIRNL
10	507	HAPLREQGAIPRLVQLLVRAHQDTQRRTSIGGTQQQFVEGVR MEEIVEGCTGALHILAR
11	583	RIVIRGLNTIPLFVQLLYSPIENIQRVAAGVLC
12	624	EAIEAEGATAPLTELLHSRNEGVATYAAAVLFRM

NCBI Conserved Domains Viewer: https://www.ncbi.nlm.nih.gov/Structure/cdd/wrpsb.cgi?INPUT_TYPE=live&SEQUENCE=AAA49670.1
AA, amino acid.

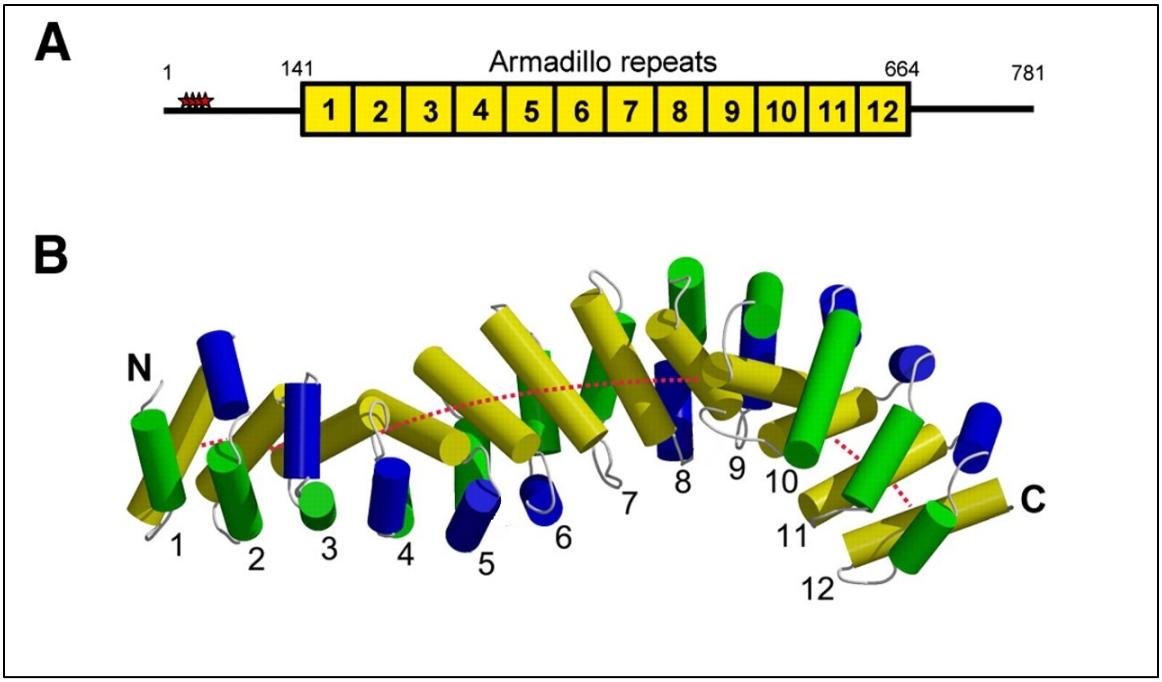

Figure 3. Structure of β-Catenin. (A) Domains of β-catenin showing intrinsically disordered termini and the 12 Armadillo repeats. Small stars on the N-terminus represent the sites phosphorylated by CK1α and GSK-3β of the destruction complex (B) Structure of the β-catenin armadillo (ARM) repeat domain. The dashed red line shows the groove of the armadillo repeat domain. Modified from [99].

One of the reasons regulation of β-catenin nuclear import remains poorly understood is because β-catenin has no identified nuclear localization sequence (NLS) [59-61]. Several ARM repeats have been shown to interact with phenylalanine-glycine (FG) repeat–rich nucleoporins (FG Nups) in the NPC [53,55,56,62], and some conformation within the β-catenin structure serves the function of an NLS. One study suggests that ARM repeats 10-12 serve this function when a residue within it, Y654, is phosphorylated [62]. Mutations in ARM 9 and ARM 12 cause loss of signaling function, but this may be because ARM 9 and ARM 10 are necessary for TCF binding [50,52].

The ARM repeats in β-catenin bear a striking resemblance to the HEAT [Huntingtin, elongation factor 3 (EF3), protein phosphatase 2A (PP2A), and the yeast kinase TOR1]

repeats of the importins that are responsible for the interaction of importins with the FG Nups, and thus translocation [55,63,64]. Importin-β is known to be a transport receptor and is known to translocate with its cargo via interaction with the FG Nups [64-67]. ARM repeats 10-12 have been shown to interact directly with Nup358, Nup62, Nup98, and Nup153, although the article in which these findings were shown was withdrawn [62,63]. Another study has shown that there is direct interaction between β-catenin and Nup62 [56]. A comparison of the ARM repeats of β-catenin with the HEAT repeats of the Importins reveals striking similarity [64,67,68]. Of the ARM repeats, 10-12 most resemble the HEAT repeats in structure [62] (Figure 4). The conformation of HEAT 4-8 of Importin-β and ARM 8-12 of β-catenin are especially similar; HEAT 6-8 are known to be necessary for translocation of Importin-β [46,69].

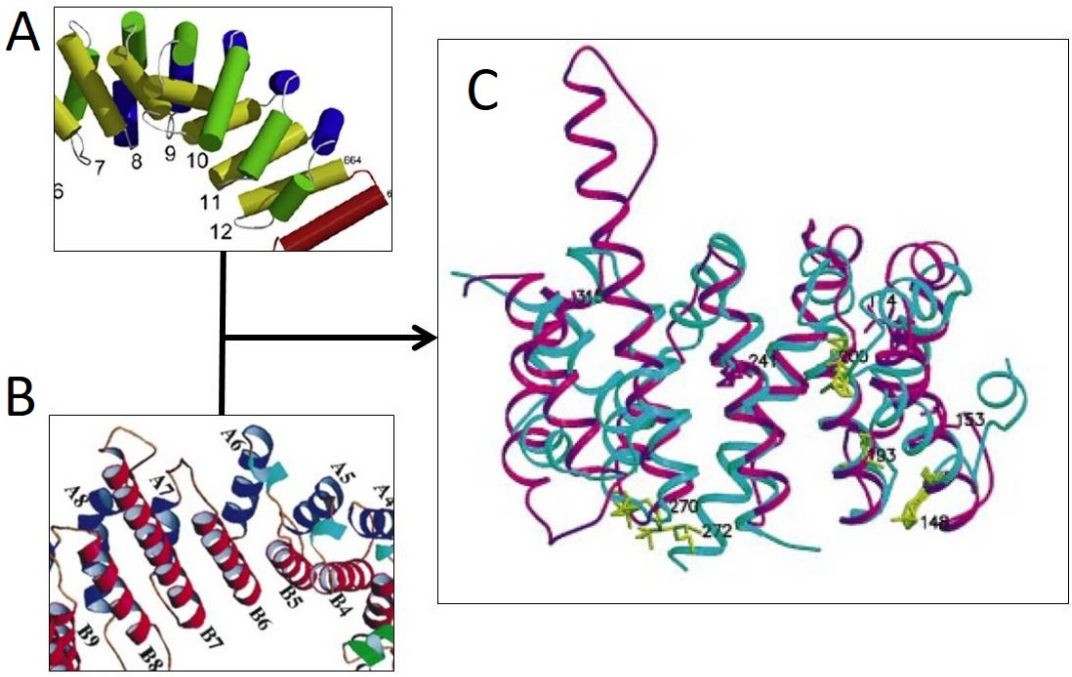

Figure 4. Comparison of β-Catenin and Importin-β. (A) Detail of the ARM repeat structure of β-catenin. (B) Detail of the HEAT repeat structure of Importin-β. (C) Superposition of HEAT 4-8 of Importin-β and ARM 8-12 of β-catenin. Modified from [46] and [54].

1.3 β-Catenin at the Nuclear Pore Complex

It has been hypothesized that there are transport receptors that facilitate import of β-catenin [60,70]; specifically, β-catenin was proposed to interact with Importin-β, although support for this proposition is not universal [71-73]. There is quite a bit of evidence that β-catenin either may translocate in the manner of a transport receptor, directly interacting with the FG Nups in the central channel of the NPC, is, or may have once been a transport receptor [68]. Some of the evidence for β-catenin's status as a current or former transport receptor given by Fagotto [68] is that translocation of β-catenin is bidirectional (*ie,* import and export), and insensitive to inhibition of the Ran GTPase cycle. Evidence for the latter assertion is not clear [59,68]. In permeabilized cells, β-catenin localizes to the nuclear envelope; β-catenin will enter the nucleus in

permeabilized cells only if ATP is added [59]. β-catenin translocation is believed to be Chromosomal Maintenance 1 (CRM1)- and Ran-independent [73,74]. If β-catenin is a transport receptor, its cargo is unknown or β-catenin may enter the nucleus without assistance but actually function as an exportin, for instance of LEF1. β-catenin has been shown to act as an export receptor for LEF1, albeit under artificial conditions [63,68]. It is possible that the unknown cargo of β-catenin may be Custos.

1.4 Custos

In a study investigating the role of Dishevelled in Wnt signaling, an effector molecule for Dishevelled, named Custos, was identified. Komiya and colleagues used the results of a previously performed yeast two-hybrid screen to identify Custos as a binding partner of Dishevelled [35,75]. In the yeast two-hydrid screen (a protein-fragment complementation assay [76-78]) of a rat brain complementary DNA (cDNA) library, the PDZ domain of Dishevelled was used as bait. Custos is a small (237–amino acid) protein (Figure 5) that is highly conserved among vertebrates. It contains phosphorylation sites near the N-terminus (all vertebrate species studied so far) and in the middle of the sequence (human, mouse, and frog), and two NLSs near the C-terminus [35,75].

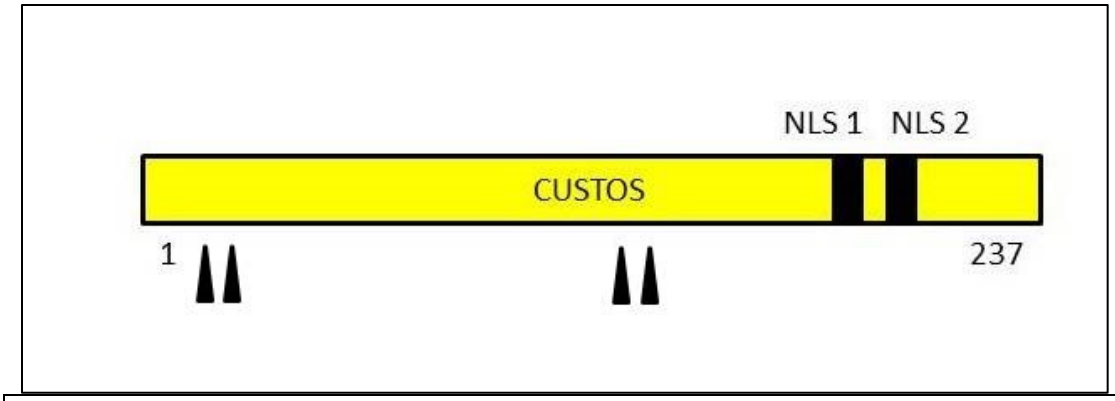

Figure 5. Custos Domains. Arrowheads indicate the CK1 phosphorylation sites, and there are two NLSs near the C-terminus [64].

Custos, found in the nucleus and at the nuclear envelope, binds to Dishevelled and β-catenin. With Wnt exposure, its binding to β-catenin is upregulated, and its binding to Dishevelled is downregulated. Custos is phosphorylated by CK1 and the interaction region of Custos with Dishevelled is located between the NLS region of the former and the PDZ region of the latter [50,75]. The domain of interaction with β-catenin is not known, but most β-catenin binding partners interact with the ARM repeat region [50,52,56,79]. Interaction with Dishevelled was shown to dephosphorylate Custos [35,75]. The function of this dephosphorylation is not known. When Dishevelled is recruited to the plasma membrane in response to Wnt, its interaction with Custos ends, and Custos remains at the nuclear envelope to interact with β-catenin. It is not yet known whether Custos interacts with the Nups or interacts with β-catenin in a way that facilitates the latter's translocation.

Custos is required for canonical Wnt signaling and β catenin nuclear translocation and regulates head development in both *Xenopus* and *Danio* embryos. Embryos depleted of Custos further lacked pigmentation in the skin and eye, suggesting a role for Custos in

neural crest development. Komiya and colleagues proposed that Custos functions to regulate the nuclear import of β-catenin.[75] Both overexpression and morpholino knockdown of Custos were shown to inhibit Wnt signaling [35,75], suggesting an optimal level of Custos required for proper regulation of Wnt signaling.

1.5 The Nuclear Pore Complex

Embedded in the nuclear envelope, the NPC is a large assembly of proteins forming a gateway between the nucleus and the cytoplasm of eukaryotic cells. The number of NPCs in the nuclear envelope of a cell varies from hundreds in yeast to thousands in human cells [80-86]. The structure of the NPC consists of an eightfold, rotationally symmetrical core channel with an associated nuclear basket structure and eight cytoplasmic fibrils [87,88]; this symmetry implies modular assembly [89,90]. A simplified diagram of the structure of the NPC is shown in Figure 6.

The NPC is approximately 60-120 MDa in mass, measures approximately 50 nm in diameter at the narrowest point and about 200 nm axially in total length in vertebrate cells [88,92]. The inner ring and the transmembrane Nups form the central scaffold of the NPC, sandwiched between the cytoplasmic ring and the nucleoplasmic ring. From the cytoplasmic ring extend the cytoplasmic filaments; from the nucleoplasmic ring extends the nuclear basket structure [91]. Approximately 30 different proteins comprise the NPC structure [93].

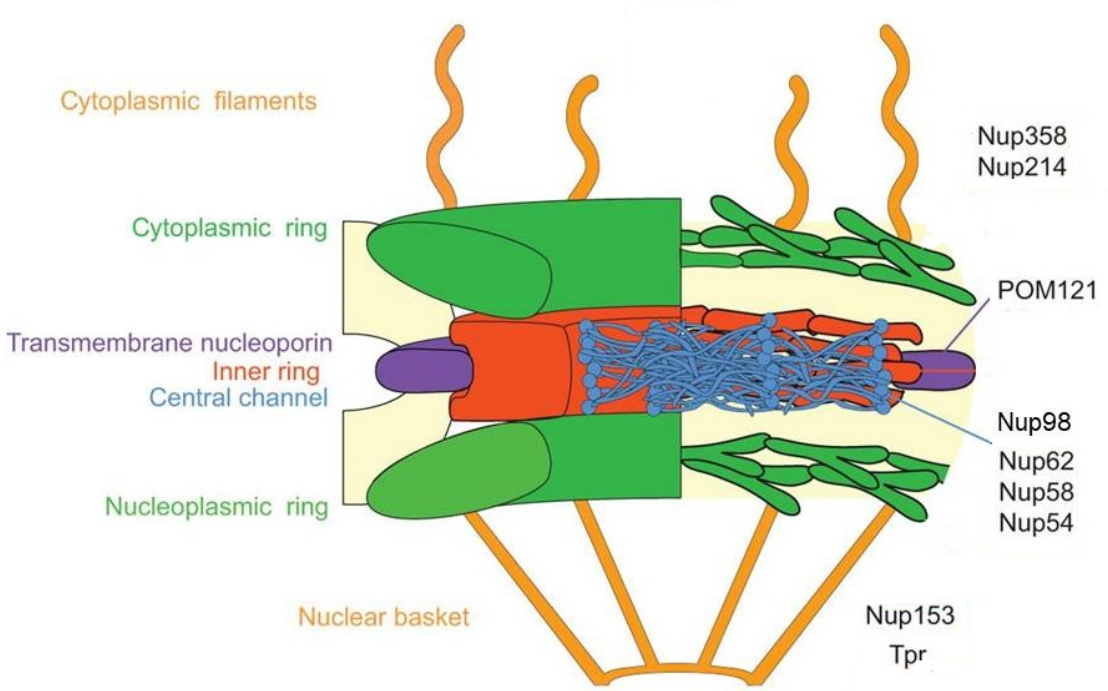

Figure 6. Simplified Diagram of the Major Structures of the NPC. Location of selected FG Nups noted. Modified from [91].

Approximately one third of the proteins that make up the NPC are filamentous linker Nups, rich in extensive FG repeats; these FG Nups are directly involved in regulating the selective transport of macromolecules through the NPC by forming a strict selective barrier in the form of a polymer brush or hydrogel meshwork in the central channel of the NPC [88,93,94-98]. Specifically, passage of small molecules (<40 kDa-60 kDa, roughly 6.0-7.5 nm [99] or even up to 9 nm [100]) across the NPC occurs by passive diffusion, whereas larger molecules (over 40-60 kDa in mass and as much as 25 nm in diameter) with an NLS or nuclear export sequence (NES) require facilitated transport [92,100-108].

Spanning the inner and outer nuclear membranes, the NPC is the major portal between the cytoplasm and the nucleus. As the major exchange pathway for proteins and genetic

materials, the NPC (as a whole or its various subunits) is closely involved in the regulation and control of many cellular processes [109-118]. Previous studies have shown an association between the NPC and gene expression and repression, mRNA export, and genome organization. The FG Nups, in particular, have been associated with gene transcription and the maintenance of chromatin structure [119-123].

1.6 β-Catenin in the Nucleus

After import into the nucleus, β-catenin interacts with multiple proteins that either inhibit or activate Wnt signaling. Inhibitor of β-catenin and TCF4 (ICAT) and Chibby are two characterized inhibitors of Wnt signaling. B-cell CLL/lymphoma 9 protein (BCL9) and CREB-binding protein/E1A binding protein p300 (CBP/p300) are known to activate Wnt signaling. Chibby and CBP are known to bind to the C-terminus of β-catenin [46,124], whereas ICAT is known to cause dissociation of β catenin from its complex with TCF [3,125,126]. The target of β-catenin in the nucleus is the TCF/LEF repressor complex; β-catenin is believed to displace repressor Groucho from the TCF/LEF complex and to recruit coactivators such as BCL9, converting it into a transcriptional activator complex to activate transcription of Wnt target genes [3,46].

1.7 Super-resolution Microscopy

The use of conventional epifluorescence microscopy in the localization of fluorescently labeled proteins has been a mainstay of biological research; however, reliance on wide-field illumination has some limitations. In the examination of the intracellular dynamics of proteins, the most important limitation is resolution. Fluorophores closer together than

the diffraction limit (~200 nm) cannot be distinguished with visible light, but super-resolution techniques can be employed to discern biostructures and the dynamics of soluble proteins in the cell [127,128]. Techniques that can achieve this breaking of the resolution limit generally take either an optical approach [*eg,* stimulated emission depletion (STED) microscopy) or a mathematical approach [*eg*, photoactivated light microscopy (PALM) and stochastic optical reconstruction microscopy (STORM)]. STED microscopy takes advantage of the nonlinear optical response of fluorophores through a subdiffraction illumination volume generated through laser modifications. PALM and STORM employ mathematical functions to localize the emitting fluorophores and then reconstitute these localizations to form super-resolution images [127-130]. Although these techniques represent a significant advance in the march toward better and better resolution (typically >50−100 nm), acquisition time remains a limitation, with seconds to hours being the state of the art at the time of this writing [127-130]. This temporal resolution is not fast enough to gain useful information about movement of molecules through the NPC, which occurs in the milliseconds range.

Further, these techniques require complex and expensive equipment. Described in more detail in the Materials and Methods section, an alternative approach was developed by and used in our laboratory, SPEED (Single-point edge-excitation subdiffraction) microscopy. This technique emphasizes comprehensive post-localization analysis and yields sub-resolution information in biological structures [65,104,131-134].

Previous microscopy methods such as confocal microscopy are limited in the level of detail that can be gleaned from examination of smaller cellular structures and dynamic biological processes [127,128]. For example, the NPC, considered among the largest of cellular structures, is below the resolution limit in width and very close to the limit in length [88,92]. Whereas electron microscopy can provide some insight on the size and structure of the NPC, sample preparation may change subtle details. Further, a fixed sample provides little information in regard to dynamic processes. Because we wanted to investigate the living process of β-catenin translocation and the role of Custos in it, a super-resolution technique was needed. In addition to the spatial resolution limit and the inability to distinguish fine enough detail for this study, conventional microscopy methods also lack the temporal resolution to distinguish the finer details of the path taken through the NPC by translocating molecules, which do so in the millisecond range. (In this study, we showed that β-catenin interaction with the NPC during translocation averaged 3.82 ms, which is too fast for conventional or most super-resolution imaging.) Even the super-resolution methods discussed previously cannot help here, as their image acquisition times are too slow [127-130]. SPEED microscopy, described in detail in the Materials and Methods section, overcomes these limitations with ~10 nm (or better) spatial resolution and 2 ms (or better) temporal resolution.

CHAPTER 2: MATERIALS AND METHODS

2.1 Tissue Culture and Transfection

HeLa cell lines (ATCC) stably expressing the GFP- or mCherry-tagged structural Nup POM121 were grown in DMEM, high glucose, GlutaMAX Supplement (Life Technologies); 10% fetal bovine serum (FBS; Fisher Scientific); and 1% penicillin-streptomycin (ThermoFisher) and split every 2-3 days to 40-50% confluency. Cells were transferred to glass-bottomed dishes (MatTek) 1-2 days before imaging and transfected with the appropriate plasmid(s). Approximately 45 minutes before imaging, cell medium was replaced with transport buffer (20 mM HEPES, 110 mM KOAc, 5 mM NaOAc, 2 mM MgOAc, and 1 mM EGTA, pH 7.3). Each cell dish was imaged for less than 1 hour.

Cells intended for Custos knockdown were serially transfected with human Custos siRNA (via DharmaFect1 transfection reagent; Dharmacon Inc) and then with wild-type *X. laevis* β-catenin (via Polyfect transfection reagent; Qiagen) 48 hours and 24 hours before imaging, respectively. The siRNA sequence used for Custos was as follows:

> Dharmacon c12orf43.L duplex;
> Sense: 5': U.C.A.G.A.U.G.A.G.C.A.G.A.A.U.G.A.A.A.U.U 3';
> Antisense: 5': U.U.U.C.A.U.U.C.U.G.C.U.C.A.U.C.U.G.A.U.U 3'.

Human Custos (wild-type) fused to mCherry or wild-type *X. laevis* β-catenin or truncates of β-catenin fused to GFP were cloned into pCS2+ vector. Wild-type β-catenin tagged at the C-terminus with GFP was used to examine the effect of a time-course of Wnt3a stimulation on translocation efficiency and also for the Custos–β-catenin FRET interaction study. For investigation of Custos knockdown effect on efficiency and for

comparison with the effect of truncation of the molecule on efficiency and 3D transport route, wild type β-catenin tagged at the N-terminus with GFP was used.
Truncates were tagged with GFP at the N-terminus. In addition, wild-type *X. laevis* β-catenin in vector pcDNA3.1 (with N-terminal GFP tag) was purchased from GenScript from which was cloned β-catenin fragments 2xGFP-[ARM]10-12C, 2xGFP-[ARM]10-12, and 2xGFP-CTF (C-Terminal fragment) (Figure 7). Cells intended for FRET study were transfected with mCherry-fused zebrafish Custos cloned in pCS2+ vector. After transfection, cells, nuclear envelopes, and NPCs were imaged. In cells expressing GFP-POM121, the pore was photobleached after imaging and before single-molecule detection. Truncate expression and expected sizes were confirmed via Western blot (Figure 8). Single-molecule tracking of GFP-β-catenin nucleocytoplasmic translocation was conducted via SPEED microscopy.

TopFlash reporters were co-transfected into HEK293T cells with expression plasmids for Axin, Dishevelled, β-catenin, dCT, CTF, 10-12C, d9, d6, and d3. After 2 hrs, cell lysates were subjected to luciferase assay [135].

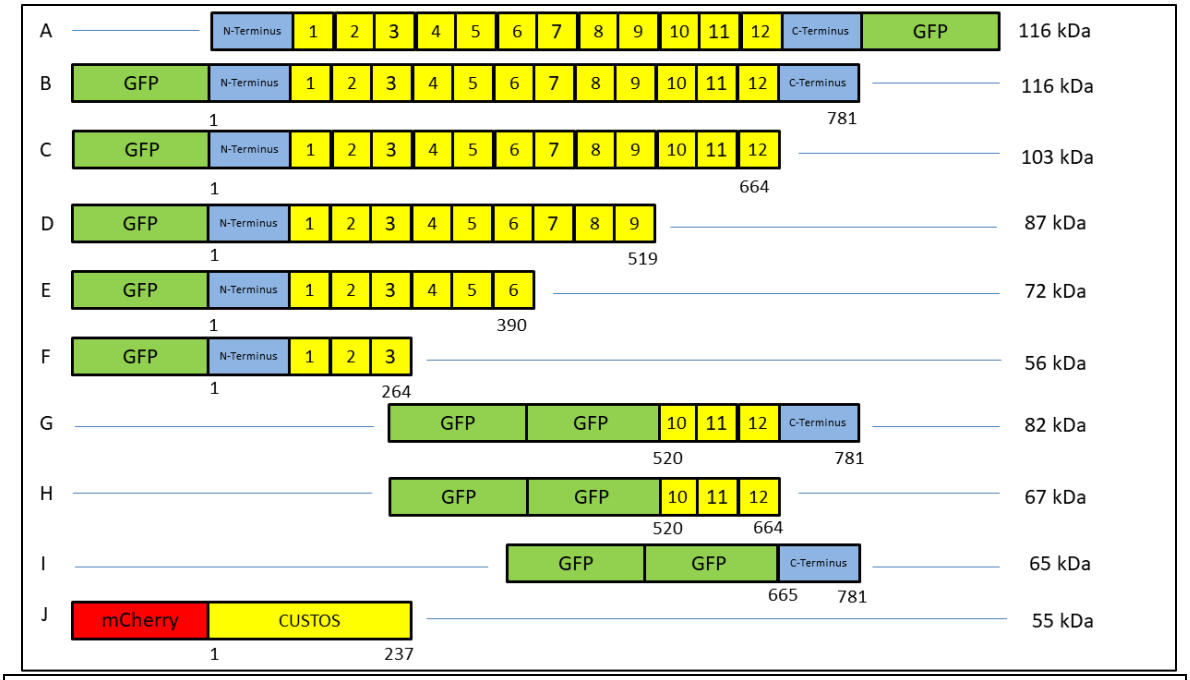

Figure 7. Constructs Used in this Study. (A) Wild-type β-catenin with C-terminal GFP. (B) wild-type β-catenin with N-terminal GFP. (C) dCT, (D) d9 (E) d6. (F) d3. (G) 10-12C. (H) 10-12. (I) CTF. (J) mCherry-Custos.

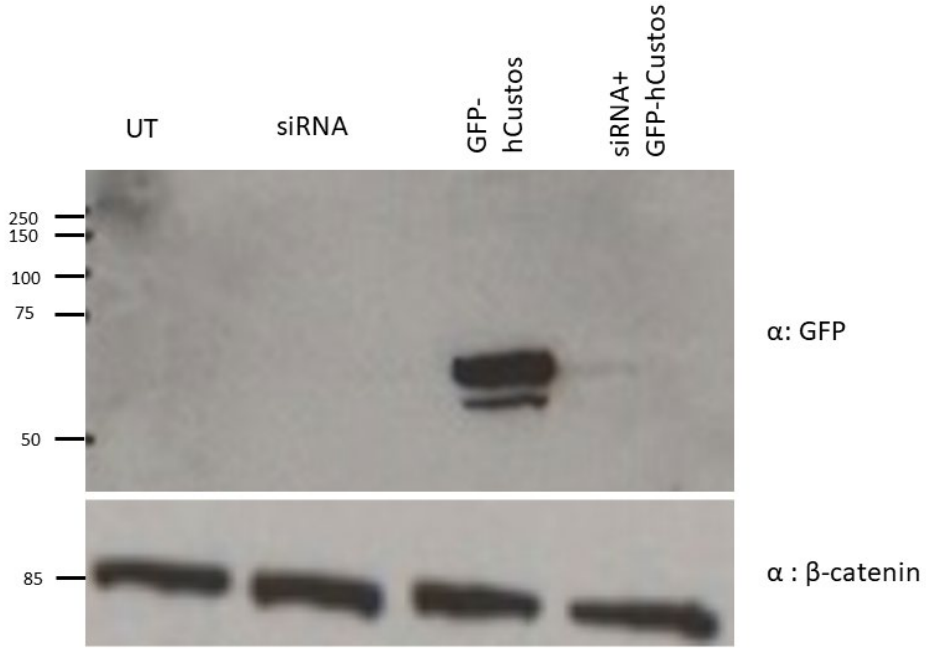

Figure 8. Expression and Size of Truncates. Western blot.

2.2. SPEED Microscopy

SPEED microscopy was developed to fill the technique niche of capturing single molecules transporting through sub–diffraction-limit biochannels (the NPC in this study) at high spatial and temporal resolution. In this study, the temporal resolution was 2 ms and the spatial resolution (for moving particles) was approximately 10 nm. SPEED microscopy achieves this level of resolution through several innovations. A vertical illumination point-spread function (PSF) allows the excitation of a single NPC on the edge (equator) of the nuclear envelope (see Figures 9 and 10) within a small volume in the focal plane. The small size of the illumination volume facilitates a high optical density (100-500 kW/cm^2), allowing the collection in a short time period of a large number of photons from the fluorophores. Further, the small illumination volume of SPEED microscopy enables the imaging of single fluorescently tagged molecules (given a sufficiently low concentration of them) within a small pixel area of the charge-coupled device (CCD) camera, resulting in a detection speed of up to 5000 frames per second (500 frames per second in this study). This fast detection speed greatly reduces the spatial localization error in determining the spatial trajectories of single moving fluorescent molecules in live cells.

Each frame must be fit with a 2D-Gaussian function. This can be accomplished with a variety of analysis software packages; our laboratory makes use of a Matlab-based program Glimpse [136] and the ImageJ plugin GDSC SMLM [137], but only the former was used in this study. These programs enable the user to filter the high number of

Gaussian fittings acquired based on a number of parameters. These include the Gaussian width of the fitting, the signal-to-noise ratio, and the intensity [136-138]. Filtering the data dependent on these factors allows researchers to limit camera noise and possible aggregate particles in the analysis. All selected points are compiled into a 2D spatial locations map. The precise alignment of the map to the fitting of the NPC is described in Figures 11 and 12 and in great detail elsewhere [138]. A minimum of 1000 data points within the selection criteria is recommended for further analysis.

After data selection by intensity and width of fitting, precision was calculated via the following formula:

$$\sigma = \sqrt{F(16(s\text{^}2 + a\text{^}2\ )/9N + 8\pi b^2(s^2 + \frac{a^2}{12})^2/a^2N^2}$$

where $F = 2$; N = number of photons collected; a = the effective pixel size of the detector; b = the standard deviation of the background in photons per pixel; and s = the following equation:

$$s = \sqrt{s_0^2 + 1/3D\Delta t}$$

where s_0 = standard deviation of the PSF in the focal plane; D = diffusion coefficient within the NPC; and Δt = the image acquisition time (2 ms in this study) [134,138-142].

To process the data for 2D-to-3D transformation, the axial length of the NPC is divided into regions (of 10 nm to 30 nm in this study) and for each of these regions the number of data points that fit into 7-nm bins along the y dimension is determined; *ie,* each x-dimensional region is divided into bins along the y dimension, and the number of fitted data points in each of these y-dimensional bins is determined (Figure 13). These numbers

are placed in the matrix equations shown in Figure 14. These equations are used to calculate the relative spatial probability density distributions for the *r*-dimension. This procedure is described in great detail elsewhere [84,105,110,138,143,144].

We employ a *Monte Carlo* simulation to demonstrate the reproducibility of our method in obtaining accurate 3D super-resolution information in the setting of rotationally symmetrical biostructures. Two critical parameters, the number of acquired single-molecule locations and the localization error of those acquired locations, are used to determine this reproducibility. The Monte Carlo simulation [145,146] and our use of it to validate our technique, as well as other details, are described elsewhere [134].

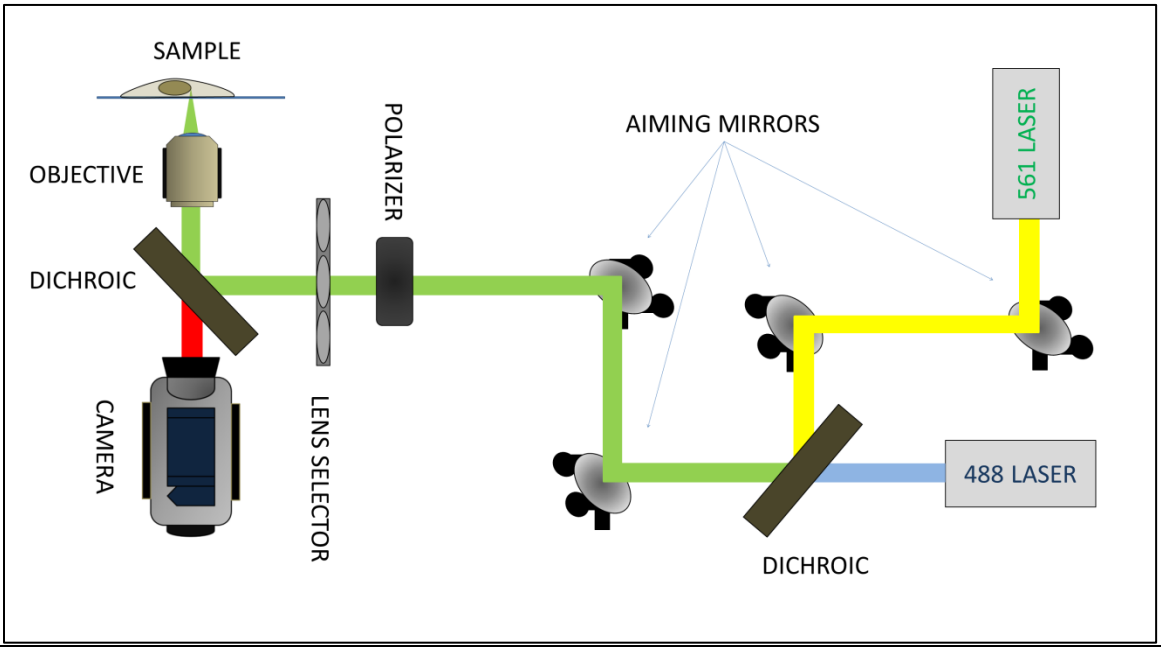

Figure 9. SPEED Microscopy Setup. Schematic of vertical version of the SPEED microscopy setup described in this protocol. (Items shown in diagram are not in scale with one another.) Light path is shown in blue (488 nm), yellow (561 nm) and green (combined) excitation and red (emission). [139].

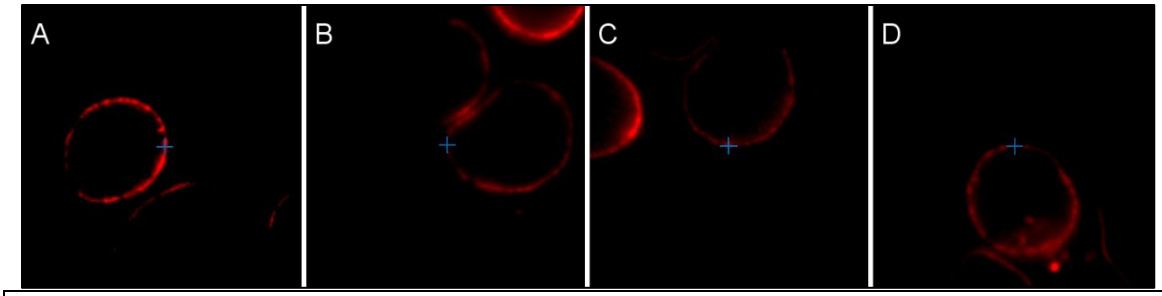

Figure 10. Examples of Nuclear Envelope Positioning for Imaging. Shown with HeLa cells expressing fluorescently tagged Nup POM121, visible as a ring. (A) Right side. (B) Left side. (C) Bottom side. (D) Top side. Crosshair falsely colored for clarity [139].

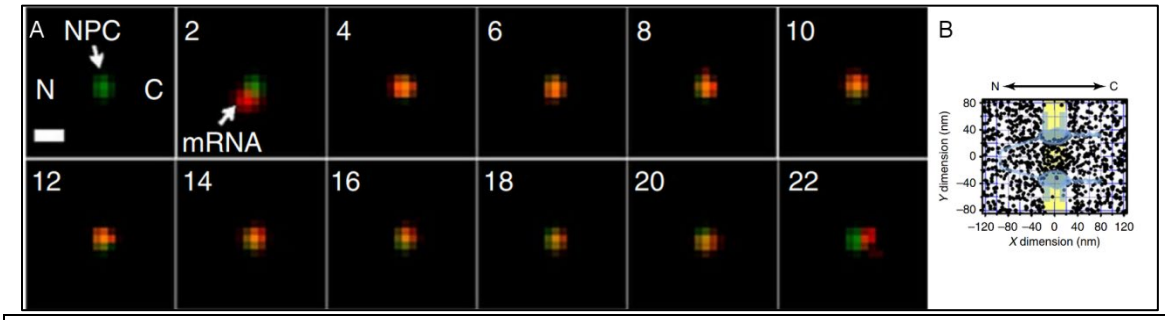

Figure 11. Captured Event and 2D Distribution. (A) A typical successful single export event captured by SPEED microscopy. The tracked molecule in this example is a messenger ribonucleoprotein (mRNP). A. A single mCherry-tagged mRNP (red spot) started from the nucleus, interacted with a single GFP-tagged NPC (green spot) and arrived in the cytoplasm. Numbers denote time in ms. (B) Single-particle tracks (black open dots) and the centroid of the NPC (red open dot) were acquired by 2D Gaussian fitting to point spread functions in a series of images for the successful event in panel A. (C) Experimentally determined 2D spatial locations of mRNPs in the NPC. A schematic of the NPC (light blue) is superimposed, and the central region of the NPC (20 nm to 20 nm) is highlighted in yellow. C, cytoplasmic side of the NPC. N, nucleoplasmic side of the NPC. Modified from [147].

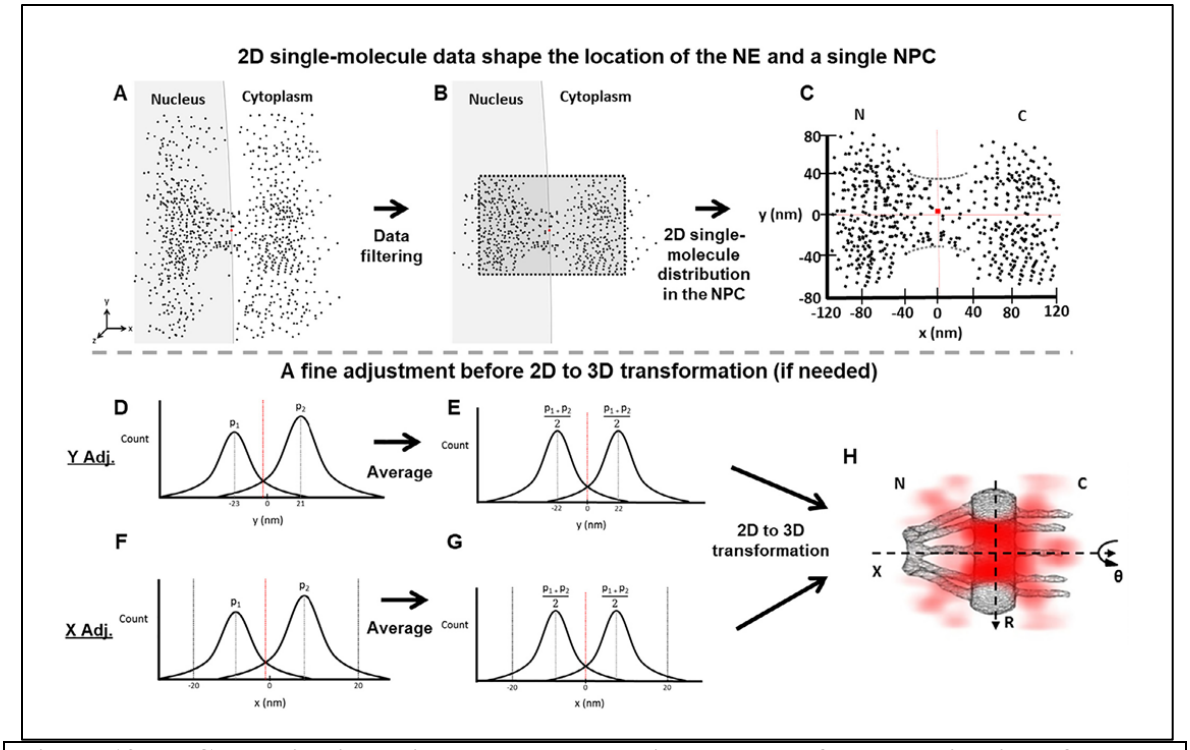

Figure 12. NPC Localization. Diagram demonstrating the steps for determination of the central axis of the NPC illuminated by SPEED microscopy. (A) The initial single-molecule tracking data (black points) are plotted around the NPC marker (red dot) collected with SPEED. (B) The collected data after filtering by using single-molecule spatial localization precision. (C) The filtered 2D single-molecule data shape the spatial location of the NE and a single NPC. The red dot represents the location of the NPC marker. (D) The plot of projected locations of these 2D single-molecule data in the y dimension will indicate if a fine adjustment for the central cytoplasmic transport axis is needed or not. (E) The two peaks are averaged as (p1 + p2) 2, resulting a fine adjustment in the NPC's central cytoplasmic transport axis. The dotted red line has shifted to the corrected central position. (F and G) Determine the precise location of the NPC central position along the x dimension by fitting the histogram of these 2D single-molecule locations within the NPC's scaffold region projected into the x dimension. (H) The 2D single-molecule data with the confirmed x and y axes will undergo the 2D to 3D transformation to produce the 3D density map of the target protein's nuclear export routes (red clouds) [138].

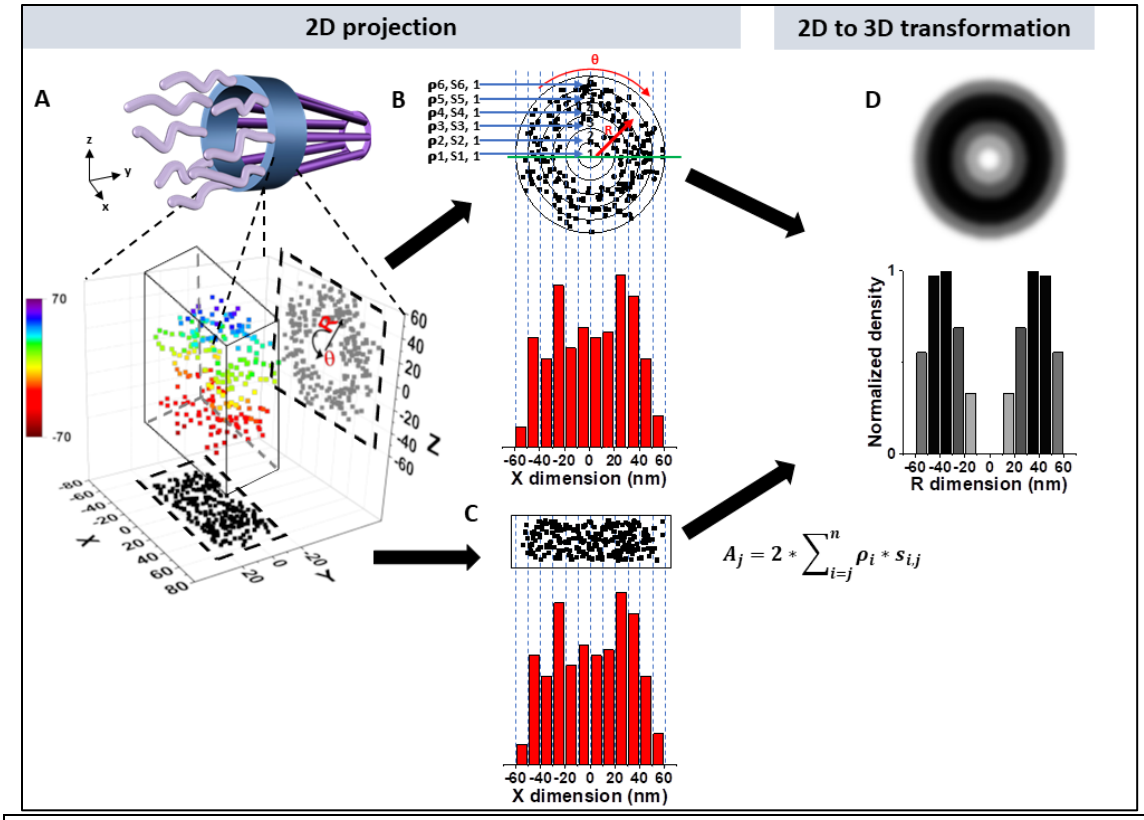

Figure 13. SPEED 2D-to-3D Algorithm. A schematic demonstration of the SPEED 2D to 3D transformation. A schematic demonstration, with simulated data, of the 2D to 3D transformation algorithms for molecules that diffuse through the NPC. (A) 3D spatial locations of randomly diffusing molecules inside the NPC can be coordinated in a cylindrical coordination system (R,Ø, Y) due to the cylindrical rotational symmetry of the NPC. The 3D molecular locations in the NPC (rainbow colored for Z position) are projected onto a 2D plane in a Cartesian coordination system (X and Y, shown as black points) by microscopy imaging (X and Z shown as gray points). (B) The cross-sectional view of all the locations shown in Panel A (same as the gray points from the X and Z dimension). These locations can be grouped into the sub-regions between concentric rings. Given the high number of randomly distributed molecules in the NPC the spatial density of locations (ρ_i) in each sub-region ($S_{(i,j)}$) between two neighboring rings will be rotationally symmetrical and uniform. These locations can be further projected into 1D along the X dimension. The locations along X dimension can be clustered in a histogram with j columns. The total number of locations in each column ($A_{(i,j)}$) is equal to $2 * \sum_{i=j}^{n} \rho_i * 8_{(i,j)}$. (C) Histograms of 2D projected data from microscopy experiments are identical to B, thereby allowing us to use the aforementioned formula to determine the density of each concentric ring. (D) Using the algorithms, 2D projected data can be used to reconstruct the 3D spatial distribution of proteins traveling through the NPC. [138]

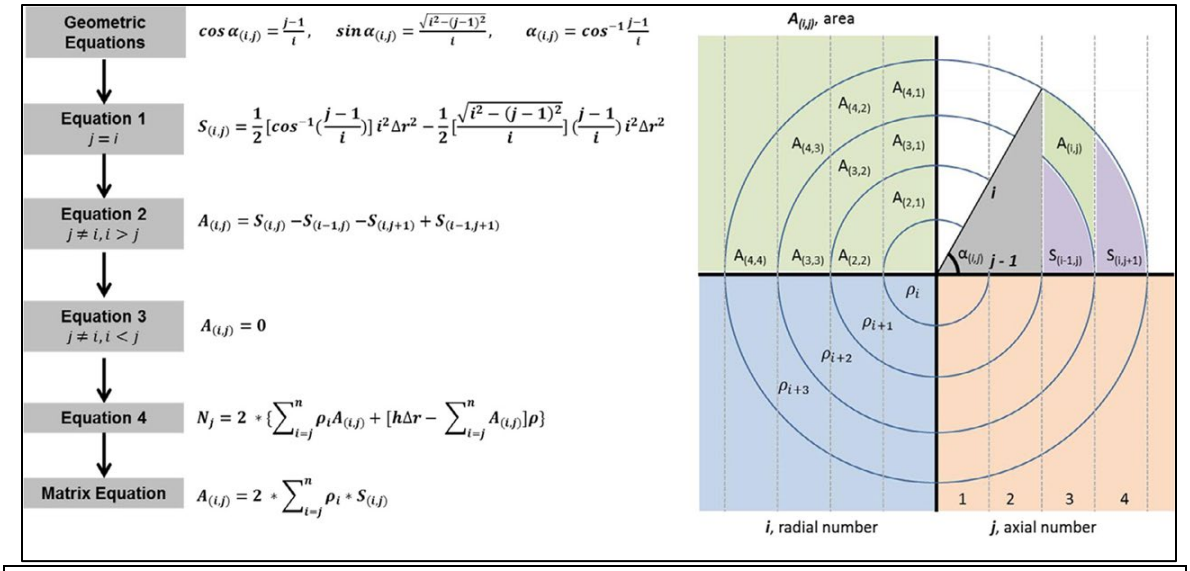

Figure 14. Matrix Equation Flowchart. ($A_{(i,j)}$), area of the sub-region, (i), radial number, (j), axial number, (ρ_i), spatial probability density in each radial ring, ($S_{(i,j)}$), area of the sub-region, (N_j), number of events, and (Δr), bin size. Eqs. (1)–(3) will determine the area of the sub-region given certain parameters (*ie, i=j*). Equation (4) will determine the number of events in the given area. Once the sub-region area ($A_{(i,j)}$) and events (N_j) are known, the spatial probability density in each radial ring (ρ_i) can be calculated. [138]

SPEED microscopy was conducted with an Olympus IX81 microscope equipped with a 1.4-NA 100× oil-immersion apochromatic objective (UPLSAPO 100×; Olympus) and an on-chip multiplication gain CCD camera (Cascade 128+; Roper Scientific); the Slidebook software package (Intelligent Imaging Innovations) was used to capture data.

Glimpse [136] was used for data analysis. For this study, two lasers were used: A 120-mW ArKr tunable 561-nm ion laser (Melles Griot) and a 50-mW 488-nm argon-ion laser (Melles Griot). Both of these lasers are run in single-line mode, and passed through one or more neutral density filters such that the laser power at the optical dish was 500 µW or less. These lasers were filtered by a dichroic filter (Di01- R405/488/561/635-25x36, Semrock) and an emission filter (NF01- 405/488/561/635-25X5.0, Semrock) and imaged

with the same CCD camera. The lasers and microscope were set up on a pneumatic isolator that is pre-mounted on a research-grade optical table (Newport, Irvine, CA)[133].

2.2.1 Localization Precision

In this study, the resulting localization error was ~10 nm for single moving particles. The localization error for FRET response was ~24 nm. Compiling the acquired localizations into 3D probability density maps of transport routes for molecules in the NPC is accomplished via a 2D-to-3D, Cartesian-to-cylindrical conversion algorithm described in detail in the previous sections and in several previous publications [65,66,104,131-134,147-149]. Data points were fit to 2D Gaussian functions using Glimpse software [136]. Data were filtered by intensity and Gaussian width, removing any data with widths <0.5 pixel and >1.1 pixel in order to avoid stochastic CCD camera noise and out-of-focus single-molecule spots.

2.2.2 Single-Particle FRET

Donor and acceptor channels were filtered with 520 ± 15-nm band-pass (CHROMA) and 593-nm long-pass (FF01-593/LP-25; CHROMA) filters, respectively. This setup provides for minimal bleed-through signal of GFP and mCherry [150,151]. Donor and acceptor fluorescence were collected with the same objective and split with a Dual View DV2 system (Teledyne Photometrics) that includes a dichroic mirror (565dcxr; CHROMA, Bellows Falls, VT). A background subtraction was performed using ImageJ for each channel, and intensity values were normalized for each channel per individual video prior to calculating FRET ratios.

To be assured that a single-particle FRET (spFRET) study of β-catenin and Custos was feasible, the predicted FRET distance of the molecules was calculated according to the following formula and compared with that of the fluorophore pair's published critical distance [99] of 5.25 nm:

$$Rmin = (\frac{3V}{4\pi})^{\frac{1}{3}} = 0.066M^{1/3}$$

where *Rmin* = minimum distance in nm; D = molecular weight in Daltons; β-catenin molecular weight at 88 kD (and a minimum hydrostatic radius of 2.9 nm); Custos molecular weight at 26 kD (and a minimum hydrostatic radius of 2 nm). The sum of the minimum radii is 4.9 nm, well within the critical distance of the FRET pair. For further assurance, FRET distance was calculated also directly from the data according to the following formulae:

$$FRET\ efficiency = E = (\frac{FRET\ intensity}{FRET\ intensity + donor\ signal\ intensity})$$

and substituting E into the following formula:

$$R = R_0 \sqrt{\frac{1-E}{E}} = 5.25 \sqrt{\frac{1-E}{E}}$$

where R = the distance between the fluorophores and R_0 = critical distance of the mCherry acceptor [79]. The calculation yields an R value of 5.3 ± 0.4 nm.

2.3 Efficiency, Net Transport Rate, and Diffusion Coefficient

For an interaction between the NPC and the molecule of study to be counted toward efficiency, the molecule must reach or pass the 40-nm axial center section of the NPC,

shown in red in Figure 15. A successful import event, wherein the molecule is detected on the cytoplasmic side of the NPC, then in the center section, then in the nucleoplasm, in shown in Figure 15A. Molecules that satisfied the criterion for inclusion but returned to the cytoplasm were counted as aborted export (Figure 15B). Translocation efficiency is expressed as a percentage and was defined as the number of times a molecule approached (from the cytoplasm for import and from the nucleoplasm for export) and interacted with the NPC divided by the number of successful translocations (into the nucleoplasm for import and into the cytoplasm for export). A diagrammatic representation of how efficiency is determined is shown in Figure 15.

Net transport rate is calculated as import efficiency minus export efficiency divided by number of frames per second acquisition time, resulting in net import events per second (NIE/s) (Figure 16).

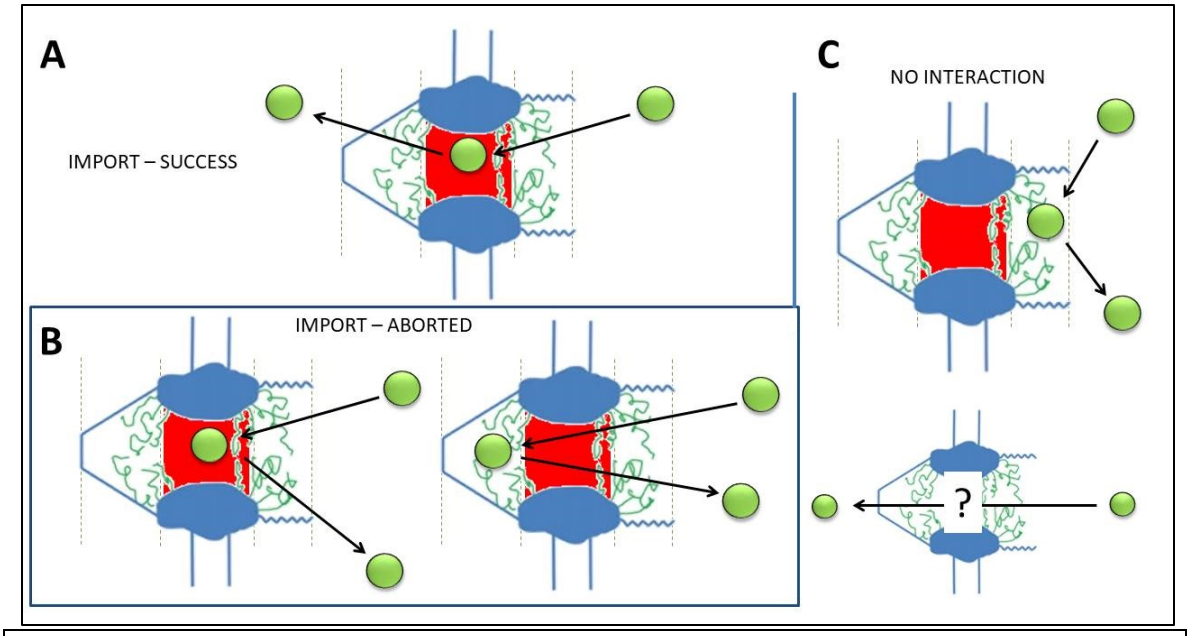

Figure 15. Efficiency Determination for Translocation through the NPC. (A) Successful import. (B) Aborted import. (C) No interaction.

Diffusion coefficient was calculated by first plotting each trajectory (>4 frames) on a Mean Square Displacement (MSD) vs. Time (t) plot. The data was fitted with the function MSD = 4Dt. [152].

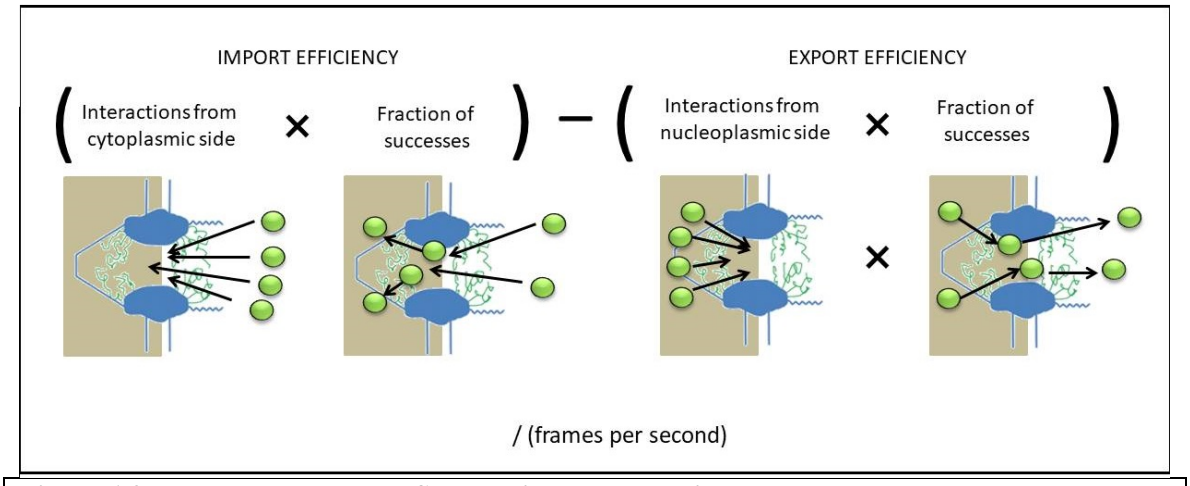

Figure 16. Net Transport Rate. Schematic representation.

2.4 Confocal Microscopy

Hela cells were transfected either with wild-type GFP–β-catenin alone or serially transfected with human Custos siRNA and then wild-type GFP–β-catenin 48 hours and 24 hours before imaging, respectively. The next day, the cells were exposed to Wnt3a ligand (250 ng/mL) for 3 hours (except for control cells). After Wnt3a exposure, cells were fixed and stained with 4′,6-diamidino-2-phenylindole (DAPI) and Texas Red and imaged with a confocal microscope.

2.5 FG Nucleoporin Comparison with β-Catenin

Unpublished single-molecule raw data for the FG Nups were collected in our lab via SPEED microscopy as described in the previous sections and will be used for publication under the title of *Probing disordered protein organization within live cells* by Kelich J, et al. The analyses and figures in this dissertation were generated from the raw FG Nup data separately by the author for comparison with β-catenin and will not be used for that publication.

2.6 Statistics

Experimental measurements were reported as mean ± standard error of the mean. An online two-tailed *t* test calculator, found at http://onlinestatbook.com/2/calculators/t_dist.html, was used to calculate significance of the difference between groups.

CHAPTER 3: RESULTS

3.1 Custos Localizes Predominantly to the Outer Nuclear Membrane and Moves with β-Catenin through the Nuclear Pore Complex

Hela cells stably expressing mCherry-tagged POM121 were co-transfected with GFP-tagged wild-type β-catenin and mCherry-tagged Custos. The next day the cells were exposed to recombinant human Wnt3a ligand (250 ng/mL) for 3 hours. After Wnt3a exposure, cell media were replaced with transport buffer for 45 minutes, after which the NPC was imaged and then photobleached. Single-molecule detection (spFRET) was performed via SPEED microscopy through the dual channel setup.

Detected FRET events were distributed from 314 nm inside the nucleoplasm to 500 nm to the cytoplasmic side (with a small number of outliers to 650 nm) at an average precision of 24 nm, showing a large bias to the cytoplasmic side (Figure 17). This provides supporting evidence for previous work of Komiya et al [75], showing that Custos preferentially localizes to the outer nuclear membrane (ONM). Custos and β-catenin were found to move together across the nuclear envelope. Representative trajectories are shown in Figures 18-20.

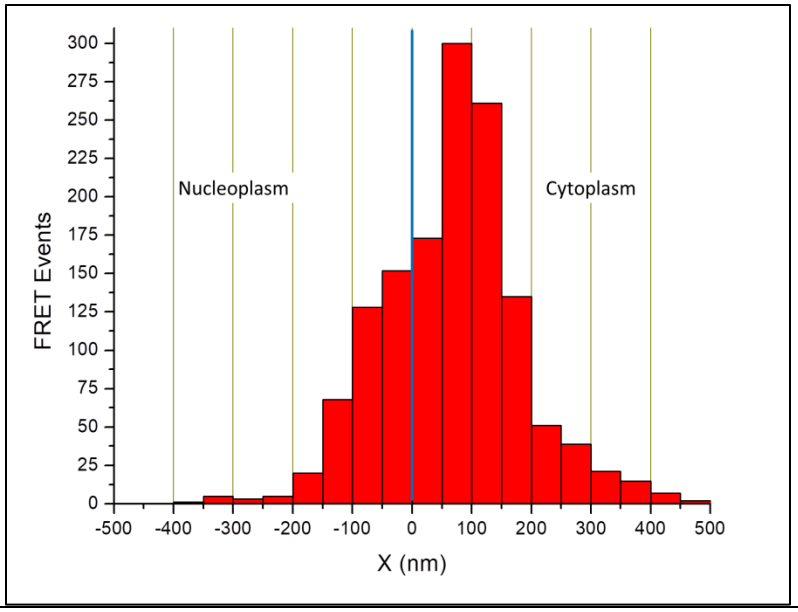

Figure 17. Distribution of Custos–β-catenin FRET events. Histogram along the axial (X) dimension of the NPC of FRET events (n=1,385).

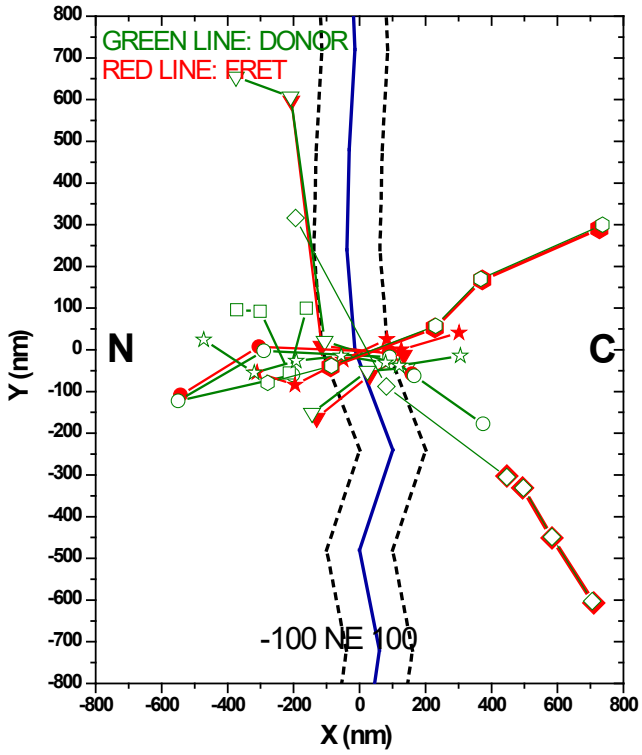

Figure 18. Custos–β-Catenin Co-movement Trajectories Across the Nuclear Envelope. N, nucleoplasm. C, cytoplasm.

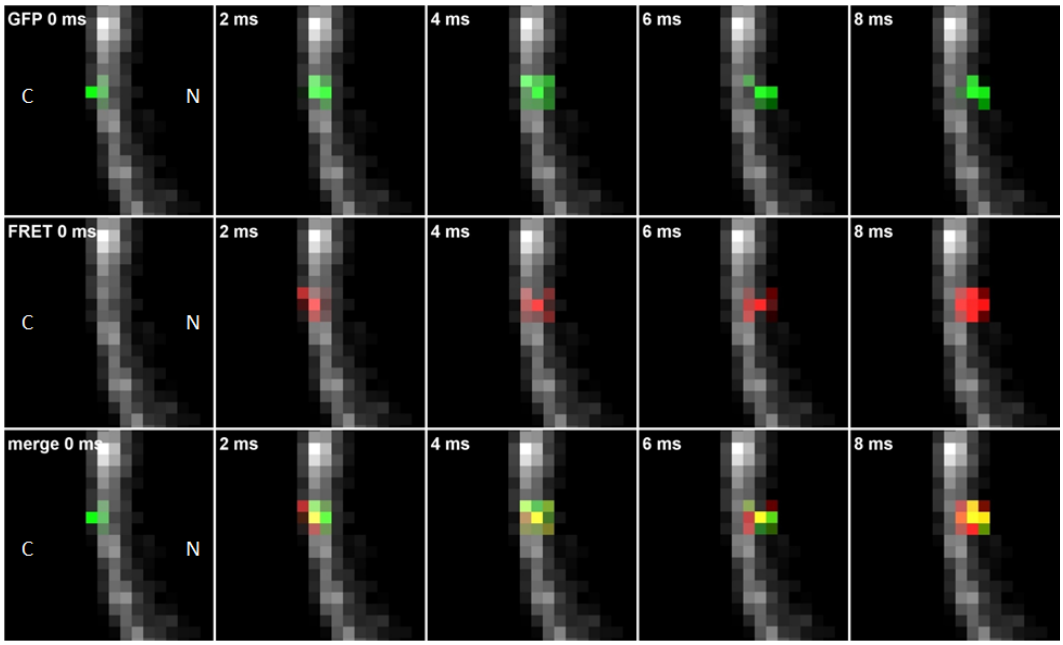

Figure 19. Custos–β-Catenin Import Trajectory Across the Nuclear Envelope. Co-tracking of Custos and β-catenin across the nuclear envelope (successful import). C, cytoplasm. N, nucleoplasm. 1 pixel = 240 nm.

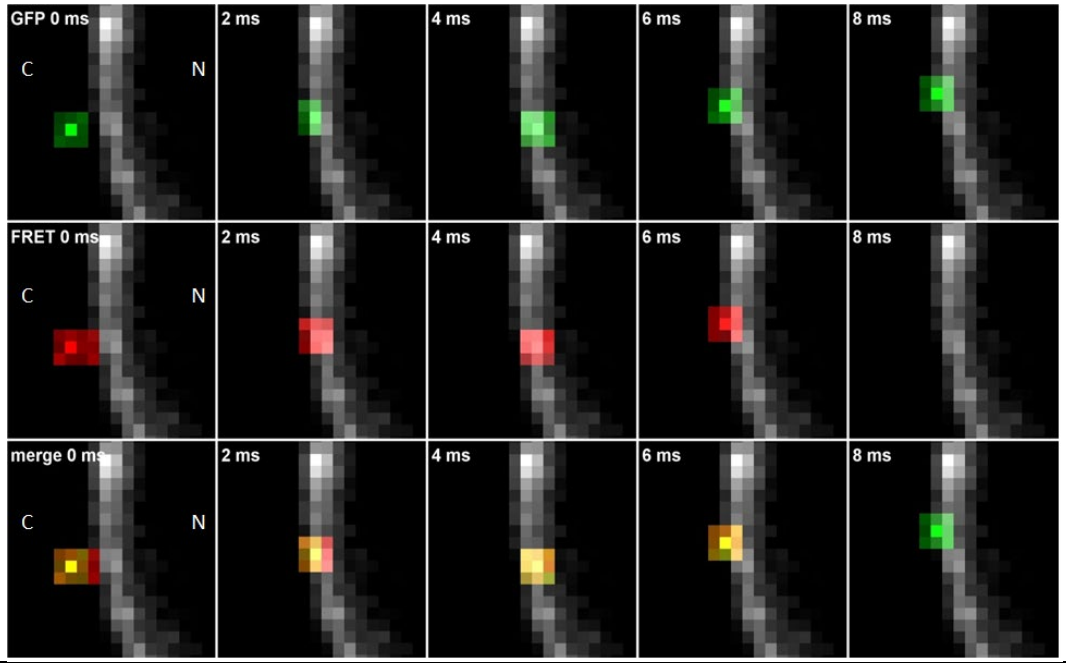

Figure 20. Custos–β-Catenin Aborted Import Trajectory at the Nuclear Envelope. Co-tracking of Custos and β-catenin during aborted import. C, cytoplasm. N, nucleoplasm. 1 pixel = 240 nm.

3.2 Knockdown of Custos Impairs Import of β-Catenin

Hela cells stably expressing mCherry-tagged POM121 were serially transfected with human Custos siRNA and then wild-type GFP–β-catenin 48 hours and 24 hours before imaging, respectively. The next day, the cells were exposed to Wnt3a ligand (250 ng/mL) for 3 hours (except for control cells). After Wnt3a exposure, cell media were replaced with transport buffer for 45 minutes, and single-molecule detection was performed via SPEED microscopy.

In the absence of Wnt3a, import efficiency was increased (although within the margin of error) by knockdown of Custos (18±3.3%) over that without knockdown (14.0±2.3%). Export efficiency of β-catenin was not affected by knockdown of Custos (36±4.8%) in comparison without knockout (38±4.9%). However, the measured N/C ratio was lower with knockdown (0.08 N/C with knockdown *vs* 0.38 N/C without knockdown). This difference in N/C ratio between two conditions with similar import and export efficiencies is likely due to the difference between calculation of N/C ratio and that of efficiency. N/C ratio is calculated using all detected points in the pore compared with efficiency percentages being calculated from full trajectories. The latter is a subset of the former. Not all points in the 2D distribution are part of a fully tracked trajectory.

In the absence of Wnt3a, the NTR of β-catenin (-0.19±0.01 NIE/s) was unaffected by knockdown (-0.20 ±0.01 NIE/s). After 3 hours of Wnt3a stimulation, import efficiency of β-catenin was reduced by knockdown of Custos (25.3±3.5%) over that without knockdown (33.6±4.1%). Knockdown of Custos increased export efficiency of β-catenin

(33.6±4.1%) over that without knockdown (26.0±4.4%). The NTR of β-catenin was 0.68±0.03 without knockdown and 0.58±0.01 with knockdown.

Under control conditions, the 2D axial distribution of detected β-catenin localizations in the pore was relatively unaffected by Custos knockdown. After Wnt3a stimulation, the 2D distribution of β-catenin was found to be shifted from a heavy bias to the nucleoplasmic side to a bias to the center and near-center cytoplasmic side of the NPC (Figure 21). This provides evidence that Custos plays a vital role in the regulation of nuclear import of β-catenin.

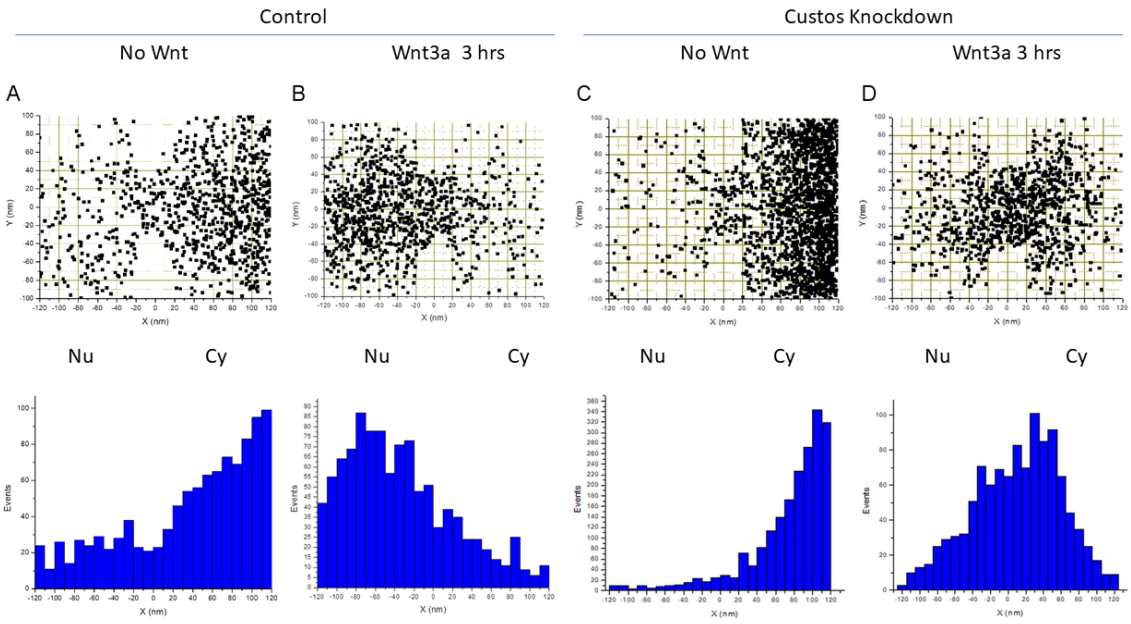

Figure 21. Knockdown of Custos Impairs the Import of β-Catenin (2D). 2D distribution (top panels) and histogram of detected events along the axis of the NPC (bottom panels). (A) Control (no Wnt3a): 1046 pts, average precision 10.8 nm. N/C ratio 0.38. (B) After 3 hrs Wnt3a (1020 pts): average precision 11.4 nm. N/C ratio 3.13. (C) Control with knockdown: 1986 pts, average precision 9.8 nm. N/C ratio 0.08. (D) After 3 Wnt3a with knockdown: (1109 pts) average precision 9.5 nm. N/C ratio 1.5. Nu, nucleoplasmic side; Cy, cytoplasmic side.

Hela cells were transfected either with wild-type GFP–β-catenin alone or serially transfected with human Custos siRNA and then wild-type GFP–β-catenin 48 hours and 24 hours before imaging, respectively. The next day, the cells were exposed to Wnt3a ligand (250 ng/mL) for 3 hours (except for control cells). After Wnt3a exposure, cells were fixed with 1:1 ratio of Acetone:Methanol and stained with DAPI and Texas Red and imaged with a confocal microscope (Figure 22). Knockdown of Custos showed an increased accumulation of GFP–β-catenin in the nucleus under control conditions. With Wnt3a stimulation, Custos knockdown decreased accumulation of GFP–β-catenin in the nucleus, when compared with that without knockdown. With knockdown and after Wnt3a stimulation, β-catenin appeared in a punctate pattern in the nuclear envelope. (Figure 22, bottom row, first panel). This punctate pattern, taken together with the 2D distribution in Figure 21D, suggests that Custos knockdown causes β-catenin to become "stuck in the pore".

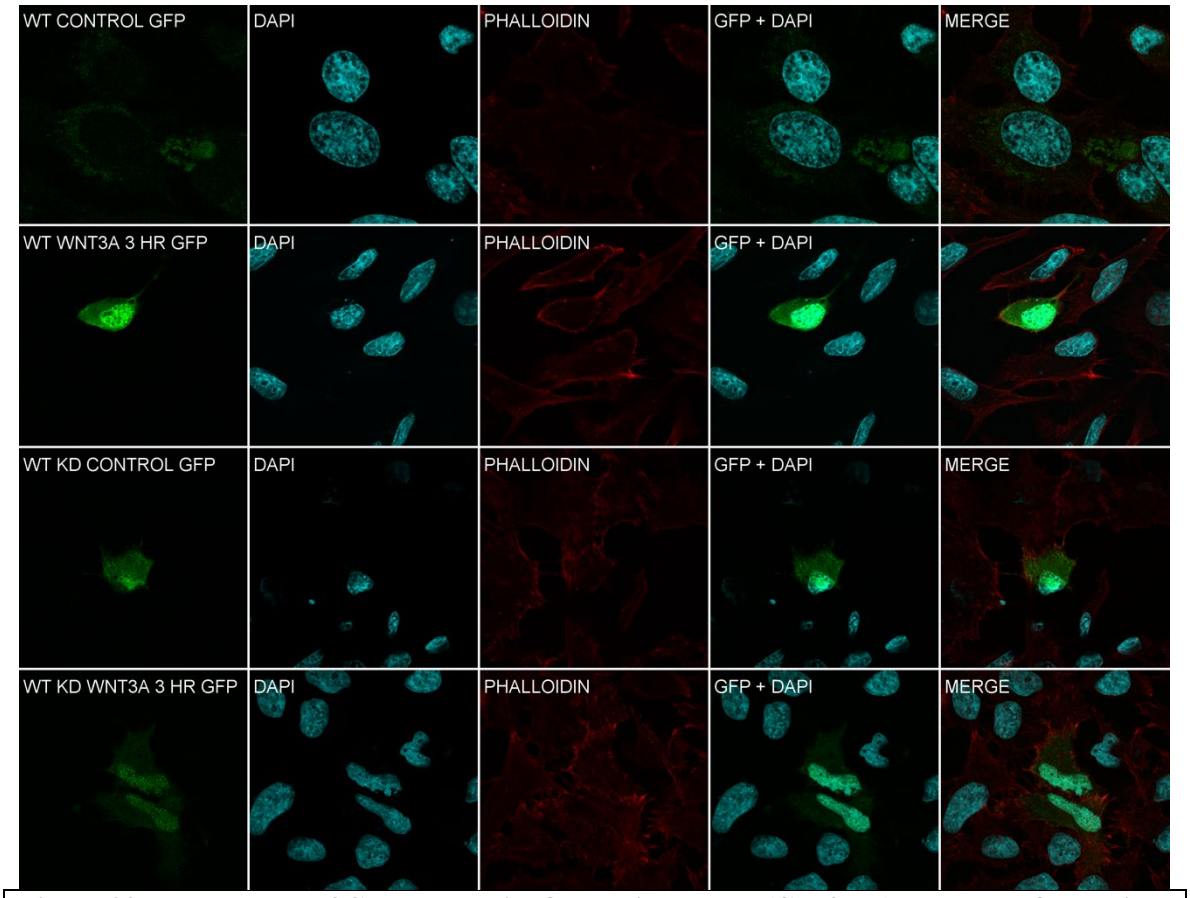

Figure 22. Knockdown of Custos Impairs β-catenin Import (Confocal). Top row, β-catenin (GFP) control. Second row, after 3 hrs Wnt3a stimulation. Third row, control with Custos knockdown. Fourth row, after 3 hrs Wnt3a stimulation with Custos knockdown.

3.3 The Role of Custos in β-Catenin Translocation May Be Limited to Import

Hela cells stably expressing mCherry-tagged POM121 were co-transfected with GFP-tagged wild-type β-catenin and mCherry tagged Custos; the next day the cells were exposed to Wnt3a ligand (250 ng/mL) for 3 hours. After Wnt3a exposure, cell media were replaced with transport buffer for 45 minutes, after which the NPC was imaged and then photobleached. Single-molecule detection (spFRET) was performed via SPEED microscopy through the dual channel setup.

FRET events that were part of a clear translocation trajectory across the NPC were classified as showing association (GFP event detected before FRET response detected), disassociation (GFP event detection continuing after FRET response no longer evident), or both. β-catenin–Custos FRET interactions were found to be initiated on the cytoplasmic side only. No association events were observed on the nuclear side of the NPC. However, disassociation events were found in roughly equal measure on either side of the NPC (Figure 23). This evidence supports the model of Custos initiating interaction with β-catenin on the outside of the NE to assist in its translocation into the nucleus (although not all events are successful). It appears that the export mechanism for β-catenin from the nucleus is not identical to that of the import mechanism and might not involve Custos.

Of 104 detected association events, all were detected in the cytoplasm. Conversely, of 42 detected disassociation events, 22 were detected in the cytoplasm and 20 were detected in the nucleus (Figure 23). Whereas Custos clearly plays a role in the import of β-catenin into the nucleus, no association event in the nucleoplasm was detected to provide evidence that Custos is involved in the export of β-catenin into the cytoplasm. Taken together with the pattern of import and export efficiency rates and NTR as well as the x-axial distribution of all detected FRET events, it appears that the role of Custos may be limited to import only.

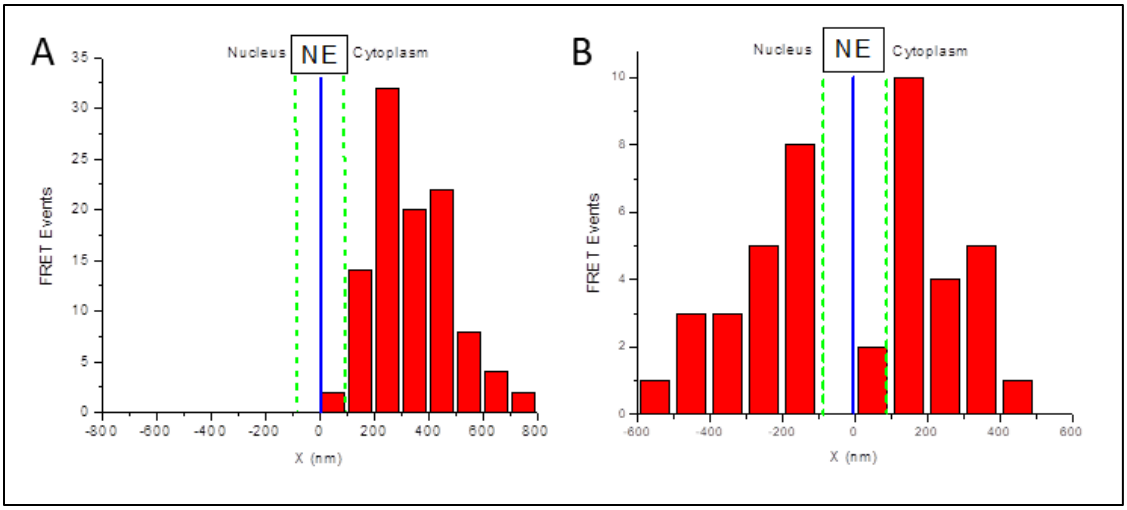

Figure 23. Custos–β-Catenin FRET Association and Disassociation Distribution.
(A) Detected association events of the β-catenin–Custos FRET complex (n=104).
(B) Detected disassociation events (n=42).

3.5 Truncation of β-catenin Dysregulates Import and Wnt3a Signal Transduction

Hela cells were transfected with truncate dCT or d9 24 hours before imaging. The next day, the cells were exposed to Wnt3a ligand (250 ng/mL) for 3 hours (except for control cells). After Wnt3a exposure, cells were fixed and stained with DAPI and Texas Red and imaged with a confocal microscope. Under control conditions, dCT accumulated in the nucleus (Figure 24, top row) at an increased level compared with wild-type (Figure 22, top row).

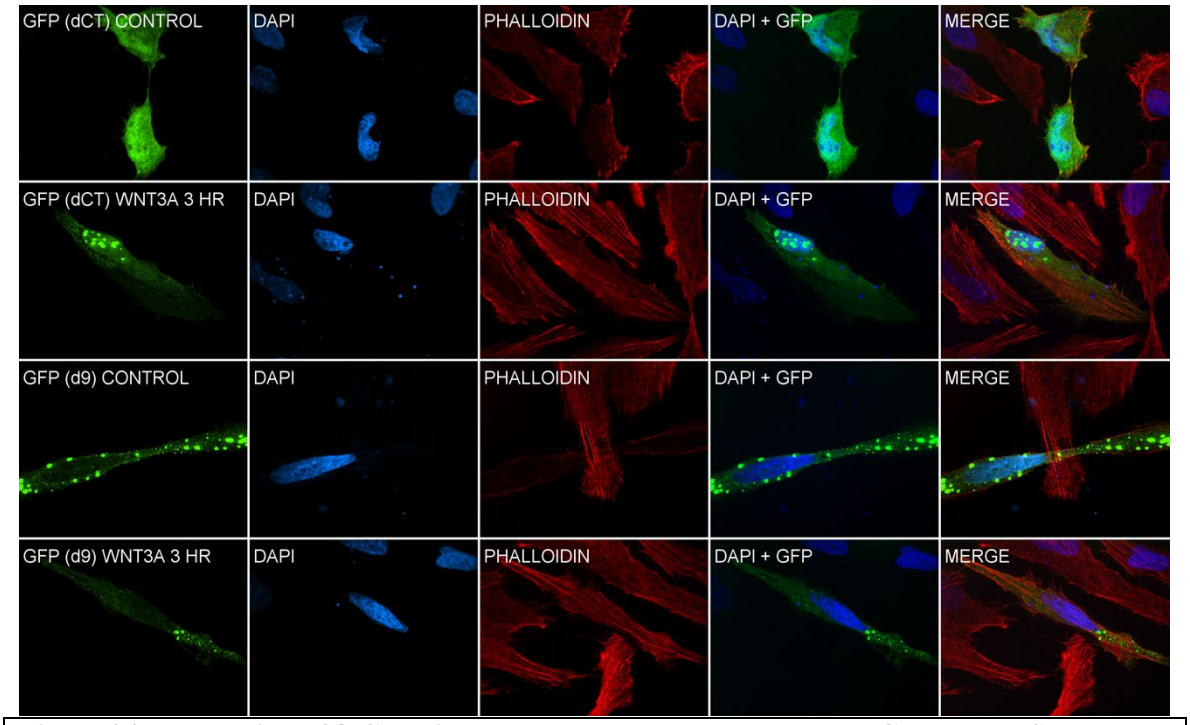

Figure 24. Truncation of β-Catenin Dysregulates Import. Top row, dCT control. Second row, dCT after 3 hrs Wnt3a stimulation. Third row, d9 control. Fourth row, d9 after 3 hrs Wnt3a stimulation.

TopFlash reporters were co-transfected into HEK293T cells with expression plasmids for β-catenin, dCT, CTF, 10-12C, d9, d6, and d3. After 48 hrs, cells were collected and the lysate was used to perform a TopFlash dual luciferase reporter assay. TopFlash is used to measure the expression of Wnt target genes, and we used it to measure the effects of the truncates on the expression of those genes [135].

Results for dCT suggest that the C-terminus of β-catenin is important in modulating nuclear import and that ARM regions 3-10 are sufficient to activate Wnt3a signaling genes via TCF binding [46,135]. Further, dCT increased transcriptional activity compared to wildtype B-catenin (Figure 25). The other truncates produced a decreased reporter activation. We reasoned that this may be due to the lack of some ARM repeats 3-

10 required for interaction with TCF or inability to enter the nucleus to affect gene transcription, or in some cases, both. Truncate 10-12C producing no reporter activation and d9 producing moderate activation further suggest that the TCF binding area on β-catenin is within ARM3-10 and the C-terminus is important in regulating nuclear import (Figure 25).

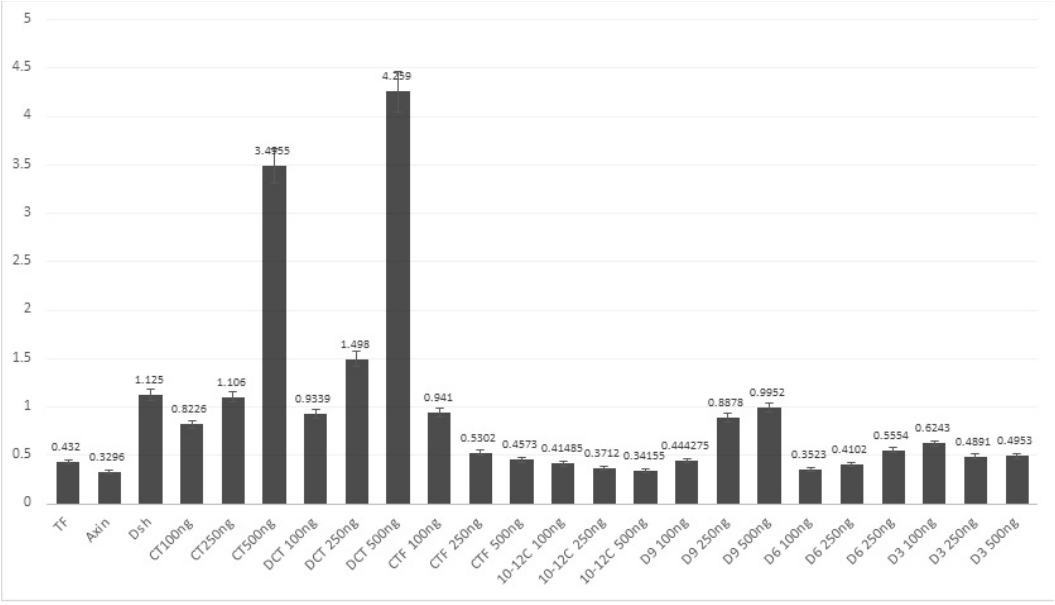

Figure 25. Removal of the C-Terminus of β-catenin Dysregulates Wnt3a Signal Transduction. Along the Y-axis are arrayed the various plasmids tested: TF, TopFlash control; Dsh, Dishevelled; CT, C-terminally GFP-tagged wild-type β-catenin; CTF, C-terminal fragment of β-catenin.

3.6 β-catenin translocates through the nuclear pore complex

Whereas β-catenin is known to enter the nucleus under Wnt3a stimulation, the exact mechanism of entry into the nucleus has heretofore not been clearly visualized. Here we used single-molecule microscopy to show images of β-catenin traversing the NPC from the cytoplasm to the nucleus in both 2D (Figure 26) and 3D (Figure 27).

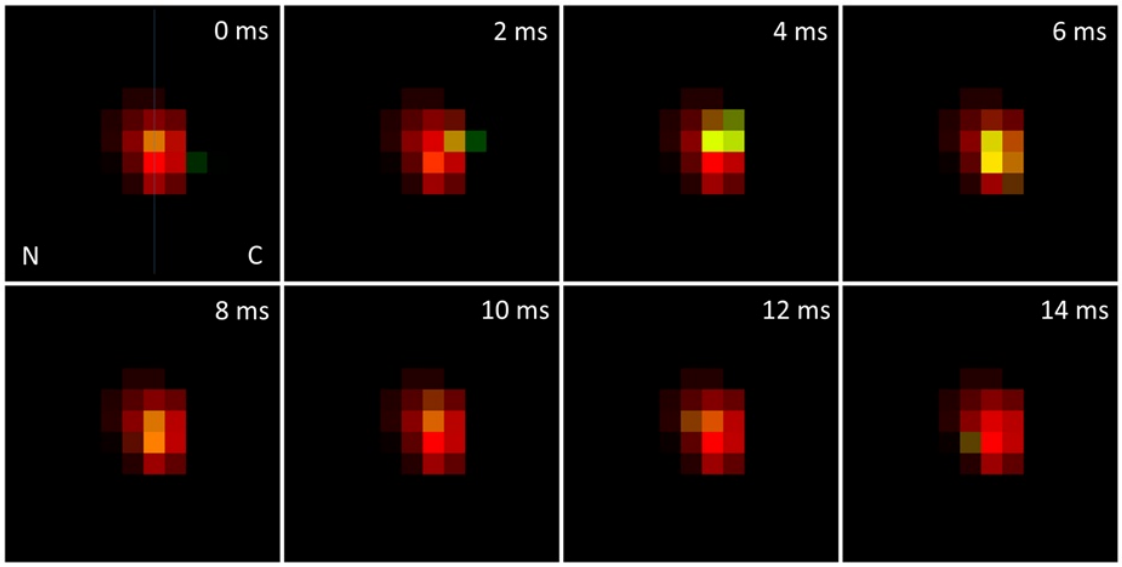

Figure 26. β-Catenin Translocates through the NPC. Series of images (2 ms per frame) taken with SPEED microscopy, showing transit of a GFP-β-catenin molecule (green) traversing the NPC (red) from cytoplasm to nucleus after stimulation with Wnt3a for 1 hour. N, nuclear side; C, cytoplasmic side. Position of the nuclear envelope indicated in the first panel with a vertical line.

Hela cells stably expressing GFP-tagged POM121 structural NPC protein were transfected with GFP-tagged wild-type β-catenin; the next day the cells were exposed to Wnt3a ligand (250 ng/mL) for 0 (control) to 8 hours in 1-hr increments. After Wnt3a exposure, cell media were replaced with transport buffer for 45 minutes, after which the NPC was imaged and then photobleached. Single-molecule detection was performed via SPEED microscopy. The average interaction time with the pore was found to be 3.82 ms. The diffusion coefficient of GFP-β-catenin was found to be 0.493 $\mu m^2/s$ in the NPC and within approximately 500 nm into the cytoplasm and approximately 500 nm into the nucleus. Efficiency of import and export and NTR were calculated.

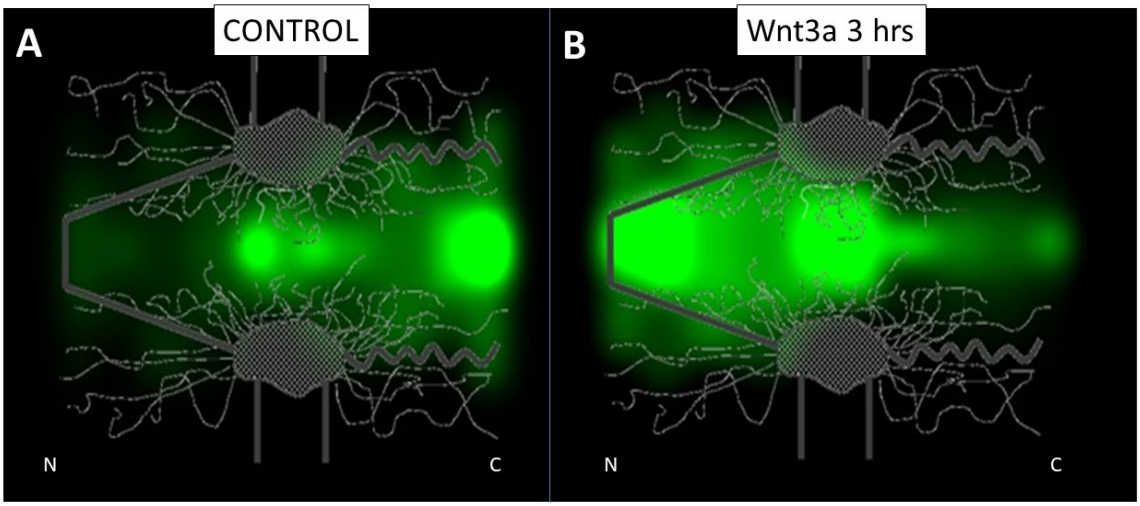

Figure 27. 3D Probability Heat Map of Detected Wild-Type β-Catenin in the NPC. A. Control. 1046 points, average precision 10.8 nm; N/C ratio 0.38. B. After 3 hrs of Wnt3a exposure. 1020 pts, average precision 11.4 nm; N/C ratio 3.13.N, nucleoplasm. C, cytoplasm.

Localizations were collected and 3D probability density maps for wild-type GFP-β-catenin were generated for the control condition and the 3-hr Wnt3a exposure, shown in Figure 27. Distribution of detected β-catenin molecules was found to be predominantly on the cytoplasmic side of the pore [nucleus-to cytoplasm (N/C) of 0.38] in the absence of Wnt3a stimulation. After 3 hrs of Wnt3a exposure the distribution is mainly in the nucleus, with an N/C ratio of 3.13 (Figure 27).

3.7 Translocation Dynamics of β-catenin are Affected by Duration of Wnt3a Ligand Exposure

The effect of Wnt3a stimulation on translocation efficiency and net transport rate (NTR) of wild-type β-catenin was measured via single-molecule localization and tracking. With Wnt3a exposure, β-catenin import efficiency increased sharply from 19% at control to 38% at 1 hr and continued to increase steadily to 51% at 4 hrs, after which it began to decrease. After 8 hours, import efficiency at 33% was still significantly higher than

control but decreasing. Export efficiency decreased steadily to 24% at 4 hrs, after which it begins to recover, steadily increasing to 43% at 8 hrs, at which point export efficiency had recovered to a level not significantly different from control (45%). (Figure 28 and Table 2).

NTR of wild-type β-catenin was calculated to be -2.47 NIE/s in the absence of Wnt3a stimulation and increased with duration of Wnt3a stimulation through 4 hrs, at which it was 3.02±0.05 NIE/s. After that, it decreased through 8 hrs (-0.97±0.03), at which time it was not fully recovered to control levels (Figure 29 and Table 2).

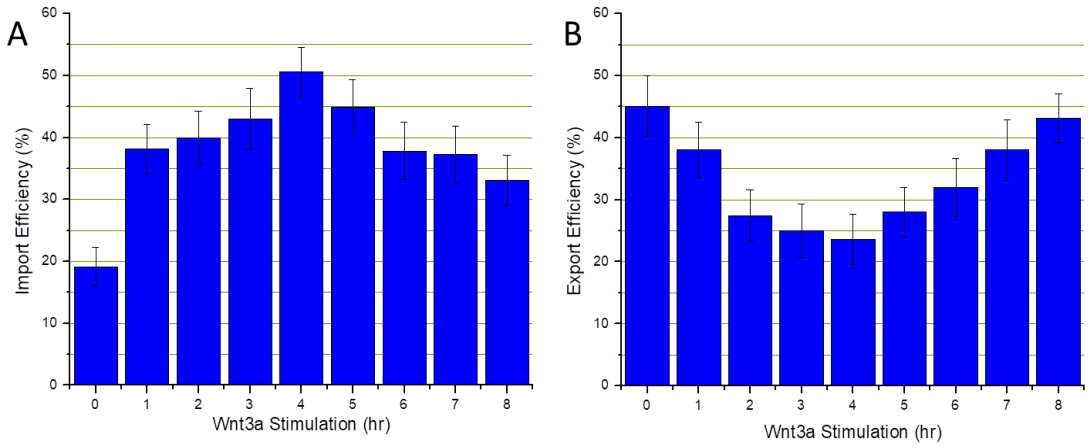

Figure 28. Translocation Efficiency of Wild-Type β-Catenin Over a Timecourse of Wnt3a Stimulation. (A) Import. (B) Export.

Table 2. Wild-Type β-Catenin Translocation Efficiency and Net Transport Rate

Wnt3a Duration (hr)	Import Efficiency	Export Efficiency	NTR (NIE/s)
0 (Control)	19.1±3.1% (n=162)	45.1±4.9% (n=102)	-2.47±0.05 (n=264)
1	38.1±4.0%*** (n=147)	38.0±4.4% (n=121)	2.07±0.05*** (n=268)
2	40.0±4.2%*** (n=135)	27.4±4.2%*** (n=113)	2.24±0.05*** (n=248)
3	43.0±5.0%*** (n=100)	25.0±4.3%*** (n=100)	2.45±0.05*** (n=200)
4	50.6±4.0%*** (n=156)	23.6±4.1%*** (n=110)	3.02±0.05*** (n=266)
5	44.9±4.4%*** (n=126)	28.0±4.0%*** (n=125)	2.54±0.05*** (n=251)
6	37.8±4.6%** (n=111)	32.0±4.7%† (n=100)	1.44±0.04*** (n=211)
7	37.3±4.6%** (n=110)	38.0±4.9% (n=100)	0.27±0.02*** (n=210)
8	33.1±4.1%* (n=130)	43.1±4.0% (n=153)	-0.97±0.03*** (n=283)

*p<0.001; ** p<0.0001; ***p<0.00001; †p<0.01.
Net transport rate (NTR) is expressed as net import events per second (NIE/s).

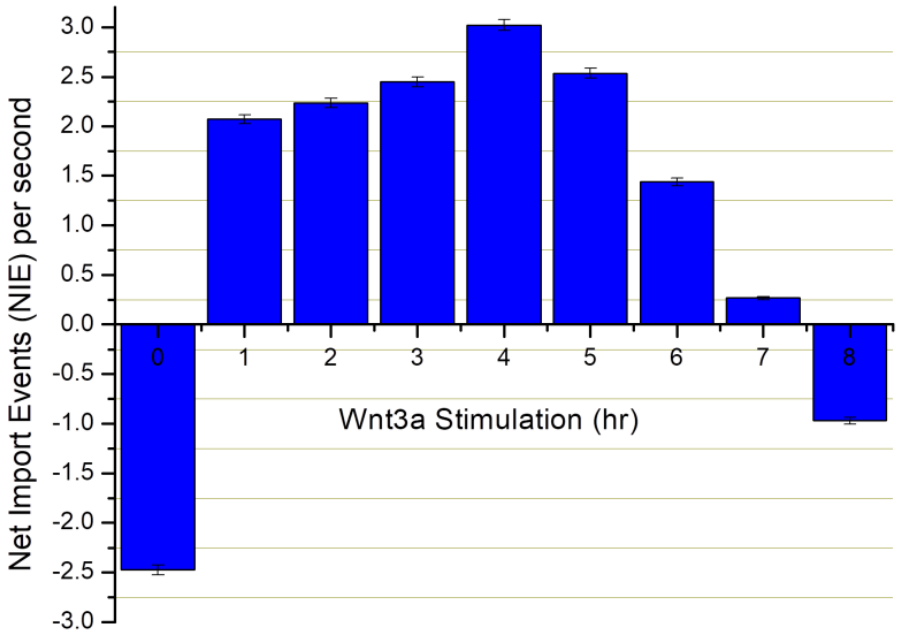

Figure 29. Net Transport Rate of Wild-Type β-Catenin Over a Timecourse of Wnt3a Stimulation.

3.8 Single-Molecule Study of β-Catenin and its Truncates

Hela cells stably expressing mCherry-tagged POM121 structural nucleoporin were transfected with GFP-tagged wild-type β-catenin and a series of truncates (Figure 7B – Figure 7H). After 24 hours cells were exposed to Wnt3a ligand (250 ng/mL) for 3 hrs.. After Wnt3a exposure, cell media were replaced with transport buffer for 45 minutes, after which the NPC was imaged and single-molecule detection was performed via SPEED microscopy. The data were compiled, and 2D, 3D, efficiency, and NTR analyses were performed. 2D and 3D data are presented in Figure 30 (control) and Figure 31 (Wnt3a 3 hrs). 2D distribution and 3D route characteristics are presented in Table 3.

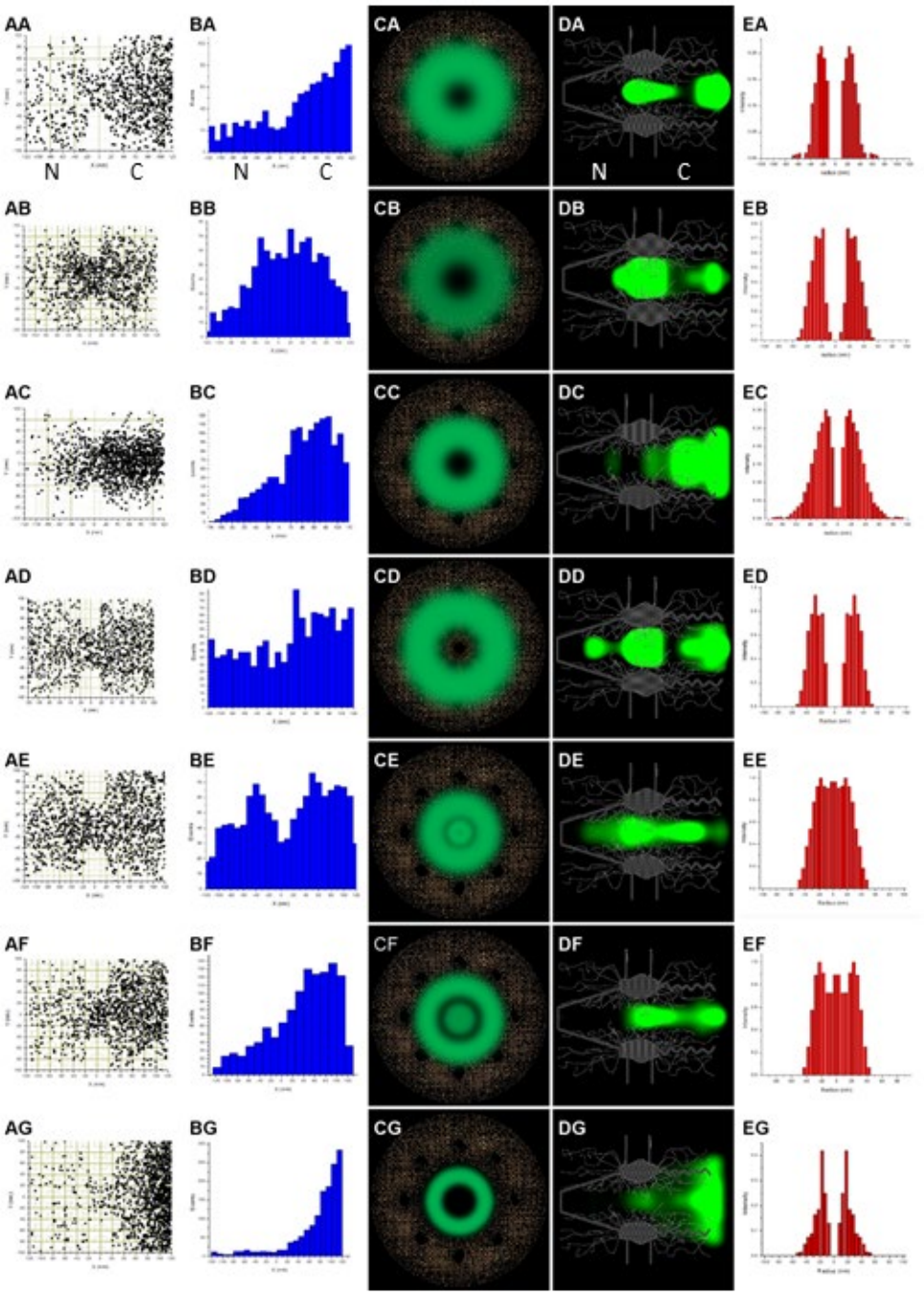

Figure 30. Single-Molecule Study of β-Catenin Truncates (Control). First column, 2D detected events; second column, 2D distribution along the x-axis; third column, 3D transport route through the central region; fourth column, 3D probability density map; fifth column, radial peaks. First row, wild-type; second row, dCT; third row, d9; fourth row, d6; fifth row, d3; sixth row, 10-12C; seventh row, 10-12. See Table 3 for associated data. N, nucleoplasmic side; C, cytoplasmic side.

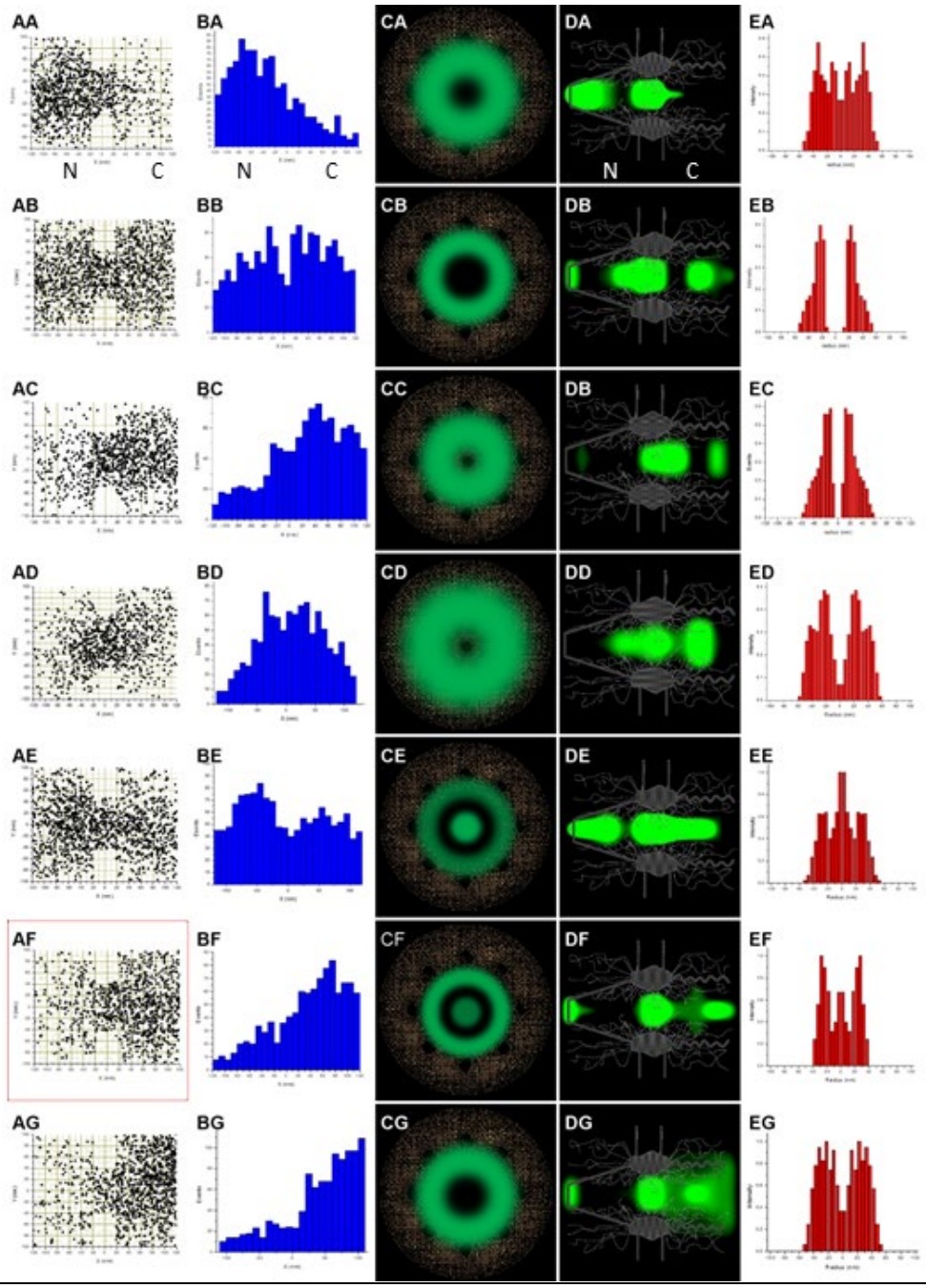

Figure 31. Single-Molecule Study of β-Catenin Truncates (After 3 hrs of Wnt3a Stimulation). First column, 2D detected events; second column, 2D distribution along the x-axis; third column, 3D transport route through the central region; fourth column, 3D probability density map; fifth column, radial peaks. First row, wild-type; second row, dCT; third row, d9; fourth row, d6; fifth row, d3; sixth row, 10-12C; seventh row, 10-12. See Table 3 for associated data. N, nucleoplasmic side; C, cytoplasmic side.

Table 3. 2D Distribution and 3D Route Characteristics of β-Catenin Compared with its Truncates (Control)

Molecule	Precision (nm)		Points		N/C Ratio		Radial Peak(s)** (nm)	
	CTL	WNT 3A	CTL	WNT 3A	CTL	WNT 3A	CTL	WNT3A
Wild-type*	10.8	11.4	1046	1020	0.38	3.13	23.9±0.6	26.1±2.3
dCT	10.9	8.4	1058	1398	0.67	0.93	25.4±0.6	24.4±0.7
d9	8.8	9.1	1436	1042	0.27	0.44	22.1±1.1	20.6±1.1
d6	10.5	10.3	1184	1024	0.68	0.76	27.1±0.5	27.4±1.2
d3	10.2	11.5	1255	1359	0.77	1.23	0.0±0.3 18.9±0.5	0.0±0.3 27.6±0.5
10-12C	10.0	10.2	1183	1009	0.30	0.35	0.0±0.2 23.0±0.2	0.0±0.3 24.8±0.2
10-12	11.0	10.2	1439	1063	0.10	0.27	17.7±0.7	25.1±1.0

*N-terminal tagged GFP-β-catenin
**At -10 to +10 nm axially
N/C, nuclear-to-cytoplasmic; CTL, control; WNT3A, 3 hrs Wnt3a stimulation.

3.9 Truncation of β-catenin Changes Efficiency of Translocation in Complex Ways

Wild-type β-catenin and a series of truncates all tagged with GFP (2xGFP in the case of truncates 10-12 and 10-12C to maintain size above the NPC exclusion limit) were tracked through the NPC. Translocation dynamics were calculated (Figures 32 and 33 and Tables 4 and 5). Truncate d9 is the sole construct not significantly different from wild-type in import efficiency, but significantly different from wild-type in export efficiency under control conditions. The similarity of d9 to wild-type and its NTR at or near zero under either condition implies a failure of d9 to interact with the NPC in a functional manner. This failure provides some evidence to support previous assertions that ARM repeats 10-12 (and the C-terminus) play a vital role in translocation [52,54-57,62].

Although the NTR of all truncates of β-catenin were significantly different from wild-type under control and Wnt3a conditions, only d3 and 10-12 showed positive NTR under control conditions. We attributed this to size and conformation (see below). Because

10-12C did not show a positive NTR under control conditions, it may be that the combination of size and lack of C-terminus has a permissive effect on nuclear import. (The lack of either disordered terminal region separates 10-12 from the other truncates.) Only 10-12C showed a negative NTR under Wnt3a conditions, pointing to the possibility of the C-terminus being a facilitator of export or have a role in inhibiting import.

3.10 The Size Exclusion Limit of the NPC is Confirmed by Truncates d6 and d3

The β-catenin truncates are fused to the fluorophore via the intrinsically disordered and presumably flexible N-terminus. It is suggested that β-catenin can adopt a linear orientation to the pore. Thus, it has an effective radius equivalent to the radius of the truncate alone, with the fluorophore preceding or trailing during translocation. Using estimated hydrostatic radius as a metric [99], and confirmed data in this study, wild-type GFP–β-catenin and truncates d9 and d6 are too large in any orientation to diffuse passively through the NPC. However, truncate d3 is small enough to translocate through the central channel of the pore when approaching in a linear orientation, but too large in other orientations. The estimated particle size at the size exclusion limit of 40 kDa is 4.6 nm, which is the estimated hydrostatic radius of truncate d6. The estimated hydrostatic radius of d3 (and 10-12C) is 4.0 nm. Truncates d3 and 10-12C were revealed to have a bimodal translocation route (Figures 30 and 31, Panels CE, CF, EE, and EF).

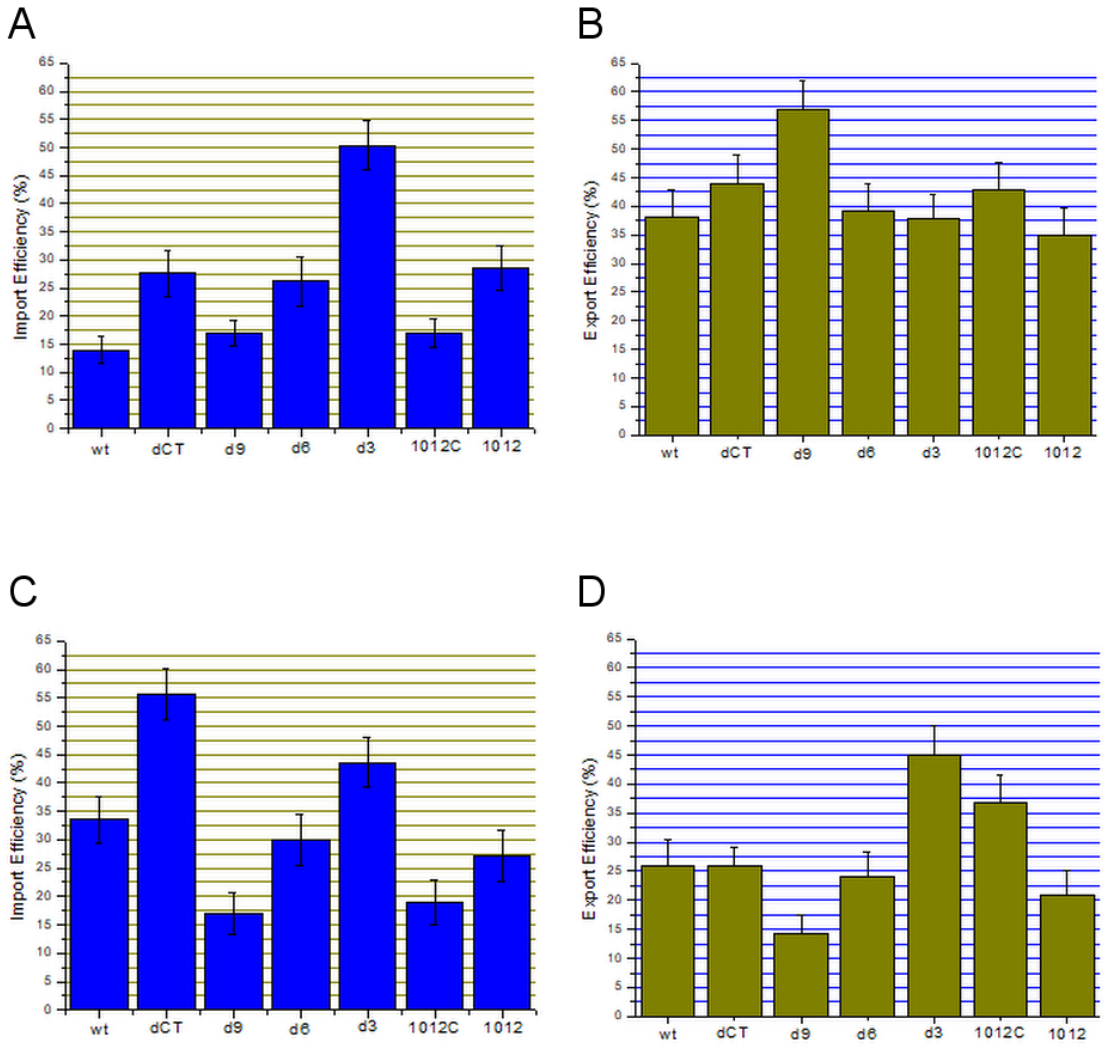

Figure 32. Translocation Efficiency β-Catenin Truncates. (A) Control import. (B) Control export. (C) Wnt3a (3 hrs) import. (D) Wnt3a (3 hrs) export.

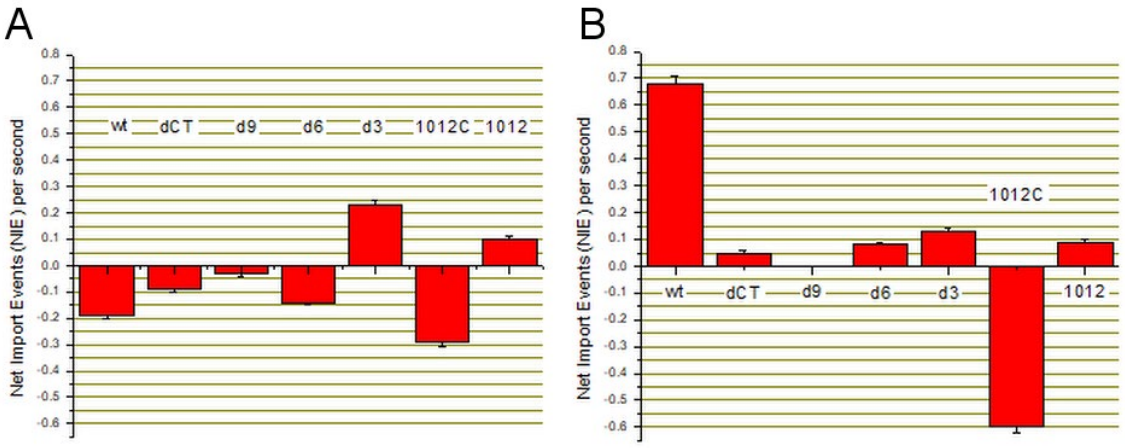

Figure 33. Net Transport Rate of β-Catenin Truncates. (A) Control. (B) Wnt3a (3 hrs).

Table 4. β-Catenin Wild-Type and Truncates Translocation Efficiency and Net Transport Rate (Control)

Molecule	Import Efficiency	Export Efficiency	NTR (NIE/s)
wild-type	14.0±2.3% (n=221)	38.0±4.9% (n=100)	-0.19±0.01 (n=321)
dCT	27.6±4.2%* (n=116)	44.0±5.0% (n=100)	-0.09±0.01*** (n=216)
d9	17.0±2.2% (n=300)	57±5.0%** (n=100)	-0.03±0.01*** (n=400)
d6	26.2±4.3%† (n=103)	39.3±4.6% (n=112)	-0.14±0.01*** (n=215)
d3	50.4±4.3%*** (n=133)	38.0±4.1% (n=137)	0.23±0.02*** (n=270)
10-12C	16.9±2.6%*** (n=201)	43.0±4.6% (n=100)	-0.29±0.02*** (n=301)
10-12	28.6±3.8%*** (n=140)	35.0±4.8% (n=100)	0.10±0.01*** (n=240)

*p<0.001; ** p<0.0001; ***p<0.00001; †p<0.01.
Net transport rate (NTR) is expressed as net import events per second (NIE/s).

Table 5. β-Catenin Wild-Type and Truncates Translocation Efficiency and Net Transport Rate (Wnt3a 3 hrs)

Molecule	Import Efficiency	Export Efficiency	NTR (NIE/s)
wild-type	33.6±4.1% (n=134)	26.0±4.4% (n=100)	0.68±0.03*** (n=234)
dCT	55.7±4.6%*** (n=131)	26.0±3.1% (n=232)	0.05±0.01*** (n=363)
d9	17.0±3.8%*** (n=100)	14.2±3.2%* (n=119)	0.0±0.0*** (n=219)
d6	30.0±4.6% (n=100)	24.1±4.1% (n=108)	0.08±0.01*** (n=208)
d3	43.6±4.3% (n=133)	45.0±5.0%* (n=100)	0.13±0.01*** (n=233)
10-12C	19.0±3.9%** (n=100)	36.9±4.8% (n=103)	-0.06±0.02*** (n=203)
10-12	27.2±4.4%† (n=103)	21.0±4.1%** (n=100)	0.09± 0.01*** (n=203)
*p<0.001; ** p<0.0001; ***p<0.00001; †p<0.01. Net transport rate (NTR) is expressed as net import events per second (NIE/s).			

3.11 Comparison of β-catenin with FG Nups

As observed in previous studies, β-catenin strongly co-localizes with the nucleoporins of the Nup62 complex (Nups 62, 58, 54, and 98) as well as POM121 (Figures 34 through 38) in the axial center of the NPC. β-catenin appears to co-localize most strongly with Nup54 at the Nup54 x-axial peak (10 nm to 20 nm cytoplasmic side) (Figure 36). This co-localization with Nup 54 is more pronounced during Wnt3a stimulation than during control conditions. β-catenin strongly co-localizes with POM121 at -10 nm to 10 nm (center) (Figure 38). Less strong but still clear are its co-localization with Nup 358 and Nup214 on the cytoplasmic side of the pore and with Wnt3a stimulation its overlap with TPR in the nuclear basket (Figures 39 through 41). Notably, the 3D probability density maps of CG1 and Nup153 do not show much overlap (Figures 42 through 44).

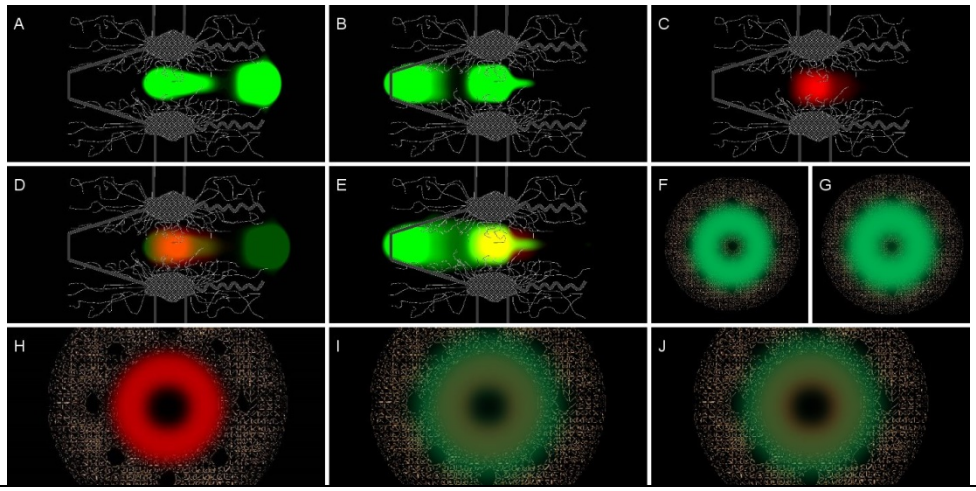

Figure 34. 3D Localization Comparison of Wild-Type β-Catenin with Nup62. Comparison at x-axial peak of Nup62 (-10 nm to 10 nm). (A) Wild-type β-catenin (control). (B) Wild-type β-catenin (Wnt3a). (C) Nup62. (D) Wild-type β-catenin (control) merged with Nup62. (E) Wild-type β-catenin (Wnt3a) merged with Nup62. (F) Wild-type β-catenin (control) axial view. (G) Wild-type β-catenin (Wnt3a) axial view. (H) Nup62 axial view. (I) Wild-type β-catenin (control) and Nup62 merged axial view. (J) Wild-type β-catenin (Wnt3a) and Nup62 merged axial view.

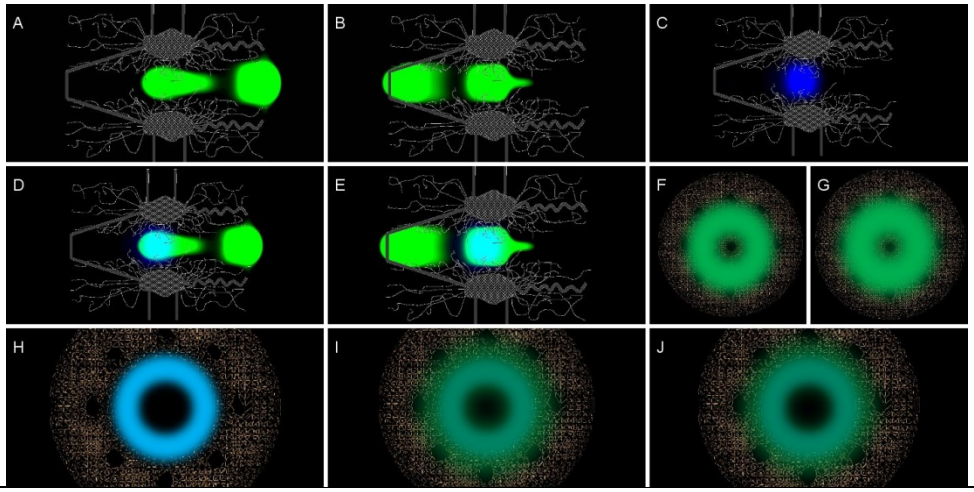

Figure 35. 3D Localization Comparison of Wild-Type β-Catenin with Nup58. Comparison at x-axial peak of Nup58 (-10 nm to 10 nm). (A) Wild-type β-catenin (control). (B) Wild-type β-catenin (Wnt3a). (C) Nup58. (D) Wild-type β-catenin (control) merged with Nup58. (E) Wild-type β-catenin (Wnt3a) merged with Nup58. (F) Wild-type β-catenin (control) axial view. (G) Wild-type β-catenin (Wnt3a) axial view. (H) Nup58 axial view. (I) Wild-type β-catenin (control) and Nup58 merged axial view. (J) Wild-type β-catenin (Wnt3a) and Nup58 merged axial view.

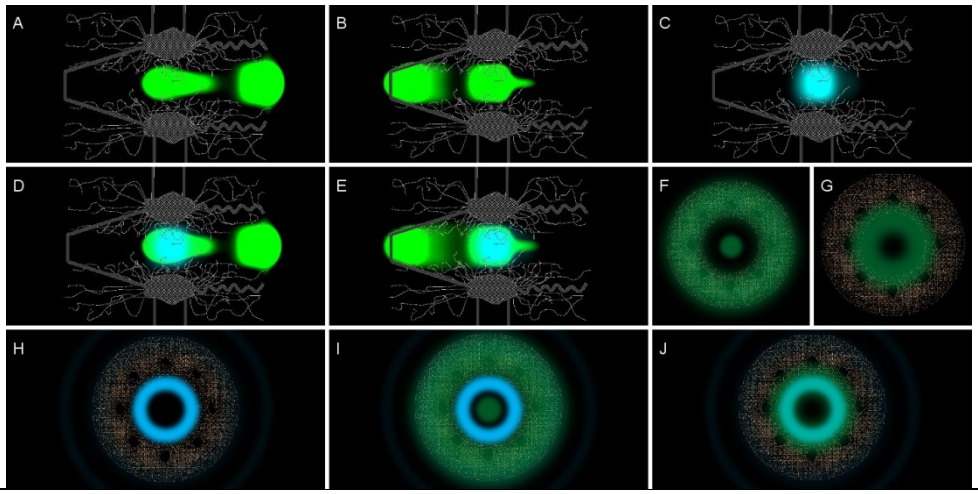

Figure 36. 3D Localization Comparison of Wild-Type β-Catenin with Nup54. Comparison at x-axial peak of Nup54 (10 nm to 20 nm cytoplasmic side). (A) Wild-type β-catenin (control). B. Wild type β-catenin (Wnt3a). (C) Nup54. D. Wild-type β-catenin (control) merged with Nup54. E. Wild-type β-catenin (Wnt3a) merged with Nup54. (F) Wild-type β-catenin (control) axial view. (G) Wild-type β-catenin (Wnt3a) axial view. (H) Nup 54 axial view. (I) Wild-type β-catenin (control) and Nup54 merged axial view. (J) Wild-type β-catenin (Wnt3a) and Nup54 merged axial view.

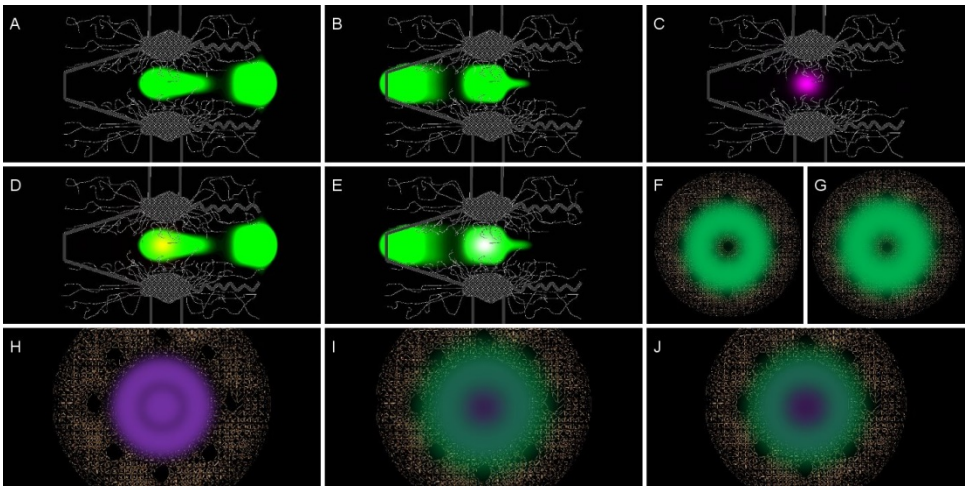

Figure 37. 3D Localization Comparison of Wild-Type β-Catenin with Nup98. Comparison at x-axial peak of Nup 98 (-10 nm to 10 nm). (A) Wild-type β-catenin (control). (B) Wild type β-catenin (Wnt3a). (C) Nup98. (D) Wild-type β-catenin (control) merged with Nup98. (E) Wild-type β-catenin (Wnt3a) merged with Nup98. (F) Wild-type β-catenin (control) axial view. (G) Wild-type β-catenin (Wnt3a) axial view. (H) Nup98 axial view. (I) Wild-type β-catenin (control) and Nup98 merged axial view. (J) Wild-type β-catenin (Wnt3a) and Nup98 merged axial view.

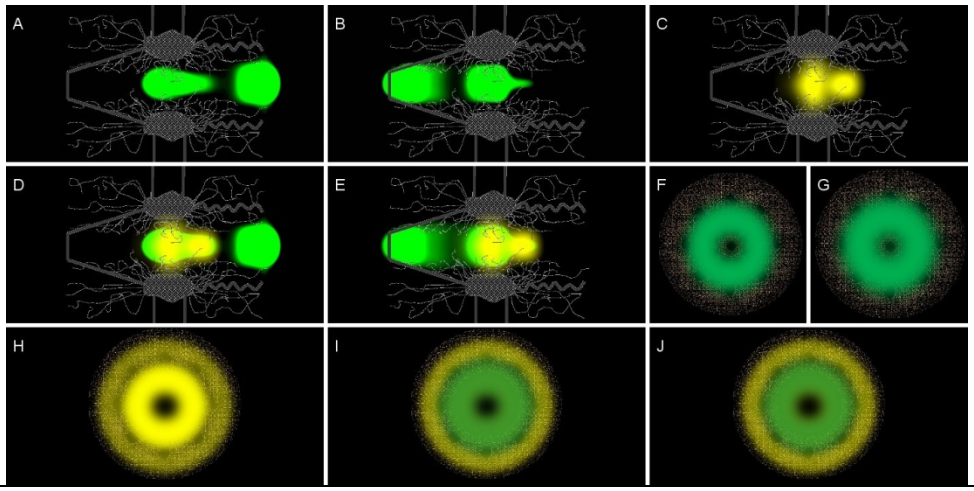

Figure 38. 3D Localization Comparison of Wild-Type β-Catenin with POM121. Comparison at x-axial peak of POM121 (-10 nm to 10 nm). (A) Wild-type β-catenin (control). (B) Wild-type β-catenin (Wnt3a). (C) POM121. D. Wild-type β-catenin (control) merged with POM121. (E) Wild-type β-catenin (Wnt3a) merged with POM121. (F) Wild-type β-catenin (control) axial view. (G) Wild-type β-catenin (Wnt3a) axial view. (H) POM121 axial view.(I) Wild-type β-catenin (control) and POM121 merged axial view. (J) Wild-type β-catenin (Wnt3a) and POM121 merged axial view.

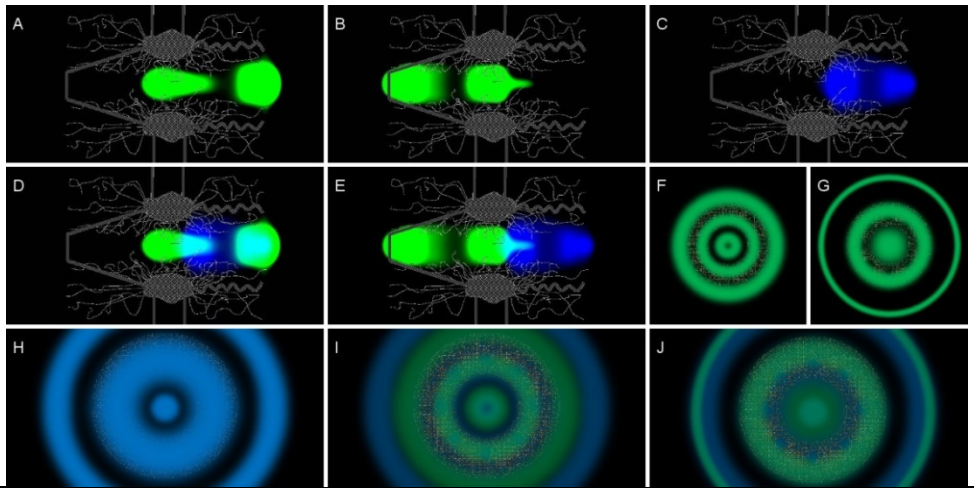

Figure 39. 3D Localization Comparison of Wild-Type β-Catenin with Nup 358. Comparison at x-axial peak of Nup358 (50 nm to 80 nm, cytoplasmic side). (A) Wild-type β-catenin (control). (B) Wild type β-catenin (Wnt3a). (C) Nup358. (D) Wild-type β-catenin (control) merged with Nup358. (E) Wild-type β-catenin (Wnt3a) merged with Nup358. (F) Wild-type β-catenin (control) axial view. (G) Wild-type β-catenin (Wnt3a) axial view. (H) Nup358 axial view. (I) Wild-type β-catenin (control) and Nup358 merged axial view. (J) Wild-type β-catenin (Wnt3a) and Nup 358 merged axial view.

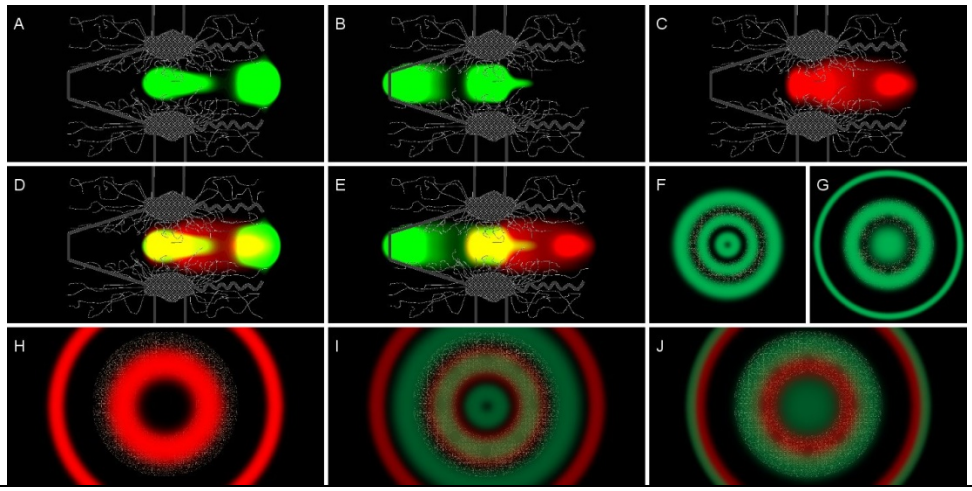

Figure 40. 3D Localization Comparison of Wild-Type β-Catenin with Nup 214. Comparison at x-axial peak of Nup214 (50 nm to 80 nm, cytoplasmic side). (A) Wild-type β-catenin (control). (B) Wild type β-catenin (Wnt3a). (C) Nup214. (D) Wild-type β-catenin (control) merged with Nup214. (E) Wild-type β-catenin (Wnt3a) merged with Nup214. (F) Wild-type β-catenin (control) axial view. (G) Wild-type β-catenin (Wnt3a) axial view. (H) Nup214 axial view. (I) Wild-type β-catenin (control) and Nup214 merged axial view. (J) Wild-type β-catenin (Wnt3a) and Nup214 merged axial view.

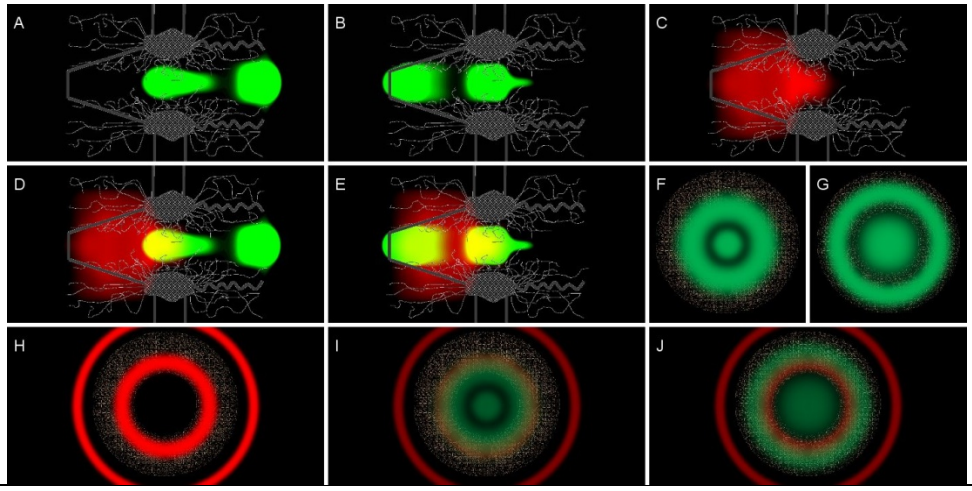

Figure 41. 3D Localization Comparison of Wild-Type β-Catenin with TPR. Comparison at x-axial peak of TPR (-20 nm to -10 nm, nucleoplasm side). (A) Wild-type β-catenin (control). (B) Wild type β-catenin (Wnt3a). (C) TPR. (D) Wild-type β-catenin (control) merged with TPR. (E) Wild-type β-catenin (Wnt3a) merged with TPR. (F) Wild-type β-catenin (control) axial view. (G) Wild-type β-catenin (Wnt3a) axial view. (H) TPR axial view. (I) Wild-type β-catenin (control) and TPR merged axial view. (J) Wild-type β-catenin (Wnt3a) and TPR merged axial view.

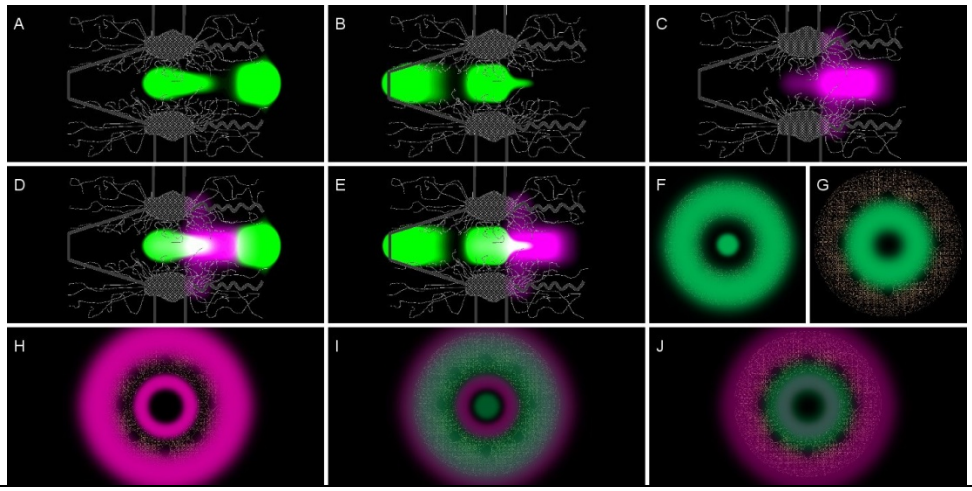

Figure 42. 3D Localization Comparison of Wild-Type β-Catenin with N-terminus of CG1. Comparison at x-axial peak of CG1(n) (10 nm to 20 nm, cytoplasmic side). (A) Wild-type β-catenin (control). (B) Wild type β-catenin (Wnt3a). (C) CG1(n). (D) Wild-type β-catenin (control) merged with CG1(n). (E) Wild-type β-catenin (Wnt3a) merged with CG1(n). (F) Wild-type β-catenin (control) axial view. (G) Wild-type β-catenin (Wnt3a) axial view . (H) CG1(n) axial view. (I) Wild-type β-catenin (control) and CG1(n) merged axial view. (J) Wild-type β-catenin (Wnt3a) and CG1(n) merged axial view.

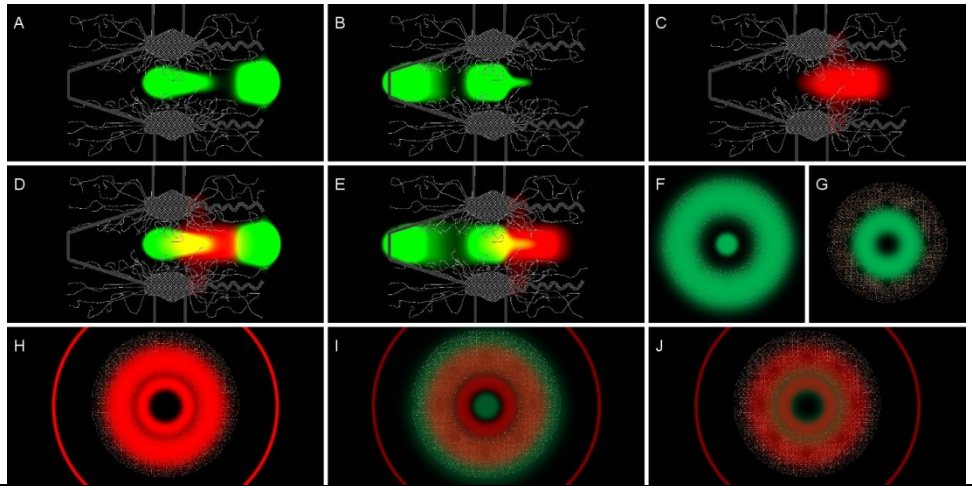

Figure 43. 3D Localization Comparison of Wild-Type β-Catenin with C-terminus of CG1. Comparison at x-axial peak of CG1(c) (20 nm to 50 nm, cytoplasmic side). (A) Wild-type β-catenin (control). (B) Wild type β-catenin (Wnt3a). (C) CG1(c). (D) Wild-type β-catenin (control) merged with CG1(c). (E) Wild-type β-catenin (Wnt3a) merged with CG1(c). (F) Wild-type β-catenin (control) axial view. (G) Wild-type β-catenin (Wnt3a) axial view. (H) CG1(c) axial view. (I) Wild-type β-catenin (control) and CG1(c) merged axial view. (J) Wild-type β-catenin (Wnt3a) and CG1(c) merged axial view.

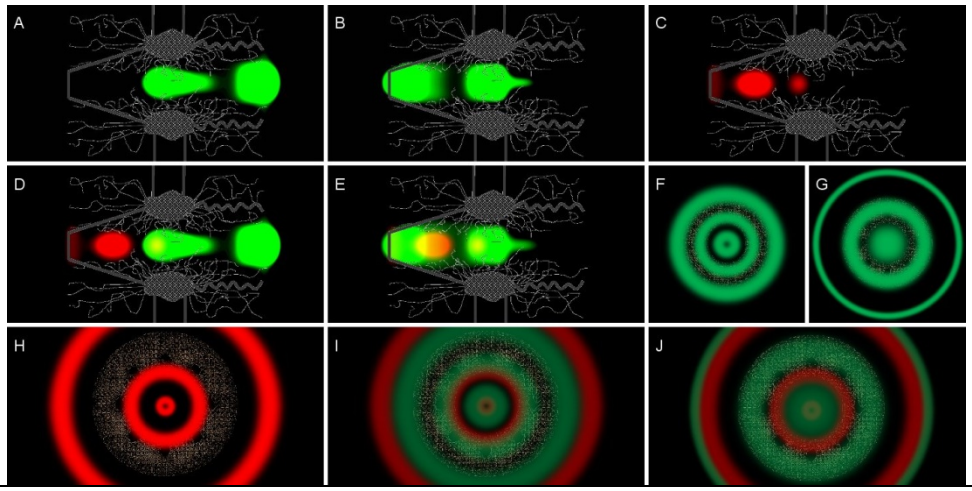

Figure 44. 3D Localization Comparison of Wild-Type β-Catenin with C-terminus of Nup153. Comparison at x-axial peak of Nup 153 (50 nm to 80 nm, cytoplasmic side). (A) Wild-type β-catenin (control). (B) Wild type β-catenin (Wnt3a). (C) Nup153. (D) Wild-type β-catenin (control) merged with Nup153. (E) Wild-type β-catenin (Wnt3a) merged with Nup153. (F) Wild-type β-catenin (control) axial view. (G) Wild-type β-catenin (Wnt3a) axial view. (H) CG1(c) axial view. (I) Wild-type β-catenin (control) and Nup153 merged axial view. (J) Wild-type β-catenin (Wnt3a) and Nup153 merged axial view.

CHAPTER 4: DISCUSSION

Refining our understanding of the Wnt signaling pathway can improve our ability to prevent birth defects and treat a variety of maladies and diseases. Such diseases are caused when Wnt signaling malfunctions or genes that express various members of the cascade are mutated. These malfunctions include missing limbs at birth, abnormal bone density in the jaw and palate, failure to form teeth, and spina bifida [1,3,153]. Further, cancer can be the result when the pathway is activated after embryonic development has ceased [1,2]. The most commonly cited examples are colon cancer resulting from mutations in APC and liver cancer resulting from mutations in Axin or in the N-terminus of β-catenin [3,46,53].

An essential focal point of the study of gene expression is the NPC. Characterization of this major selective barrier to nucleocytoplasmic translocation is important to understanding many cellular processes. Refinement of the measure of transport kinetics provides important contributions to the understanding of the details of the role of the NPC, such as regulating access to the nucleus. Failure of this regulation can have consequences such as developmental defects or cancer. These processes involve the interaction of the NPC with various proteins [154-160]. Additionally, it is believed that precise localization of molecular interactions within the NPC central channel itself is directly relevant to cancer-drug targeting [161-164].

The protein Custos, a binding partner of β-catenin, and a member of the canonical Wnt signaling cascade [1], is shown in this study to localize (at the level of the nuclear envelope) primarily to the ONM. There it serves as a docking protein for β-catenin import to the nucleus, as evidenced via FRET. Although co-moving spFRET trajectories exiting the nucleus were detected, the role of Custos in export is less clear. The FRET data, along with the results of truncation of β-catenin on translocation efficiency, provide strong evidence that the import and export mechanisms of β catenin through the NPC are likely not the same. The role of Custos in the translocation of β-catenin is possibly limited to import, and no β-catenin-Custos FRET complexes were shown to begin their association in the nucleus. Further, we provide clear evidence that β-catenin enters the nucleus via translocation through the NPC. Over many thousand events, we never observed β-catenin or any of its truncates traverse the nuclear envelope at any point other than the NPC.

Fagotto and colleagues showed that in permeabilized cells [59], β-catenin localized to nuclear envelope and failed to enter the nucleus. This failure could be caused by Custos being washed away during the permeabilization. We propose that Custos is this missing cytosolic factor required for translocating β-catenin into the nucleus. Knockdown of Custos appeared to have a muted effect on translocation of β-catenin in the absence of Wnt3a. However, the effect of Custos knockdown on the nuclear import of β-catenin is clearly observed in the presence of the ligand. With Custos knocked down and in the absence of Wnt3a, there is less β-catenin detected even on the cytoplasmic side of the

pore than at baseline, specifically at approximately +40 nm to +60 nm to the cytoplasmic side of the central plane of the pore (Figure 21 column B in comparison with Figure 21 column D). Note that baseline here refers to the low level of β-catenin that enters the nucleus even under control conditions. This baseline is presumably below the threshold required to activate transcription of Wnt target genes.

The efficiency of the knockdown may be roughly estimated from the results of the single-molecule analysis. Before knockdown of Custos, the N/C ratio of β-catenin in the NPC was 0.38. After knockdown, the N/C ratio decreased to 0.08. This may be due to the sharply decreased presence of β-catenin in the region between +20 nm to +60 nm in the cytoplasmic side of the pore with Custos knockdown. There may be a missing interaction in that region that requires Custos at normal levels. After 3 hrs of Wnt3a stimulation, the N/C ratio of β-catenin in the NPC is decreased from 3.13 without knockdown to 1.5, a decrease of 67%. Further, with knockdown, there appears to be an accumulation of β-catenin in this same region, providing more evidence for an interaction in that area that requires normal levels of Custos. It is possible also that Custos interacts with one of the FG Nups, whether through β-catenin or independently. Nup358, CG1, and Nup98 have 3D probability density map peaks in this region (unpublished data, see Materials and Methods). Several Nups interact with β-catenin, such as Nup62, Nup98, Nup358, and Nup153 [56,62], all of these present, according to our data, in the +40 nm to +60 nm region in question. (Note that the co-localization of β-catenin with TPR is not particularly convincing.)

Normally with Wnt3a stimulation, the 2D distribution of β-catenin in the NPC is biased strongly to the nucleoplasmic side of the pore. However, when Custos is knocked down, β-catenin appears to be concentrated in the central channel area of the NPC (-40 nm to 60 nm), with a bias to the cytoplasmic side (Figure 21 column B in comparison with Figure 21 column D). This clumping of β-catenin suggests that some factor is missing to translocate β-catenin through the NPC. Our data suggest that this factor is Custos. (Nups that show peaks in this region are Nup98, Nup62, Nup54, Nup58, POM121, Nup153, and TPR.) It may be that Custos facilitates interaction between these Nups and β-catenin in this region. Knockdown of Custos appears to cause β-catenin translocation to stall in the central channel area. Taken together, these data suggest strongly that that Custos plays a vital role in the regulation of nuclear import of β-catenin. In this study we refine a model previously proposed [35], in which Wnt3a stimulation frees Custos from binding with Dishevelled and CK1. We add to this model that Custos travels with β-catenin into the nucleus where they dissociate (Figure 45). Whether β-catenin is a transport receptor and Custos is the cargo on its way to another role in the nucleus is not known. Future work is required to determine the role, if any, Custos plays in β-catenin export.

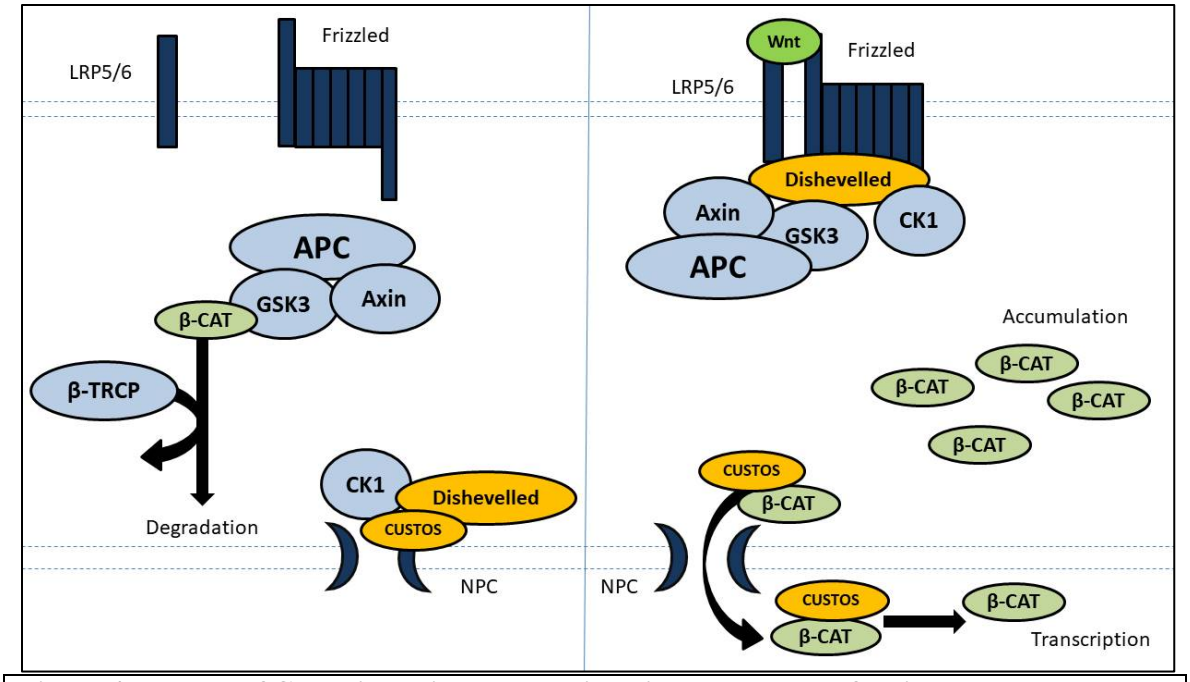

Figure 45. Model of Custos' role in the Wnt signaling Pathway. Left, without Wnt stimulation, Dishevelled and CK1 are in a complex with Custos at the NPC. Right, With Wnt stimulation, recruitment of CK1 and Dishevelled free Custos act as a docking protein for β-catenin translocation and dissociating in the nucleus. After [1] and [35].

Translocation dynamics of wild-type β-catenin are affected by the duration of Wnt3a stimulation. Import efficiency of β-catenin quickly shows a sharp increase by 1 hour and continues to increase until 4 hours in response to Wnt3a stimulation. Import efficiency decreases through 8 hours, the longest timepoint tested in this study. The return to control levels of import efficiency takes longer than 8 hours, based on the still-elevated import efficiency at 8 hours. Export efficiency showed a reverse pattern, decreasing through 4 hours, after which it increases through 8 hours, reaching level not significantly different from control. Import efficiency remains elevated (33%) at 8 hours (*vs* 19% at control) whereas export efficiency has recovered at that timepoint. This implies that β-catenin remains in the nucleus at higher than basal levels for a period longer than 8 hours.

Translocation dynamics differed between β-catenin tagged with GFP on the C-terminus and β-catenin tagged with GFP on the N-terminus. C-terminus tagged β-catenin was used in this study for investigation of timecourse of wnt stimulation, spFRET, and TopFlash assay. N-terminus tagged β-catenin was used for Custos knockdown, comparison with the truncates, and interaction with the FG Nups. Import and export efficiency of the C-terminus tagged β-catenin (19.1±3.1% and 45.1±4.9%, respectively) were elevated over N-terminal GFP β-catenin (14.0±2.3% import and 38.0±4.9% export). Although unexpected, this finding is not entirely surprising. Dar and colleagues [53] showed that removal of part of the C terminus reduces transcriptional activity. Further, deletion of the C-terminus appears to increase nuclear localization of β-catenin. It is possible that fusing GFP to the C-terminus of the molecule may sterically interfere with the function of the C-terminus or cause a conformational change that reduces the efficacy of C-terminus function [54,57] in its interaction with the NPC, ARM repeats [58,165], or both. The way in which translocation efficiency was measured in this study takes into account concentration of β-catenin, at least in the vicinity of the NPC (within approximately 500 nm of it). That is, efficiency is a fraction of interactions with the NPC. This is evidence that import of β-catenin is not merely the result of a concentration gradient.

Truncation of the β-catenin protein changes the efficiency of translocation in complex ways, with the effect on import more defined than on export. Removing the C-terminus and subsequent groups of three ARM repeats yields a cyclic pattern of increase and decrease of import efficiency. That is, removing the C-terminus from the wild-type molecule (dCT) results in an increase of import efficiency. Removal of three more (d9)

results in a decrease in import efficiency. Removal of further truncations (d6 and d3) result in further increase (Figure 29). This cyclic change in import efficiency with progressive truncation of the molecule may reflect the repeating structure of the β-catenin ARM region. This pattern does hold for NTR also under control conditions. However, this cyclic pattern was not seen in export efficiency. Export efficiency does not show a clear pattern of change with truncation of the molecule. There was a relatively large increase in export efficiency of d9 under control conditions and a similar increase in export efficiency of d3 under Wnt3a stimulation. The latter perhaps cannot be weighted heavily because of the possibility of the size-related effect of d3 interfering with measurable facilitated export.

Several previous studies have found ARM repeats 10-12, along with the C-terminus, to be necessary for import of β-catenin into the nucleus, although there is not universal agreement on the necessity of the C-terminus for interaction with the NPC. The most important region in the structure of β-catenin (in terms of regulation of import) is the C-terminus. Truncation of the C-terminus results in increased and inappropriate import into the nucleus combined with increased TCF-mediated gene expression. Other truncations of the molecule resulted in varied levels of dysregulation of translocation, including the increased import of d3 and the failure to interact functionally with the NPC of d9. However, only truncation of the C-terminus resulted in increased gene transcription. Wnt3a stimulation may activate β-catenin signaling not only by increasing its cytosolic levels, but by regulating the conformation of C-terminus [57]. It has been shown that changes to the C-terminus conformation cause upregulation of transcriptional activity

[54]. It may be that the C-terminus of β-catenin may change conformation in response to Wnt stimulation, which may expose ARM repeats to interaction with the NPC [55,57].

Several previous studies have reported that ARM 10-12 is necessary for import of β-catenin into the nucleus [52,54-57,62]. We find here that its necessity is ambiguous. (Both d3 and d6 lack this region but do show some import activity). Further, although 10-12 most resembles the HEAT repeats of Importin-β [62], we find it is not sufficient for import, as shown in the translocation dynamics of 10-12 and 10-12C. The C-terminus also has been suggested as unnecessary for import of β-catenin [56], and we find evidence here, in the translocation dynamics of dCT, to support that assertion. Our TopFlash results suggest the role of the C-terminus to be a bit more complex, and provide evidence here that the C-terminus, among other roles, may be an important regulator preventing the import of β-catenin into the nucleus in the absence of Wnt3a stimulation.

Truncate d3 at a mass of 56 kDa, is in the gray zone of the NPCs size exclusion limit (considered 40 60 kDa), whereas d6 is well above the limit at 72 kDa. Predictably, no translocating d6 molecules were detected in the central passive diffusion channel of the NPC. On the other hand, truncates d3 and 10-12C showed a bimodal transport route [Figure 30 (panels CE, DE, EE, CF, DF, and EF) and 31 (panels CE, DE, EE, CF, DF, and EF) and Table 3] being found in both the facilitated transport channel of the pore and in the passive diffusion central channel of the pore. We propose that this bimodal transport route is explained by the structure of the flexible structure of the molecules. In a linear conformation and perhaps approaching the NPC in a linear orientation, d3 or 10-

12C is just small enough to diffuse passively through the center of the NPC. On the other hand, if it encounters the pore in any other conformation or perhaps in another orientation, the primary interaction of the molecule is with the FG Nups and the translocation occurs through the facilitated transport route.

Because it is larger at 82 kDa, the similarity between truncate 10-12C and d3 is unexpected. Truncate 10-12, at 67 kDa, does not show this bimodal transport route. Truncate 10-12 differs from d3 and 10-12C in that it lacks either terminus. These results suggest is possible that this bimodal transport route phenomenon requires the presence of a disordered region to occur. Further, in all truncates that include either disordered terminus, the fluorophore is separated from the ARM repeats by a disordered region, whether N-terminus or C-terminus.

Therefore, it is possible that the d3 and 10-12C ARM repeat regions interact with the FG Nups during translocation, whereas the fluorophore can either be detected in the FG repeat region (facilitated transport channel) or being pulled along through the central diffusion channel. Truncate 10-12, having no disordered region and presumably more rigid, does not show this pattern perhaps because the fluorophore does not have the freedom to be in the central diffusion channel while the ARM repeats interact with the FG Nups in the facilitated transport channel. With Wnt3a stimulation, the NTR of the truncates does not appear to show a clear pattern. However, it can be noted that the only truncate lacking a disordered region (10-12) shows a very negative NTR compared with the other truncates; this may imply that the C-terminus (or at least either disordered

terminus) is required for the molecule to be retained in the nucleus. The low NTR of truncate 10-12 is attributable to the low import efficiency combined with a high export efficiency. The only truncate with a comparable export efficiency is d3; however, the high export efficiency of d3 is offset by its very high import efficiency, explained above, resulting in an unremarkable NTR.

It is often asserted that import of β-catenin is a result of rising levels of the molecule in the cytoplasm, the mechanism being that of a concentration gradient. However, it is not clear whether this alone is the mechanism. The structure and interactions of β-catenin as described in the previous paragraphs provide some doubt and reason to investigate this assumption further. It is possible that translocation of β-catenin is a regulatory event in the manner of other events upstream in the signaling cascade, such as the recruitment of the destruction complex to the plasma membrane. Import may be a regulatory event at the NPC, and this regulation seems to involve the C-terminus. Truncation of the β-catenin molecule interferes with its translocation, clearly implying that its structure itself is a regulatory mechanism. When the C-terminus is removed from the molecule (resulting in dCT), translocation is dysregulated such that the molecule is imported to the nucleus inappropriately (*ie*, increased translocation efficiency in the absence of Wnt3a), possibly causing inappropriate timing of gene expression. Further truncation of the molecule, however, meets with the "next step" of regulatory mechanism, *ie*, the need for nearly the entire ARM repeat region to be intact for interaction with TCF and thus gene expression.

β-catenin and all of the truncates used in this study contain significant regions of disorder, with the exception of truncate 10-12. Most eukaryotic proteins contain regions of disorder, and approximately one third of have little or no secondary structure. Many of these intrinsically disordered proteins (IDPs) are known to localize in the nucleus, and in the NPC, where they play important roles in signaling, genome fidelity, and regulatory functions [166-173]. It has been proposed that the transport route of proteins with significant regions of disorder depend not only on size but on another criterion, the ratio of charged to hydrophobic residues in the amino acid sequence (C/H ratio). Further, C/H ratio appears to be the dominant criterion in proteins with a C/H ratio over approximately 0.37 [166]. Proteins with a C/H ratio over this value have an increased probability of translocating through the central diffusion channel despite being too large. The C/H ratio of GFP-d3 is 0.67; the C/H ratio of 2xGFP-10-12C is 0.73. These values are both high enough (for disordered proteins) to traverse the central diffusion channel despite their mass. Although the C/H ratio of 2xGFP-10-12 is 0.71, this construct contains no predicted region of disorder. It is comprised of three ARM repeats and the fluorophore. We reason that this is why 10-12 does not show the bimodal transport route of d3 and 1012C.

In this study we provide support for a model of β-catenin import that requires Custos as a docking protein. Custos and β-catenin form a complex in the cytoplasm and move together through the NPC into the nucleus, where they dissociate in the nucleus. During import, β-catenin co-localizes with FG Nups such as the Nup62 complex, POM121, and Nup153. Further, we provide support for the hypothesis that import of β-catenin into the

nucleus is a regulatory event at the NPC rather than merely the result of a concentration gradient forming from the accumulation of β-catenin in the cytoplasm. The role of Custos in the export of β-catenin is less clear, and our understanding of the interactions between the Custos–β-catenin complex and the Nups needs refinement.

Although it is shown that the interactions between Custos, β-catenin, and the NPC comprise a regulatory checkpoint in the Wnt signaling pathway, the details of this interaction are not clear. Future studies are required to investigate the configuration of this interaction. One possibility is that Custos and β-catenin form a trimeric complex with one or more FG Nups. Another possibility is that either Custos or β-catenin act as a scaffold for the other's interaction with the FG Nups. Future studies may take a finer-grained approach to mutation of the ARM repeat region of β-catenin to study its effect on translocation. It does not appear the transcription activation function of β-catenin can be separated entirely from its translocation function. However, additional study of the ARM repeat region and comparison of it with the HEAT repeats of Importin-β1 may provide an improved understanding of this important regulatory mechanism. SPEED microscopy is poised to take a leading role in this study, and help lead to innovations in human health care.

REFERENCES

1. Komiya, Y.; Habas, R. Wnt signal transduction pathways. Organogenesis 2008, 4, 68–75.

2. Reya T, Clevers H. Wnt signalling in stem cells and cancer. Nature. 2005;434(7035):843-50.

3. Logan CY, Nusse R. The Wnt signaling pathway in development and disease. Annual review of cell and developmental biology. 2004;20:781-810.

4. Perrimon N, Pitsouli C, Shilo B-Z. Signaling Mechanisms Controlling Cell Fate and Embryonic Patterning. Cold Spring Harbor Perspectives in Biology. 2012;4(8).

5. Editorial: Signaling Pathways in Embryonic Development
Juan J. Sanz-Ezquerro1*, Andrea E. Münsterberg2 and Sigmar Stricker Front. Cell Dev. Biol., 31 August 2017

6. Nusse, Ft., Brown, A., Papkoff, J., Scambler, P., Shackleford, G., McMahon, A., Moon, R., and Varmus, H. (1991). A new nomenclature for int-l and related genes: the Wnt gene family. Cell 64, 231.

7. Roel Nusse and Harold E. Varmus. Wnt Genes. Cell, Vol. 69, 1073-1067, June 26, 1992.

8. Huelsken, J. and W. Birchmeier, New aspects of Wnt signaling pathways in higher vertebrates. Curr Opin Genet Dev, 2001. 11(5): p. 547-53.

9. Keller, R., Shaping the vertebrate body plan by polarized embryonic cell movements. Science, 2002. 298(5600): p. 1950-4.

10. Sokol, S., A role for Wnts in morpho-genesis and tissue polarity. Nat Cell Biol, 2000. 2(7): p. E124-5.

11. Wodarz, A. and R. Nusse, Mechanisms of Wnt signaling in development. Annu Rev Cell Dev Biol, 1998. 14: p. 59-88.

12. Yamaguchi, T.P., Heads or tails: Wnts and anterior-posterior patterning. Curr Biol, 2001. 11(17): p. R713-24.

13. Filiz Tepekoy, Gokhan Akkoyunlu, Ramazan Demir. The role of Wnt signaling members in the uterus and embryo during pre-implantation and implantation. J Assist Reprod Genet. 2015 Mar; 32(3): 337–346.

14. Nusse R. "Wnt signaling in disease and in development". Cell Research. 2005:15 (1): 28–32.

15. Giles, R.H., J.H. van Es, and H. Clevers, Caught up in a Wnt storm: Wnt signaling in cancer. Biochim Biophys Acta, 2003. 1653(1): p. 1-24.

16. Lustig, B. and J. Behrens, The Wnt signaling pathway and its role in tumor development. J Cancer Res Clin Oncol, 2003. 129(4): p. 199-221.

17. Habas R and Dawid IB. Dishevelled and Wnt signaling: is the nucleus the final frontier? J Biol 2005;4:2.

18. Astrid S. Pfister, Michael Kühl. WNT Signaling in Health and Disease, in Progress in Molecular Biology and Translational Science, 2018

19. Bryan T. MacDonald, Keiko Tamai, and Xi He. Wnt/β-catenin signaling: components, mechanisms, and diseases. Dev Cell. 2009 Jul; 17(1): 9–26.

20. Cadigan KM, Fish MP, Rulifson EJ, Nusse R. 1998. Wingless repression of Drosophila frizzled 2 expression shapes the Wingless morphogen gradient in the wing. Cell 93:767–77

21. Strigini M, Cohen SM. 2000. Wingless gradient formation in the Drosophila wing. Curr. Biol. 10:293–300

22. Zecca M, Basler K, Struhl G. 1996. Direct and long-range action of a wingless morphogen gradient. Cell 87: 833–44

23. Daniel Routledge, Steffen Scholpp. Mechanisms of intercellular Wnt transport. Development 2019 146: dev176073. 15 May 2019

24. Greco V, Hannus M, Eaton S. 2001. Argosomes: a potential vehicle for the spread of morphogens through epithelia. Cell 106: 633–45

25. Ramirez-Weber FA, Kornberg TB. 1999. Cytonemes: cellular processes that project to the principal signaling center in Drosophila imaginal discs. Cell 97: 599–607

26. Willert K, Brown JD, Danenberg E, Duncan AW, Weissman IL, Reya T, Yates JR, 3rd, Nusse R. Wnt proteins are lipid-modified and can act as stem cell growth factors. Nature. 2003;423:448–452.

27. Hoang B, Moos M Jr, Vukicevic S, Luyten FP. 1996. Primary structure and tissue distribution of FRZB, a novel protein related to Drosophila frizzled, suggest a role in skeletal morphogenesis. J. Biol. Chem. 271: 26131–37

28. Rattner A, Hsieh JC, Smallwood PM, Gilbert DJ, Copeland NG, et al. 1997. A family of secreted proteins contains homology to the cysteine-rich ligand-binding domain of frizzled receptors. Proc. Natl. Acad. Sci. USA 94: 2859–63

29. Bafico A, Gazit A, Pramila T, Finch PW, Yaniv A, Aaronson SA. 1999. Interaction of frizzled related protein (FRP) with Wnt ligands and the Frizzled receptor suggests alternative mechanisms for FRP inhibition of Wnt signaling. J. Biol. Chem. 274: 16180–87

30. Uren A, Reichsman F, Anest V, Taylor WG, Muraiso K, et al. 2000. Secreted frizzled-related protein-1 binds directly to Wingless and is a biphasic modulator of Wnt signaling. J. Biol. Chem. 275: 4374–82

31. Glinka A, Wu W, Delius H, Monaghan AP, Blumenstock C, Niehrs C. 1998. Dickkopf-1 is a member of a new family of secreted proteins and functions in head induction. Nature 391: 357–62

32. Itasaki N, Jones CM, Mercurio S, Rowe A, Domingos PM, et al. 2003. Wise, a context-dependent activator and inhibitor of Wnt signalling. Development 130: 4295–305

33. Kimelman, D., Xu, W. β-Catenin destruction complex: insights and questions from a structural perspective. Oncogene 25, 7482–7491 (2006).

34. Daniel B. Lybrand, Misha Naiman, Jessie May Laumann, Mitzi Boardman, Samuel Petshow, Kevin Hansen, Gregory Scott, Marcel Wehrli. Destruction complex dynamics: Wnt/β-catenin signaling alters Axin-GSK3β interactions in vivo. Development 2019 146: dev164145 doi: 10.1242/dev.164145 Published 2 July 2019

35. Mandrekar, Noopur. “Characterization of a novel component of Wnt signaling pathway using zebrafish as a model organism.” PhD diss., Temple University, 2016.

36. Chan Gao, Ye-Guang Chen. Dishevelled: The hub of Wnt signaling. Cellular Signalling. Volume 22, Issue 5, May 2010, Pages 717-727

37. Fahmy OG, Fahmy MJ. Differential Gene Response to Mutagens in Drosophila Melanogaster. Genetics. 1959 Nov;44(6):1149-71.

38. Wallingford J and Habas R. The developmental biology of Dishevelled: an enigmatic protein governing cell fate and cell polarity. Development 2005;132:4421-4436.

39. Boutros M, Mlodzik M. Dishevelled: at the crossroads of divergent intracellular signaling pathways. Mech Dev. 1999 May;83(1-2):27-37.

40. Habas R. Dawid IB. Dishevelled and Wnt signaling: is the nucleus the final frontier? Journal of Biology volume 4, 2 (2005).

41. Su B. “The role of Ric8a during early vertebrate development.” PhD diss., Temple University, 2018.

42. Habas R. Canonical Wnt Signaling: An Unexpected New Player. Developmental Cell 2006;11:138-139.

43. Prilusky, J et al. FoldIndex©: a simple tool to predict whether a given protein sequence is intrinsically unfolded. Bioinformatics 2005;21: 3435–3438. http://www.vazymolo.org/MeDor/

44. Wong HC, Bourdelas A, Krauss A, Lee HJ, Shao Y, Wu D, Mlodzik M, Shi DL, Zheng J. Direct binding of the PDZ domain of Dishevelled to a conserved internal sequence in the C-terminal region of Frizzled. Mol Cell. 2003 Nov;12(5):1251-60.

45. A. Cliffe, F. Hamada, M. Bienz. A role of Dishevelled in relocating Axin to the plasma membrane during wingless signaling. Curr. Biol., 13 (11) (2003), p. 960

46. Xu W, et al. Mechanistic insights from structural studies of β-catenin and its binding partners. Journal of Cell Science 120, 3337-3344.

47. Kidd, A. R., 3rd, Miskowski, J. A., Siegfried, K. R., Sawa, H. and Kimble, J. (2005). A β-catenin identified by functional rather than sequence criteria and its role in Wnt/MAPK signaling. Cell 121, 761-772.

48. Korswagen, H. C., Herman, M. A. and Clevers, H. C. (2000). Distinct β-catenins mediate adhesion and signalling functions in C. elegans. Nature 406, 527-532.

49. Kraus C, Liehr T, Hülsken J, Behrens J, Birchmeier W, Grzeschik KH, Ballhausen WG (September 1994). "Localization of the human beta-catenin gene (CTNNB1) to 3p21: a region implicated in tumor development". Genomics. 23 (1): 272–4.

50. Thomas A. Graham, Carole Weaver, Feng Mao, David Kimelman, Wenqing Xu. Crystal Structure of a b-Catenin/Tcf Complex. Cell, Vol. 103, 885–896, December 8, 2000.

51. Fang, D., Hawke, D., Zheng, Y., Xia, Y., Meisenhelder, J., Nika, H., Mills, G. B., Kobayashi, R., Hunter, T. and Lu, Z. (2007). Phosphorylation of β-catenin by AKT promotes β-catenin transcriptional activity. J. Biol. Chem. 282, 11221-11229.

52. Bienz M, et al. Armadillo/β-catenin signals in the nucleus – proof beyond a reasonable doubt? Nature Cell Biology volume 5, pages179–182(2003).

53. Dar MS et al. Terminal regions of β-catenin are critical for regulating its adhesion and transcription functions. Biochimica et Biophysica Acta (BBA) - Molecular Cell Research Volume 1863, Issue 9, September 2016, Pages 2345-2357

54. Brembeck FH, et al. Balancing cell adhesion and Wnt signaling, the key role of β-catenin. Current Opinion in Genetics & Development Volume 16, Issue 1, February 2006, Pages 51-59.

55. Koike M, Kose S, Furuta M, Taniguchi N, Yokoya F, Yoneda Y, Imamoto N. beta-Catenin shows an overlapping sequence requirement but distinct molecular interactions for its bidirectional passage through nuclear pores.J Biol Chem. 2004 Aug 6; 279(32):34038-47.

56. Yang X, et al. Nucleoporin 62-Like Protein Activates Canonical Wnt Signaling through Facilitating the Nuclear Import of β-Catenin in Zebrafish. Molecular and Cellular Biology Mar 2015, 35 (7) 1110-1124; DOI: 10.1128/MCB.01181-14

57. Gottardi CJ, et al. Distinct molecular forms of β-catenin are targeted to adhesive or transcriptional complexes. J Cell Biol. 2004 Oct 25; 167(2): 339–349.

58. Heuberger, et al. Interplay of Cadherin-Mediated Cell Adhesion and Canonical Wnt Signaling. Cold Spring Harb Perspect Biol. 2010 Feb; 2(2): a002915.

59. Fagotto, F., U. Gluck, and B.M. Gumbiner, Nuclear localization signal-independent and importin/karyopherin-independent nuclear import of beta-catenin. Curr Biol, 1998. 8(4): p. 181

60. Henderson, B.R., Nuclear-cytoplasmic shuttling of APC regulates beta-catenin subcellular localization and turnover. Nat Cell Biol, 2000. 2(9): p. 653-60.

61. Henderson, B.R. and F. Fagotto, The ins and outs of APC and beta-catenin nuclear transport. EMBO Rep, 2002. 3(9): p. 834-9.

62. Jamieson C, et al. Targeting the β-catenin nuclear transport pathway in cancer. Seminars in Cancer Biology Volume 27, August 2014, Pages 20-29.

63. Sharma, M., et al., Specific armadillo repeat sequences facilitate beta-catenin nuclear transport in live cells via direct binding to nucleoporins Nup62, Nup153, and RanBP2/Nup358. J Biol Chem, 2012. 287(2): p. 819-31.

64. Lee SJ, Imamoto N, Sakai H, Nakagawa A, Kose S, Koike M, Yamamoto M, Kumasaka T, Yoneda Y, Tsukihara T. The adoption of a twisted structure of importin-

beta is essential for the protein-protein interaction required for nuclear transport. J Mol Biol. 2000 Sep 8; 302(1):251-64.

65. Yang, W. & Musser, S.M. Nuclear import time and transport efficiency depend on importin beta concentration. J. Cell Biol. 174, 951–961 (2006).

66. Sun, C., Yang, W., Tu, L.C. & Musser, S.M. Single-molecule measurements of importin alpha/cargo complex dissociation at the nuclear pore. Proc. Natl. Acad. Sci. USA 105, 8613–8618 (2008).

67. Bayliss R, et al. Structural Basis for the Interaction between FxFG Nucleoporin Repeats and Importin-b in Nuclear Trafficking. Cell, Vol. 102, 99–108, July 7, 2000.

68. Fagotto F. Looking beyond the Wnt pathway for the deep nature of β-catenin, EMBO Rep. 14 (2013) 422–433.

69. S. Kose, N. Imamoto, T. Tachibana, M. Yoshida, Y. Yoneda. β-Subunit of nuclear pore-targeting complex (importin-β) can be exported from the nucleus in a Ran-independent manner. J. Biol. Chem., 274 (1999), pp. 3946-3952

70. Cong, F. and H. Varmus, Nuclear-cytoplasmic shuttling of Axin regulates subcellular localization of beta-catenin. Proc Natl Acad Sci U S A, 2004. 101(9): p. 2882-7.

71. Suh, E.K. and B.M. Gumbiner, Translocation of beta-catenin into the nucleus independent of interactions with FG-rich nucleoporins. Exp Cell Res, 2003. 290(2): p. 447-56.

72. Asally, M. and Y. Yoneda, Beta-catenin can act as a nuclear import receptor for its partner transcription factor, lymphocyte enhancer factor-1 (lef-1). Exp Cell Res, 2005. 308(2): p. 357-63.

73. Nicola Wiechens and François Fagotto. CRM1- and Ran-independent nuclear export of β-catenin. Current Biology VOLUME 11, ISSUE 1, P18-28, JANUARY 09, 2001.

74. F. Yokoya, N. Imamoto, T. Tachibana, Y. Yoneda. β-Catenin can be transported into the nucleus in a Ran-unassisted manner. Mol. Biol. Cell, 10 (1999), pp. 1119-1131

75. Komiya Y.; Mandrekar, N.; Sato, A.; Dawid, I.B.; Habas, R. Custos controls β-catenin to regulate head development during vertebrate embryogenesis. Proc. Natl. Acad. Sci. USA 2014, 36, 13099–13104.

76. Young KH (February 1998). "Yeast two-hybrid: so many interactions, (in) so little time". Biology of Reproduction. 58 (2): 302–11.

77. Joung JK, Ramm EI, Pabo CO (June 2000). "A bacterial two-hybrid selection system for studying protein-DNA and protein-protein interactions". Proceedings of the National Academy of Sciences of the United States of America. 97 (13): 7382–7.

78. Hurt JA, Thibodeau SA, Hirsh AS, Pabo CO, Joung JK (October 2003). "Highly specific zinc finger proteins obtained by directed domain shuffling and cell-based selection". Proceedings of the National Academy of Sciences of the United States of America. 100 (21): 12271–6.

79. Akrap N et al. Förster distances for FRET between mCherry and other Visible Fluorescent Proteins. Anal Biochem. 2010 Jul 1; 402(1): 105–106.

80. Rout, M.P.; Blobel, G. Isolation of the yeast nuclear pore complex. J. Cell. Biol. 1993, 123, 771–783.

81. Gorlich, D.; Kutay, U. Transport between the nucleus and cytoplasm. Annu. Rev. Cell Dev. Biol. 1999, 15, 607–660.

82. Maul, G.G. Nuclear pore complexes. Elimination and reconstruction during Mitosis. J. Cell Biol. 1977, 74, 492–500.

83. Macara, I.G. Transport into and out of the Nucleus. Microbiol. Mol. Biol. Rev. 2001, 65, 570–594.

84. Yang, W. Distinct, but not completely separate spatial transport routes in the nuclear pore complex. Nucleus 2013, 4, 166–175.

85. Maimon, T.; Nadav, E.; Dahan, I.; Medalia, O. The human nuclear pore complex as revealed by cryo-electron tomography. Structure 2012, 20, 998–1006.

86. Maeshima, K.; Iino, H.; Hihara, S.; Funakoshi, T.; Watanabe, A.; Nishimura, M.; Nakatomi, R.; Yahata, K.; Imamoto, F.; Hashikawa, T.; et al. Nuclear pore formation but not nuclear growth is governed by cyclin-dependent kinases (CDKS) during interphase. Nat. Struct. Mol. Biol. 2010, 17, 1065–1072.

87. Arias, I.M. Nuclear pore complex. In Chichester; John Wiley & Sons: West Sussex, UK; pp. 147–155.

88. Wente, S.R.; Rout, M.P. The nuclear pore complex and nuclear transport. Cold Spring Harb. Perspect. Biol. 2010, 2, doi:10.1101/cshperspect.a000562.

89. Gant TM, Goldberg MW, Allen TD: Nuclear envelope and nuclear pore assembly: analysis of assembly intermediates by electron microscopy. Curr Opin Cell Biol. 1998, 10: 409-415. 10.1016/S0955-0674(98)80018-5.

90. Hinshaw JE, Carragher BO, Milligan RA: Architecture and design of the pore complex. Cell. 1992, 69: 1133-1141.

91. Weberruss, M. and W. Antonin, Perforating the nuclear boundary - how nuclear pore complexes assemble. J Cell Sci, 2016. 129(24): p. 4439-4447.

92. Vasu, S.K.; Forbes, D.J. Nuclear pores and nuclear assembly. Curr. Opin. Cell Biol. 2001, 13, 363–375.

93. Lim, R.Y.; Fahrenkrog, B. The nuclear pore complex up close. Curr. Opin. Cell Biol. 2006, 18, 342–347.

94. Strawn, L.A.; Shen, T.; Shulga, N.; Goldfarb, D.S.; Wente, S.R. Minimal nuclear pore complexes define FG repeat domains essential for transport. Nat. Cell Biol. 2004, 6, 197–206.

95. Milles, S.; Lemke, E.A. Single molecule study of the intrinsically disordered FG-repeat nucleoporin 153. Biophys. J. 2011, 101, 1710–1719.

96. Lim, R.Y.; Huang, N.P.; Koser, J.; Deng, J.; Lau, K.A.; Schwarz-Herion, K.; Fahrenkrog, B.; Aebi, U. Flexible phenylalanine-glycine nucleoporins as entropic barriers to nucleocytoplasmic transport. Proc. Natl. Acad. Sci. USA 2006, 103, 9512–9517.

97. Miao, L.; Schulten, K. Transport-related structures and processes of the nuclear pore complex studied through molecular dynamics. Structure 2009, 17, 449–459.

98. Yang W. Natively unfolded nucleoporins in nucleocytoplasmic transport. Clustered or evenly distributed? Nucleus 2011;2:10-16.

99. Erickson HP. Size and shape of protein molecules at the nanometer level determined by sedimentation, gel filtration, and electron microscopy. Biol Proceed Online. 2009;11:32-51. Published 2009 May 15. doi:10.1007/s12575-009-9008-x

100. Görlich D, Kutay U: Transport between the cell nucleus and the cytoplasm. Annu Rev Cell Dev Biol. 1999, 15: 607-660. 10.1146/annurev.cellbio.15.1.607.

101. Mattaj, I.W.; Englmeier, L. Nuclecytoplasmic transport: The soluble phase. Annu. Rev. Biochem. 1998, 67, 265–306.

102. Terry, L.J.; Shows, E.B.; Wente, S.R. Crossing the nuclear envelope: Hierarchical regulation of nucleocytoplasmic transport. Science 2007, 318, 1412–1416.

103. Patel, S.S.; Belmont, B.J.; Sante, J.M.; Rexach, M.F. Natively unfolded nucleoporins gate protein diffusion across the nuclear pore complex. Cell 2007, 129, 83–96.

104. Ma, J.; Yang, W. Three-dimensional distribution of transient interactions in the nuclear pore complex obtained from single-molecule snapshots. Proc. Natl. Acad. Sci. USA 2010, 107, 7305–7310.

105. Ma, J.; Liu, Z.; Michelotti, N.; Pitchiaya, S.; Veerapaneni, R.; Androsavich, J.R.; Walter, N.G.; Yang, W. High-resolution three-dimensional mapping of mRNA export through the nuclear pore. Nat. Commun. 2013, 4, doi:10.1038/ncomms3414.

106. Shahin, V.; Danker, T.; Enss, K.; Ossig, R.; Oberleithner, H. Evidence for Ca2+- and ATP-sensitive peripheral channels in nuclear pore complexes. FASEB J. 2001, 15, 1895–1901.

107. Weiss, K. Regulating access to the genome: Nucleocytoplasmic transport throughout the cell cycle. Cell 2003, 112, 441–451.

108. Akey CW, Goldfarb DS: Protein import through the nuclear pore is a multistep process. J Cell Biol. 1989, 109: 971-982.

109. Kohler, A.; Hurt, E. Exporting RNA from the nucleus to the cytoplasm. Nat. Rev. Mol. Cell Biol. 2007, 8, 761–773.

110. Goryaynov, A.; Ma, J.; Yang, W. Single-molecule studies of nucleocytoplasmic transport: From one dimension to three dimensions. Integr. Biol. 2012, 4, 10–21.

111. Bilokapic, S.; Schwartz, T.U. 3D ultrastructure of the nuclear pore complex. Curr. Opin. Cell Biol. 2012, 24, 86–91.

112. Hoelz, A.; Debler, E.W.; Blobel, G. The structure of the nuclear pore complex. Annu. Rev. Biochem. 2011, 80, 613–643.

113. Strambio-De-Castillia, C.; Niepel, M.; Rout, M.P. The nuclear pore complex: Bridging nuclear transport and gene regulation. Nat. Rev. Mol. Cell Biol. 2010, 11, 490–501.

114. Fahrenkrog, B.; Aebi, U. The nuclear pore complex: Nucleocytoplasmic transport and beyond. Nat. Mol. Cell Biol. 2003, 4, 757–766.

115. Chatel, G.; Fahrenkrog, B. Dynamics and diverse functions of nuclear pore complex proteins. Nucleus 2012, 3, 162–171.

116. Grimaldi, M.R. Cozzolino, L.; Malva, C.; Graziani, F.; Gigliotti, S. nup154 genetically interacts with cup and plays a cell-type-specific function during Drosophila melanogaster egg-chamber development. Genetics 2007, 175, 1751–1759.

117. Tang, S.; Presgrabes, D.C. Evolution of the Drosophila nuclear pore complex results in multiple hybrid incompatibilities. Science 2009, 323, 779–782.

118. Chakraborty, P.; Wang, Y.; Wei, J.H.; van Deursen, J.; Yu, H.; Malureanu, L.; Dasso, M.; Forbes, D.J.; Levy, D.E.; et al. Nucleoporin levels regulate cell cycle progression and phase-specific gene expression. Dev. Cell 2008, 15, 657–667.

119. Deng et al, Chromatin dynamics and genome organization in development and disease. In: Epigenetic Gene Expression and Regulation. Suming Huang, , Michael D. Litt, , and C. Ann Blakey, Eds. Elsevier Science & Technology 2015

120. Casolari JM, Brown CR, Komili S, West J, Hieronymus H, Silver PA. Genome-wide localization of the nuclear transport machinery couples transcriptional status and nuclear organization. Cell May 14, 2004;117(4):427– 39.

121. Capelson M, Liang Y, Schulte R, Mair W, Wagner U, Hetzer MW. Chromatin-bound nuclear pore components regulate gene expression in higher eukaryotes. Cell February 5, 2010;140(3):372– 83.

122. Laura T. Burns, Susan R. Wente. From Hypothesis to Mechanism: Uncovering Nuclear Pore Complex Links to Gene Expression. Molecular and Cellular Biology May 2014, 34 (12) 2114-2120; DOI: 10.1128/MCB.01730-13

123. Christopher Ptak, John D Aitchison, Richard W Wozniak. The multifunctional nuclear pore complex: a platform for controlling gene expression. Current Opinion in Cell Biology. Volume 28, June 2014, Pages 46-53

124. Takemaru K, Yamaguchi S, Lee YS, Zhang Y, Carthew RW, Moon RT. 2003. Chibby, a nuclear beta-catenin-associated antagonist of the Wnt/Wingless pathway. Nature 422:905–9.

125. Tago K, Nakamura T, Nishita M, Hyodo J, Nagai S, et al. 2000. Inhibition of Wnt signaling by ICAT, a novel beta-catenin-interacting protein. Genes Dev. 14:1741–49.

126. Daniels DL, Weis WI. 2002. ICAT inhibits beta-catenin binding to Tcf/Lef-family transcription factors and the general coactivator p300 using independent structural modules. Mol. Cell. 10:573–84.

127. Huang, B., Bates, M. & Zhuang, X. Super-resolution fluorescence microscopy. Annu.

Rev. Biochem. 78, 993-1016 doi:10.1146/annurev.biochem.77.061906.092014 (2009).

128. Leung, B. O. & Chou, K. C. Review of super-resolution fluorescence microscopy for
biology. Appl. Spectrosc. 65, 967-980 doi:10.1366/11-06398 (2011).

129. Hell, S. W.; Wichmann, J. Breaking the diffraction resolution
limit by stimulated emission: stimulated-emission-depletion fluorescence microscopy. Opt. Lett. 1994, 19, 780−782.

130. Betzig, E.; Patterson, G. H.; Sougrat, R.; Lindwasser, O. W.; Olenych, S.; Bonifacino, J. S.; Davidson, M. W.; Lippincott-Schwartz, 93.J.; Hess, H. F. Imaging intracellular fluorescent proteins at nanometer
resolution. Science 2006, 313, 1642−1645

131. Yang, W., Gelles, J. & Musser, S.M. Imaging of single-molecule translocation through nuclear pore complexes. Proc. Natl. Acad. Sci. USA 101, 12887–12892 (2004).

132. Yang, W. & Musser, S.M. Visualizing single molecules interacting with nuclear pore complexes by narrow-field epifluorescence microscopy. Methods 39, 316–328 (2006).

133. Schnell SJ, Tingey M. Single-molecule localization via SPEED microscopy of translocating soluble proteins in the nuclear pore complex in live mammalian cells. Methods in Molecular Biology: Springer Science+Business Media 2020 (submitted)

134. Ruba A, et al. 3D Tracking-Free Approach for Obtaining 3D Super-Resolution Information in Rotationally Symmetric Biostructures. J. Phys. Chem. B 2019, 123, 5107−5120

135. Fortes, P. and Razquin, N. In Vivo Evaluation of Regulatory Sequences by Analysis of Luciferase Expression. [Internet] 2009. [cited: 2020-MAY-13]. Available from: https://www.promega.com/resources/pubhub/in-vivo-evaluation-of-regulatory-sequences-by-analysis-of-luciferase-expression/

136. Gelles J (2014) Glimpse. Brandeis University

137. Herbert A (2013) Single Molecule Light Microscopy ImageJ Plugins. University of Sussex

138. Li Y, Junod SL, Ruba A, Kelich JM, Yang W (2019) Nuclear export of mRNA molecules studied by SPEED microscopy. Methods 153:46-62. doi:10.1016/j.ymeth.2018.08.005

139. Schnell SJ, Tingey M, Yang W: Single-molecule localization via SPEED microscopy of translocating soluble proteins in the nuclear pore complex in live mammalian cells. (Springer Protocols - Methods in Molecular Biology), in press.

140. Kelich JM, Ma J, Dong B, Wang Q, Chin M, Magura CM, Xiao W, Yang W (2015) Super-resolution imaging of nuclear import of adeno-associated virus in live cells. Molecular Therapy-Methods & Clinical Development 2:15047

141. Mortensen KI, Churchman LS, Spudich JA, Flyvbjerg H (2010) Optimized localization analysis for single-molecule tracking and super-resolution microscopy. Nature methods 7 (5):377

142. Quan T, Zeng S, Huang Z (2010) Localization capability and limitation of electron-multiplying charge-coupled, scientific complementary metal-oxide semiconductor, and charge-coupled devices for superresolution imaging. Journal of biomedical optics 15 (6):066005

143. Thompson RE, Larson DR, Webb WW (2002) Precise nanometer localization analysis for individual fluorescent probes. Biophysical journal 82 (5):2775-2783

144. Schnell SJ, Ma J, Yang W (2014) Three-dimensional mapping of mRNA export through the nuclear pore complex. Genes 5 (4):1032-1049

145. Mooney CZ (1997) Monte carlo simulation, vol 116. Sage publications

146. Mahadevan S (1997) Monte carlo simulation. Marcel Dekker, New York and Basel, Switzerland

147. Ma, J. et al. High-resolution three-dimensional mapping of mRNA export through the nuclear pore. Nat. Commun. 4, 2414 (2013).

148. Ma J, Goryaynov A, Yang W. Super-resolution 3D tomography of interactions and competition in the nuclear pore complex. Nature Structural & Molecular Biology 23, 239–247 (2016)

149. Ma, J., Goryaynov, A., Sarma, A. & Yang, W. Self-regulated viscous channel in the nuclear pore complex. Proc. Natl. Acad. Sci. USA 109, 7326–7331 (2012).

150. Li Y., Luo W. and Yang W. (2018) Signal-Regulated Nuclear Transport and Accumulation of Smad Proteins studied by High-Speed Single-Molecule Microscopy. Biophysical J. 114, 2243. https://doi.org/10.1016/j.bpj.2018.03.018

151. Albertazzi L, et al. Quantitative FRET analysis with the EGFP-mCherry fluorescent protein pair. Photochem. Photobiol. 2009; 85: 287-297.

152. Ruba, Andrew. “Studying transmembrane protein transport in primary cilia with single molecule tracking.” PhD diss., Temple University, 2019.

153. Yang, Y. Wnt signaling in development and disease. Cell Biosci 2, 14 (2012).

154. Gilboa, E.; Vieweg, J. Cancer immunotherapy with mRNA-transfected dendritic cells. Immunol. Rev. 2004, 199, 251–263.

155. Schlake, T.; Thess, A.; Fotin-Mleczek, M.; Kallen, K. Developing mRNA-vaccine technologies. RNA Biol. 2012, 9, 1319–1330.

156. Malina, A.; Mills, J.R.; Pelletier, J. Emerging therapeutics targeting mRNA translation. Cold Spring Harb. Perspect. Biol. 2012, 4, doi:10.1101/cshperspect.a012377.

157. McIvor, R.S. Therapeutic Delivery of mRNA: The Medium Is the Message. Mol. Ther. 2011, 19, 822–823.

158. Hill, R.; Cautain, B.; de Pedro, N.; Link, W. Targeting nucleocytoplasmic transport in cancer therapy. Oncotarget 2013, 5, 11–28.

159. Rodriguez, J.A.; Schüchner, S.; Au, W.W.; Fabbro, M.; Henderson, B.R. Nuclear-cytoplasmic shuttling of BARD1 contributes to its proapoptotic activity and is regulated by dimerization with BRCA1. Oncogene 2004, 23, 1809–1820.

160. Jamali, T.; Jamali, Y.; Mehrbod, M.; Mofrad, M.R.K. Nuclear pore complex: Biochemistry and biophysics of nucleocytoplasmic transport in health and disease. Int. Rev. Cell Mol. Biol. 2011, 287, 233–286.

161. Snow, C.M.; Senior, A.; Gerace, L. Monoclonal antibodies identify a group of nuclear pore complex glycoproteins. J. Cell Biol. 1987, 104, 1143–1156.

162. Gasiorowski, J.Z.; Dean, D.A. Mechanisms of nuclear transport and interventions. Adv. Drug Deliv. Rev. 2003, 55, 703–716.

163. Turner, J.G.; Dawson, J.; Cubitt, C.L.; Bazc, R.; Sullivana, D.M. Inhibition of CRM1-dependent nuclear export sensitizes malignant cells to cytotoxic and targeted agents. Semin. Cancer Biol. 2014, 27, 62–73.

164. Harland, R. and J. Gerhart, Formation and function of Spemann's organizer. Annu Rev Cell Dev Biol, 1997. 13: p. 611-67.

165. Choi H-J, et al. Thermodynamics of β-Catenin-Ligand Interactions. The roles of the n- and c-terminal tails in modulating binding affinity. The Journal of Biological Chemistry 281, 1027-1038.

166. Samuel L. Junod, Joseph M. Kelich, Jiong Ma, Weidong Yang. Nucleocytoplasmic transport of intrinsically disordered proteins studied by high-speed super-resolution microscopy. Protein Science. 2020;1–14.

167. Oldfield CJ, Cheng Y, Cortese MS, Brown CJ, Uversky VN, Dunker AK. Comparing and combining predictors of mostly disordered proteins. Biochemistry. 2005; 44: 1989– 2000.

168. Rabut G, Ellenberg J: Nucleocytoplasmic transport: diffusion channel or phase transition?. Curr Biol. 2001, 11: R551-554. 10.1016/S0960-9822(01)00340-2.

169. Dunker AK, Obradovic Z, Romero P, Garner EC, Brown CJ. Intrinsic protein disorder in complete genomes. Intrinsic protein disorder in complete genomes. Genome Inform Ser Workshop Genome Inform. 2000; 11: 161– 171.

170. Iakoucheva LM, Brown CJ, Lawson JD, Obradović Z, Dunker AK. Intrinsic disorder in cell-signaling and cancer-associated proteins. J Mol Biol. 2002; 323: 573–584.

171. Frege T, Uversky VN. Intrinsically disordered proteins in the nucleus of human cells. Biochem Biophys Rep. 2015; 1: 33– 51.

172. Fink AL. Natively unfolded proteins. Curr Opin Struct Biol. 2005; 15: 35– 41.

173. Tompa P. Intrinsically unstructured proteins. Trends Biochem Sci. 2002; 27: 527–533.